

NOTICE

This is a FULL translation of the original E2 blue book from German to English.

The translation was performed in the summer of 2017 by an undergraduate student at UC Berkeley, Tara Mellor, with native fluency in German, under the supervision of Dr. Chadi Salem at the Space Sciences Laboratory of UC Berkeley.

Thanks to Ina Fischer for her German expertise.

University of California Berkeley does not claim the copyright of the original document or this translation.

**Chadi Salem & Tara Mellor,
University of California, Berkeley, October 2017.**

BMFT-FB-W 81-039

Federal Ministry for Research and Technology

**Research Report W81-039
Air and Space Travel**

- Space Research / Space Technology -

**Routine data processing and physical interpretation of the measured data
from the fluxgate probe magnetometer (E2) and the search coil
magnetometer (E4) on the Helios 1 and Helios 2 space probes**

By

**F. M. Neubauer
H. Barnstorf
H. -J. Beinroth
K. U. Denskat
G. Musmann
H. Ruprecht
P. Volkmer**

**Institute for Geophysics and Meteorology
Braunschweig Technical University**

November 1981

Document control sheet

1. Report No. **BMFT-FB-W 81-039** 2. Type of Report **Final Report** 3. Space Research / Space Technology

4. Report Title.
Routine data processing and physical interpretation of data obtained by the fluxgate and search-coil magnetometer experiments onboard Helios 1 and Helios 2

5. Author(s) (Family name, First name(s))
Neubauer, Fritz Manfred; Barnstorf, Henning; Beinroth, Hans-Jürgen; Denskat, Kurt Ulrich; Musmann, Günter; Ruprecht, Hinrich;

6. Report date **June 1981**
7. Publication Date

8. Performing Organization (Name, Address)

9. Originator's Report No.

Braunschweig Technological University
Institute for Geophysics and Meteorology
Mendelssohn St. 1A
3300 Braunschweig

10. BMFT-reference no.
01QCO16A/WRS01081

11. No. of Pages
107

13. No. Of References
38

14. No. of Tables
4

15. No. of Figures
39

12. Sponsoring Agency (Name, Address)

Federal Ministry for Research and Technology (BMFT)

P.o. box 200706

5300 Bonn 2

16. Supplementary Notes

17. Presented at (Title, Place, Date)

18. Abstract

The methods used and problems encountered during the routine data processing of the fluxgate and search-coil magnetometer experiments onboard Helios 1 and Helios 2 are described. Subsequently the numerous new scientific results are summarized in detail.

19. Keywords

Interplanetary magnetic field
Solar magnetic field
Solar physics

20.	21.	22. Price DM 22,70
-----	-----	------------------------------

Federal Ministry for Research and Technology

Research Paper W 81-039

Air and Space Travel

- Space Research / Space Technology -

Routine data processing and physical interpretation of the measured data from the fluxgate probe magnetometer (E2) and the search coil magnetometer (E4) on the Helios 1 and Helios 2 space probes

By

Prof. Fritz Manfred Neubauer
Dr. Henning Barnstorf
Hans-Jürgen Beinroth
Kurt Ulrich Denskat
Dr. Günter Musmann
Hinrich Ruprecht
Peter Volkmer

Institute for Geophysics and Meteorology
Technical University of Braunschweig

Institute Director:
Prof. Dr. Walter Kertz

Project Director:
Prof. Dr. Fritz M. Neubauer

November 1981

Table of Contents

	Page
1. Introduction	5
2. Routine Processing E2	10
2.1 Data reduction	10
2.2 Routine presentation of reduced data	19
3. Routine Data Processing E4	23
3.1 Data reduction	23
3.2 Routine presentation of reduced data	25
4. Shock-Mode	26
4.1 Working principles	26
4.2 Processing of the shock-mode data	28
5. Data Exchange with Other Groups	30
6. Scientific Evaluation	32
6.1 General information	32
6.2 Macrostructure of interplanetary magnetic fields	33
6.3 Interference from interplanetary mediums through shock waves	42
6.4 MHD waves	53
6.5 High frequency wave fields in "whistler-mode" range	67
6.6 Discontinuities in interplanetary plasma	80
6.7 Fine structure of discontinuities	88
6.8 Fine structure of shock waves	97
7. Summary and Conclusion	105
8. Acknowledgements	107
9. Bibliography	108

1. Introduction

On December 10, 1974, the Helios 1 space probe was launched from NASA's Kennedy Space Center. Helios 1 had a perihelion distance of 0.31 AU and an orbital period around the Sun of 190 days. Helios 2 followed on January 15, 1976 with a perihelion distance of 0.29 AU and an orbital period of 185 days. The purpose of ten active experiments as well as ten passive experiments was and is to study the fields and matter in the interplanetary medium between 0.29 AU and 1 AU.

The Institute for Geophysics and Meteorology at Braunschweig Technical University contributed to the fluxgate probe (E2) and search coil (E4) experiments. The scientific objective of these experiments concerns different issues including the total area of the sun's magnetic field and interplanetary magnetic field, solar wind, and cosmic radiation. Most of the following points of scientific objectives will only be fully answered by close cooperation with more experiments. The contributions of E2 and E4 are shown in parentheses and are listed in order of importance:

- A. Macrostructure of the interplanetary magnetic field relating to the stream structure and characteristic areas on the sun, in particular, sector structure as a function of distance, longitude, and to limited degree latitude. The dependence of the sunspot cycle (E2).
- B. Dynamic processes in the interplanetary medium such as the propagation of shock waves and "coronal transients" (E2).
- C. Analysis of discontinuities in the interplanetary magnetoplasma including the type, orientation, frequency, jump properties, thickness etc. (E2).
- D. Analysis of the properties of MHD waves in the interplanetary magnetoplasma with the aim of understanding their propagation, formation, and damping (E2).

- E. Study of the plasma-physical fine structure of most common discontinuities such as tangential and rotational discontinuities (E4, E2).
- F. Fine structure of collision-less shock waves (E4, E2).
- G. Investigation of high-frequency electromagnetic wave fields, in particular, the occurrence of waves in the "whistler-mode" (E4).

Naturally, close coordination is necessary between the plasma experiment (E1), plasma wave experiment (E5), as well as the instruments measuring cosmic radiation (E6, E7, E8).

The analysis of the questions and issues mentioned above provides contributions to geophysics in connection with the propagation of interferences that affect the magnetosphere and upper atmosphere of the Earth. Contributions to astrophysics result from the study of the sun's environment, the only star available for in-situ measurements. Also, the use of the interplanetary magnetoplasma as a plasma laboratory gives contributions to plasma physics.

The E2 and E4 experiments on Helios were already described by Musmann et al. [1975], Dehmel et al. [1975], and Gliem et al. [1976]. The raw data from the experiments are routinely transmitted from telemetry onboard the spacecraft to the Deep Space Network (DSN) via NASA and the GSOC in Oberpfaffenhofen as EDR bands to the experimenters (EDR = Experiment Data Record). The routine data processing occurs between the EDR-bands and ADR-bands (ADR = Analysis Data Record). Here, a large number of small experimental errors are eliminated and the data is put into an easily usable form for further use. This task is simple in comparison to the development and construction of the experiments in terms of effort and complexity. This applies in particular to E2.

After retrieving the raw data from the magnetic field vectors,

the fluxgate probe experiment (E2) must correct for the phase shift through the aliasing filter, the zero point shifts through variable spacecraft fields, magnetometer zero points, as well as the the deflection of the whole measured triplet. The correct zero point displacement and "misalignment" angle must be determined in flight. This correction method is not specific to Helios, at least in principle, and must be applied in all magnetic field experiments on spinning spacecraft. Different coordinate transformations and so on are applied before reaching the ADR.

Essentially, only the calibration factors measured on the ground must be included in the routine processing of the E4 spectral data. The situation is somewhat more complicated with the so-called waveform data, in which variable frequency bands from the noise magnetic fields (B_d) on Helios-1 and the time derivative $\frac{dB_d}{dt}$ on Helios 2 are both measured. Here, extensive coordinate transformations etc. must be carried out.

In the planning of both the routine and scientific processing of the Helios data, a mission duration of 18 months, and a mission extension of 12 months, were assumed. In planning, a compromise between the routine processing and the scientific processing had to be found. The first part naturally decreases with time, while the latter part increases. The actual data processing costs far surpassed what was expected because of two developments which occurred after the Helios mission began.

Although both Helios spacecraft fulfilled the technical specifications to a great extent, one anomaly hit the E2 fluxgate probe experiment onboard Helios 1 particularly hard. Due to the flawed model for the required thermal insulation of the sensor box on E2, temperatures that were too high were reached at perihelion. It should be noted that the thermal insulation of the E2 sensor box does not lie within the area of

responsibility of the experimenters. At first perihelion, a temperature of 75°C was measured on the sensor, which rose until the 12th perihelion. The temperature at perihelion increased to 89 °C. As a result, the mechanical folding mechanism ("flipper") on board Helios 1, which had the purpose of calibrating instrument zero points for the 90° rotation of two sensors, stopped functioning just before the first perihelion. Since the micro-switch necessary to indicate the flipper's position also failed, the flipper's position had to be constantly monitored and reconstructed with the aid of the data because of the possibility of spontaneous flips. Furthermore, for reasons which have not been completely clarified due to the problem described before, jumps in the sensitivity of the instruments occurred followed by successive, reversible jumps back. These rare events are identifiable from the simultaneous leaps of zero points at high data rates with the temporal resolution of spin variations (i.e. for 1024 bps and 2048 bps). Since this observation is not possible with lower bit rates, suspected sensitivity changes must be identified through simultaneous jumps of the same factor for all three components. In order to ensure the certainty of the identification, a final inspection was introduced during routine processing, in which plots from processed data were examined. Due to the problems just mentioned, the data processing expenditures increased considerably. Extensive tests showed that the magnetometer worked flawlessly aside from the sensitivity changes mentioned. In the final analysis, the sensitivity calibration cycles and the internal consistency of the data were taken into account.

The thermal system [for Helios 2] had to be changed because of the problem with the E2 thermal insulation on the Helios 1 sensor box; this led to much lower temperatures. A problem occurred with Helios 2 on January 17, 1976 when the "flipper" was left hanging between the two rest positions because too low a temperature was reached during a flip test. The system then

"crawled" slowly by another 6° in the direction of the rest position. Then on April 7, 1976, the mechanism began working fully due to the now-increased temperature. Extensive modifications and tests were once again necessary in order to rectify the valuable data from this interval at the beginning of the Helios 2 mission. After the "freezing interval" the folding command was only given for temperatures above 20°C enabling the flipper to work flawlessly until the end of the Helios 2 mission. Another problem with Helios 2 arose from variations of the spacecraft field, these had periods of several hours and amplitudes of a few nT. They were noticeable only after the primary mission.

Aside from the previously mentioned undesirable technical problems, the work devoted to the routine data processing increased over the long lifespan of both space craft, this time in a desirable manner. At the time this report was written, Helios 1 still provided valuable data while the Helios 2 mission ended on March 3, 1980. With this data, it will be possible to continue investigations of the interplanetary magnetic fields until the solar maximum is reached. In the future, this data will be priceless.

The search coil experiment (E4) experienced only small problems, so the processing of the data recorded during the mission was free of major obstacles. The E2 experiment on Helios 1 stopped working during the 12th perihelion when too high sensor temperatures were reached (>150°C). The instrument (E2) worked on Helios-2 until the end of the mission on March 3, 1980.

3200 EDR bands have been analyzed so far in the processing of the E2 and E4 Helios experiments. This has resulted in 265 ADR bands from the fluxgate probe experiment (E2), 494 ADR-bands from the search coil experiment (E4), and 10 bands containing data from the so-called shock-mode. The routine processing and subsequent scientific processing was performed on a rented HP-

3000 computer system with appropriate peripheral equipment such as Band devices, printers, plotters, etc. Figure 1 shows the number of staff available for the Helios data processing as a function of time.

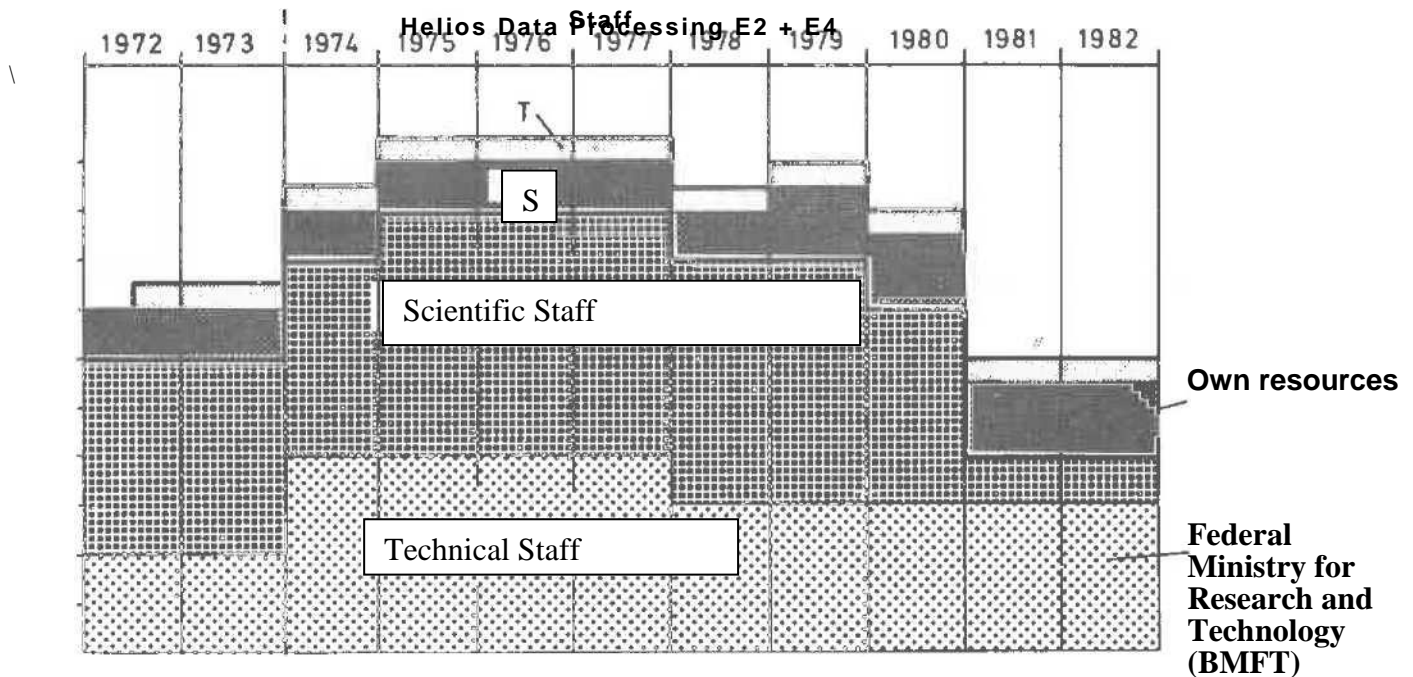


Fig.1: Staffing of the Helios data processing

2. Routine Processing of E2

2.1 Data Reduction

The raw material for data processing was sent in the form of EDR bands by the GSOC in Oberpfaffenhoffen containing raw data from the fluxgate probe experiment (E2). The first step of processing the data is cataloging the bands in a computerised database.

For data backup and to simplify the later processing, all EDR-bands (with a few exceptions), were copied. Because this required copying all the data from extra long output bands (1200 copied bands and 370 which have still not been copied), it has resulted in 112 copy tapes. The raw data analysis begins with the time allocation of the measured values. Since the magnetic

field has a fixed sampling frequency per revolution (i.e. is measured spin-synchronously), and the data transfer takes place in a fixed time grid, the data is given via a memory buffer in the telemetry. So that no data is lost, it is ensured that all measured data values are taken from the telemetry. The memory buffer is emptied periodically and the fill vector is transferred. Because of transition errors in the telemetry, which were known and displayed by the GSOC, it is possible that some of the data records are unnecessary, but in general this does not apply to any whole number of vectors contained. As a result, information about the measuring direction (sector), which is only contained in the first three vectors of the main frame, is often also lost. All this must be taken into account when regenerating the directional information and time allocation.

The bulk of the data reduction consists of the elimination of some usually small systematic errors due to the presence of a spacecraft field from magnetometer zero point errors, including the deviations from the orientation of sensor triplets from the nominal direction - in which one component is exactly parallel to the real direction of the spin vector.

Figure 2 shows the geometry of the true axes of the sensors denoted as RAW_1 , RAW_2 , and RAW_3 . The ideal axis of the payload coordinate system are the PAY_1 , PAY_2 , and PAY_3 axes. The PAY_3 axis is exactly parallel to the true spin axis. This true spin axis direction usually deviates from the planned spin direction, on the figure axis of the spacecraft - this is due to inaccuracies in the balancing of the spacecraft. The RAW_2 axis in figure 2 was assumed to lie in the meridian plane of PAY_3 and PAY_2 axes. While all the angular magnitudes in Fig. 2 can be determined from the data in flight, the exact angle between the PAY_2 or PAY_1 directions and the sun cannot be determined from the data itself.

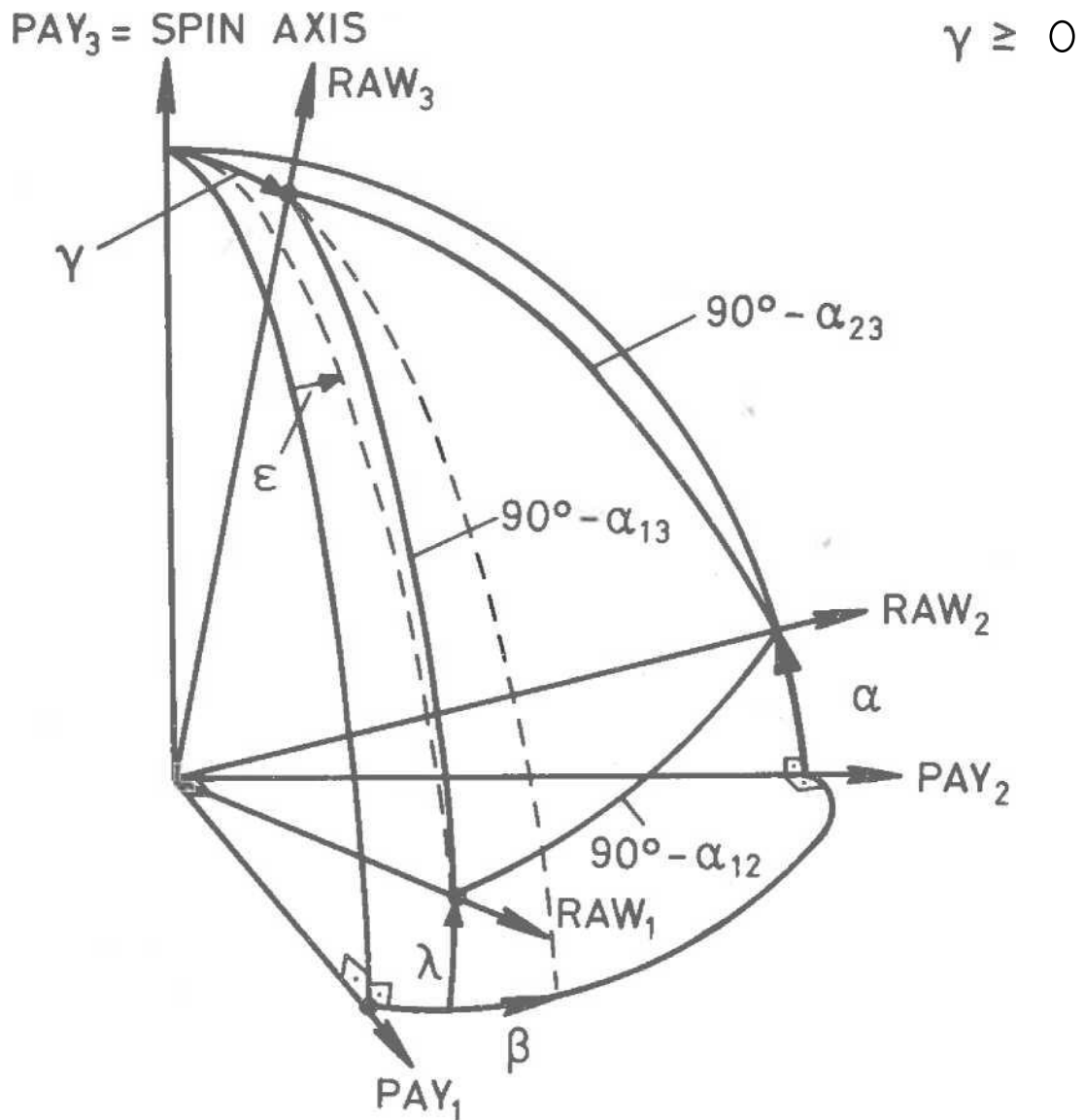


Fig. 2:

Planned outline for missalignment of the true magnetic sensor axis directions RAW_1 , RAW_2 , and RAW_3 .

The accuracy with which this angle can be known, is then given by the precision of the mechanical construction of the spacecraft. The direction of the spin axis in elliptical coordinates is routinely provided on the AOI-bands from the project (AOI = Attitude Orbit Information). The angles α_{12} , α_{13} , and α_{23} represent the deviations of the sensor triple from an orthogonal measuring system. These angles are known, and have an order of magnitude of several arc minutes. The mechanical design of the sensor system does not account for variations in these angles. The limited accuracy requirements of the Helios mission

allow for the assumption of an ideal trihedron, i.e. $\alpha_{12} \approx 0$, $\alpha_{13} \approx 0$, and $\alpha_{23} \approx 0$, respectively. From the angles shown in Fig. 2, only two are freely selectable, e.g. α and γ .

We can now provide a formalism to study the various systematic and statistical errors. The magnetic field in an inertial system is given by the quantities F_{\parallel} , F_{\perp} and the angle ϕ . The components in the direction of the axes $HPAY_j$ ($j = 1, 2, 3$) in the rotating system of the spacecraft can be represented as follows:

$$\begin{aligned} HPAY_1 &= F_{\perp} \cos(\Omega t + \phi) \\ HPAY_2 &= -F_{\perp} \sin(\Omega t + \phi) \\ HPAY_3 &= F_{\parallel} \end{aligned} \quad (1)$$

For a constant vector in the inertial frame of reference F_{\parallel} , F_{\perp} , and ϕ are constant. The exact components of the magnetic field in the direction of true sensor axis RAW_j ($j = 1, 2, 3$) are given by:

$$\begin{aligned} HMAG_1 &= F_{\parallel} \sin\lambda + F_{\perp} \cos\lambda \cos(\Omega t + \phi + \varepsilon) \\ HMAG_2 &= F_{\parallel} \sin\alpha - F_{\perp} \cos\alpha \sin(\Omega t + \phi) \\ HMAG_3 &= F_{\parallel} \cos\gamma + F_{\perp} \sin\gamma \cos(\Omega t + \phi + \beta) \end{aligned} \quad (2)$$

The spin frequency, Ω , has a rotational period of about 1s. These exact magnetic field components are measured by a magnetometer on the spacecraft and therefore can be subject to measurement errors. Firstly, signal distortions are generated by the aliasing filter with the transfer function $T(\omega) = T_A(\omega) \cdot e^{i\phi_T(\omega)}$, where $T_A(\omega)$ and $\phi_T(\omega)$ are known real measured functions of frequency with $T_A(\omega) \rightarrow 1$ and $\phi_T(\omega) \rightarrow 0$ for $\omega \rightarrow 0$. Secondly, spacecraft fields and sensor zero point displacements cause total zero-point shifts, HN_j , for the sensors $j = 1, 2, 3$. The latter two errors can in principle be determined with some effort. The digitization error HD_j can not be eliminated. We can then get the raw magnetic field vectors $HRAW_j$ from $HMAG_j$

$$\begin{aligned} HRAW_1 &= HN_1 + F_{\parallel} \sin\lambda + F_{\perp} T_A(\Omega) \cos\lambda \cos(\Omega t + \phi + \phi_T) + HD_1 \\ HRAW_2 &= HN_2 + F_{\parallel} \sin\alpha - F_{\perp} T_A(\Omega) \cos\alpha \sin(\Omega t + \phi + \phi_T) + HD_2 \\ HRAW_3 &= HN_3 + F_{\parallel} \cos\gamma + F_{\perp} T_A(\Omega) \sin\gamma \cos(\Omega t + \phi + \phi_T) + HD_2 \end{aligned} \quad (3)$$

under the only assumption that the magnetic field variations in the inertial system F_{\parallel}, F_{\perp} , and ϕ only vary slowly with time, i.e. $\omega \ll \Omega$. Assuming arbitrary frequency values of F_{\parallel}, F_{\perp} , and ϕ equation 3 must be replaced by a complex expression. In the most important measuring range with digitization windows of the size 0.4 nT applies to $|HD_j| \leq 0.2 \text{ nT}$.

Equation 3 gives the various distortions of the measured signals through the systematic errors. The $HRAW_1$ component for example had small spin variances, the projection of the magnetic field vectors on the spin plane was rotated by the aliasing filter, and so on.

We now use equation 3 for the case of constant magnetic fields in the inertial system ($F_{\parallel}, F_{\perp}, \phi, \text{constant}$) to determine the necessary correction quantities. For this purpose, the measured time variation is decomposed according to the Fourier transform with the result:

$$HRAW_j(t) = HRAWO_j + HRAWS_j \sin \Omega t + HRAWC_j \cos \Omega t + HR_j \quad (4)$$

The Fourier coefficients $HRAWO_j$, $HRAWS_j$. And $HRAWC_j$ for $j= 1, 2, 3$ are constant for a given analysis interval. In the case that F_{\parallel}, F_{\perp} , and ϕ are constant, HR_j disappears. A comparison of equations 3 and gives:

$$\begin{aligned}
\text{HRAWO}_1 &= \text{HN}_1 + F_{11} \sin\lambda \\
\text{HRAWO}_2 &= \text{HN}_2 + F_{11} \sin\alpha \\
\text{HRAWO}_3 &= \text{HN}_3 + F_{11} \cos\gamma
\end{aligned} \tag{5a}$$

$$\begin{aligned}
\text{HRAWS}_1 &= - F_{\perp} T_A \cos\lambda \sin(\phi + \varepsilon + \phi_T) \\
\text{HRAWS}_2 &= - F_{\perp} T_A \cos\alpha \cos(\phi + \phi_T) \\
\text{HRAWS}_3 &= - F_{\perp} T_A \sin\gamma \cos(\phi + \beta + \phi_T)
\end{aligned} \tag{5b}$$

$$\begin{aligned}
\text{HRAWC}_1 &= F_{\perp} T_A \cos\lambda \cos(\phi + \phi_T + \varepsilon) \\
\text{HRAWC}_2 &= - F_{\perp} T_A \cos\alpha \sin(\phi + \phi_T) \\
\text{HRAWC}_3 &= F_{\perp} T_A \sin\gamma \cos(\phi + \beta + \phi_T)
\end{aligned} \tag{5c}$$

The amplitude of spin variations from 5b and 5c are given

$$\frac{\sin\gamma}{\cos\lambda} = \sqrt{\frac{(\text{HRAWC}_3^2 + \text{HRAWS}_3^2)}{(\text{HRAWC}_1^2 + \text{HRAWS}_1^2)}} \tag{6a}$$

and

$$\frac{\sin\gamma}{\cos\alpha} = \sqrt{\frac{(\text{HRAWC}_3^2 + \text{HRAWS}_3^2)}{(\text{HRAWC}_2^2 + \text{HRAWS}_2^2)}} \tag{6b}$$

Further we have:

$$\text{tg}(\phi + \varepsilon + \phi_T) = -\frac{\text{HRAWS}_1}{\text{HRAWC}_2} \tag{6c}$$

and

$$\text{tg}(\phi + \phi_T) = \frac{\text{HRAWC}_2}{\text{HRAWS}_2} \tag{6d}$$

Equations 5 and 6 can only be used with the highest slow varying angle magnitudes such as HN_j for the correction of the raw measured data. When selecting which equations to use, the sensitivity to small residual HR_j and digitalization errors HD_j must not be considered.

The procedure is then run in such a way that the data is continuously searched through in intervals of several minutes, i.e. with many spin rotations. These data intervals contain sufficiently pure sine and cosine variations - i.e. with small $HR = \sqrt{HR_1^2 + HR_2^2 + HR_3^2}$. They also have sufficient amplitudes of the spin variations $HRAW_1$ and $HRAW_2$ to fulfill the necessary conditions. The γ and ε angles are calculated with the aid of equations 6. This assumption is justified because γ , λ , and α are small angles with $\cos\lambda \approx 1$ and $\cos\alpha \approx 1$, (in equations 6a and 6b), this makes calculations considerably simpler. All other angles can be found using known spherical trigonometric relations. With the help of the derived quantities $\alpha, \beta, \gamma, \varepsilon$, and λ , the magnetic field variations can be corrected so that only zero point errors remain. The measured values of the magnetic field are transformed to the system in the coordinate direction PAY_j ($j = 1, 2, 3$), they can also be regarded as the measured values of fictitious sensors with an ideal orientation. The zero points for the coordinate direction PAY_j ($j = 1, 2, 3$) will now be determined according to the vector equation 5a and are denoted $HN_j^{\ddot{}}$, $HN_1^{\ddot{}}$, and $HN_2^{\ddot{}}$. After this, only the zero point displacement in the PAY_3 direction are undetermined i.e. $HN_3^{\ddot{}}$.

In addition to the standard procedure described above, further programs were developed for special time intervals or tasks, i.e. programming and testing. From January 17 to April 7, 1976, the sensor system on Helios-2 was "frozen" between the two rest positions. The angle γ varied from 20° to 26° . In

this case, the assumption that $\alpha \approx 0$, $\varepsilon \approx 0$, and $\beta \approx 0$ or 180° was made which gives

$$tg \gamma = \left(\frac{HRAWC_3^2 + HRAWS_3^2}{HRAWC_1^2 \beta HRAWS_1^2} \right)^{1/2}$$

This approximation results in small precision losses at desired time resolutions, and is preferable to a second spin period.

A further program called COMPIS was developed so that the determination of α_{12} , α_{13} , and α_{23} was possible independently. Despite the achievable accuracy, the complexity of this procedure makes standard application impractical.

The techniques just described are only applicable when the data rate is high enough to resolve the spin variations temporally. The measurements are essentially spin synchronous. An optimum resolution will produce format 1 at 2048 bps. At this interval, both the angles and the zero-point shifts, $HN_1^{\ddot{}}$, and $HN_2^{\ddot{}}$, are routinely calculated. At 1024 bps only zero points can be calculated since there are only 2 vectors per revolution. In all intervals with bit rates below 2048 bps, the correction angles from adjacent 2048 bps interval are interpolated or extrapolated.

In addition to using zero points, utilizing spin variation allows for the determination of the zero point shifts in the spin plane, aside from $HN_3^{\ddot{}}$. $HN_3^{\ddot{}}$ must therefore always be determined in a different way, whereas $HN_1^{\ddot{}}$, and $HN_2^{\ddot{}}$ can be determined relatively frequently (at least at intervals with high data rates).

The zero-point shifts $HN_3^{\ddot{}}$ and small data rates $HN_1^{\ddot{}}$, and $HN_2^{\ddot{}}$ are determined by a technique developed by Hedgecock (1975). It is

based on the statistically plausible hypothesis that for large values of N , the true interplanetary magnetic field quantities that are of magnitude:

$$S_j = \sum_{i=1}^N (H_{j,i+1} - H_{j,i})(F_{i+1} - F_i) \quad (7)$$

become insignificant. The interplanetary magnetic field has a value of F_i and components $H_{1,i}$, $H_{2,i}$, and $H_{3,i}$ in the inertial frame of reference; the index, i , describes the equidistant measured values in the data series. A zero point displacement of the measurement magnetometer causes a resulting asymmetry in the $F_{i+1} - F_i$ term so that S_j no longer disappears. To keep the static fluctuations of S_j ($j= 1,2,3$) as small as possible, N must be sufficiently large. Experiments of the [hedgecock] method in Earth orbit and also on Helios at other known zero points yielded satisfactory results. One disadvantage of the method is that short-term variations of the zero points can remain undetected. In Helios' case, data intervals of 8 hours are a convenient compromise between time resolution and accuracy.

The final zero points are determined for $HN_3^{\ddot{}}$ by the interpolation of the 8 hour difference in values. Three cases had to be determined for the $HN_1^{\ddot{}}$ and $HN_2^{\ddot{}}$ zero points. For higher data rates, the zero points obtained from spin variations are used. At a distance of more than 24 hours from an interval with sufficient time resolution, ≥ 1024 bps, only the Hedgecock method was used. During the transition, interpolations were made between the two values. The fixed zero points $HN_j^{\ddot{}}$ ($j = 1,2,3$) are stored separately in the computer so that they will be available later to be used for the zero point corrections of the data at different time resolutions.

The magnetic field data without zero-point corrections are ultimately rotated into a non-rotating coordinate system whose coordinate directions correspond approximately to the solar ecliptic coordinate system, which will be introduced in the next section. This system X, Y, Z is first defined by the true spin axis as the Z axis. The plane from the spin axis and the direction to the sun includes the coordinate direction, X. The right-handed, orthogonal trihedron is completed by the Y-axis, perpendicular to the latter plane. The magnetic field components calculated in this way form the starting point for the preparation of the ADR bands described in the next section (2.2).

2.2 Routine Presentation of Reduced Data

The ADR bands (ADR = Analysis Data Record) produced are the output of the data reduction; in addition to the processed magnetic field data, they contain all other EDR data including house-keeping, attitude-orbit, and command-data records (HKI, AOI, and CMD). The number representation, however, is adapted by the local computer. In addition, times are given in days and fractions of days beginning from January 1 of the start year. The records are stored in chronological order.

In the case of a later data evaluation, it is preferable to have all the required data together, the magnetic field data sets are stored in a data header, which is the same for E2 and E4, the most important information about the transfer mode (bit rate, format, data handling mode), the position of the helios probe, as well as the correction values (angles and zero point shifts) are determined during the data processing. For each magnetic field vector related to the spacecraft based X,Y,Z coordinate system, there is a status update with information on the position of the flipper, the sector in which the vector was measured, and the quality of the data.

The data quality is used to identify missing vectors, and vectors during which inconsistencies or errors occurred during the raw data processing. Inconsistencies determined on board are detected by the flipper position display from regenerated sector information that contains errors and unexplained jumps in the magnetic field data or in the zero shifts.

The default outputs of the ADR bands are 8 second mean values. The record format used for the bands is the same as for the ADR. In addition, magnetic field vectors are stored in separate data sets with the same leader in the solar ecliptic coordinate system and have an additional specification of the standard deviations and mean value. In the status update, instead of the sector information, there is an identifier for the number of vectors used. From the other data sets (HKI, AOI, CMD), only one selection with a smaller time resolution is accepted.

The mean value bands are used to determine zero point correction values with the help of the Hedgecock Method (see 2.1) and are then corrected.

In order to simplify further evaluations, outputs of corrected 8 second mean value bands, one hour mean value band, and 40.5 second mean value bands were generated. However, in principle, any time resolution can generate average bands.

The average value bands determined for data exchange contain corrected 8 second average values for standard deviations and magnitudes

In order to obtain an overview of the data, daily, monthly, and hourly plots (during the primary mission) were created. The GMD microfilm plotter was widely used for these plots. The plots have a uniform format and are based on mean values (8 seconds for the hour plots, 2 minutes for the 1 day plot, and

1 hour for the monthly plot). The magnitude of the ecliptic angle (ϕ), angle of elevation (θ), and the standard deviation of the magnitude and data quality are shown. A sample plot is shown in figure 3, where the ground data has been omitted.

For specific "suspicious" time periods, in reference to the quality of the data, HKI day plots are generated for control and are determined by the space craft and the data processing, and include fixed zero point shifts and flipper settings and the as the paramter of the data transmission.

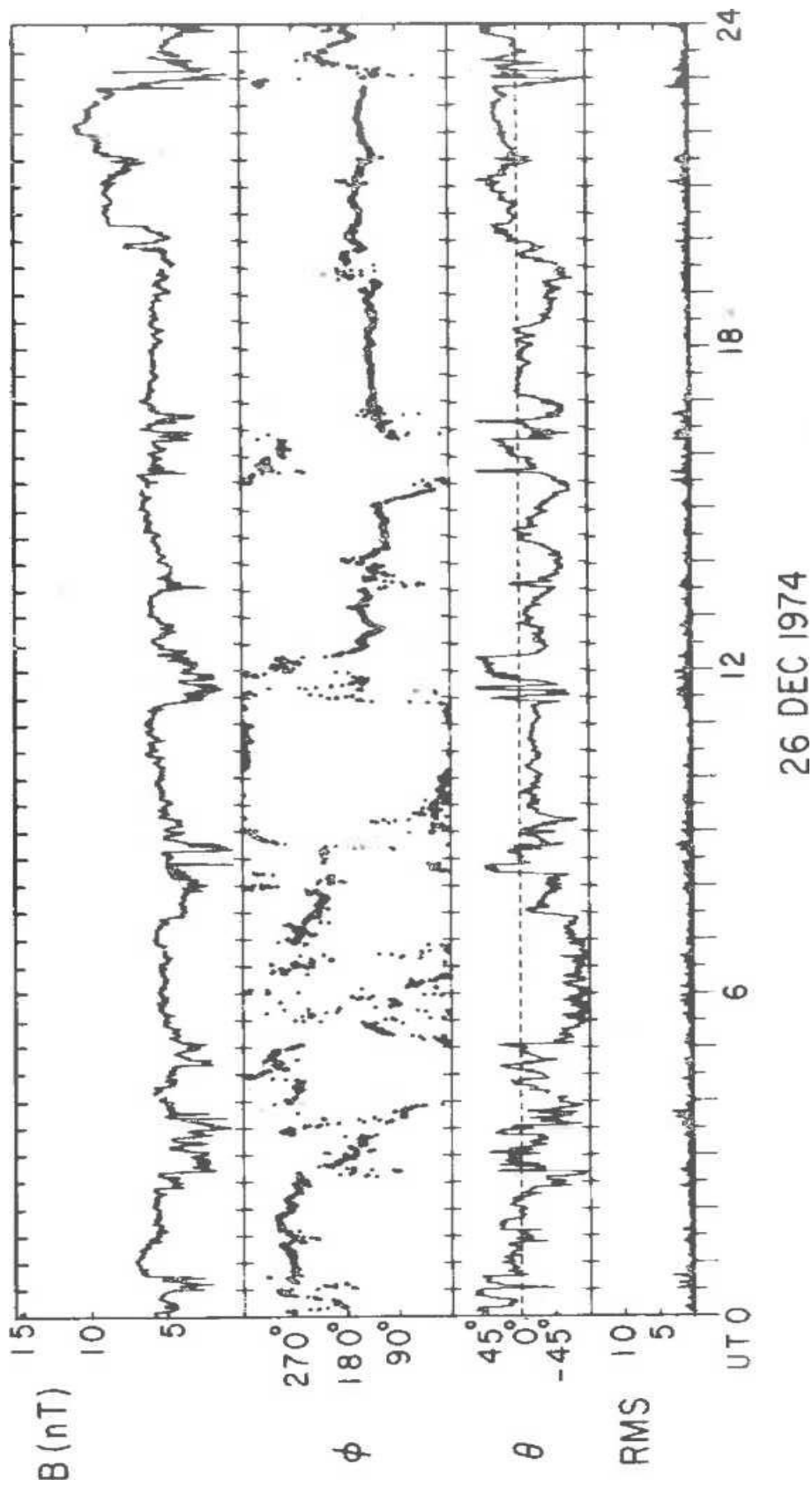


Fig. 3: Complicated sector structure from the 26th of December as an example of the E2 routine plots.

For further analysis it is possible to create high-resolution plots (each vector is plotted) and long-term plots of any time period. Finally, there are programs for the collation of data sets of EDR, ADR and mean value bands, as well as for the direct establishment of mean value lists in the solar ecliptic coordinate system with any time resolution.

3. Routine Data Processing E4

3.1 Data reduction

Data processing for E2 begins with computer-assisted cataloging. Afterwards, the EDR bands supplied by GSOC are copied for the reasons mentioned above (data backup, better utilization of the band stations, etc.)

The search coil magnetometer experiment E4 is characterized by an extremely high internal data generation rate. For this reason, various techniques of redundancy and information reduction, which provide different data streams, are used in the experiment.

In most formats and data modes, only spectral data are telemetered. The spectral data contains intermittent consecutive time intervals that are a minimum of 1,125 seconds, the average squares of the output signals for the eight band passes in the experiment for the two components, and the maximum value of the signals. There are $2 \times 8 = 16$ average values and 16 maximum values. Since the measurements are time synchronized, the time order for the individual measured values of the spectral data is simple. According to the time allocation, the raw measured data values are multiplied by calibration factors obtained on the ground in order to obtain the spectral densities in nT/\sqrt{Hz} . The maximum values with corresponding calibration factors are provided such that the ratio between the maximum and mean values for a monochromatic scale is $\sqrt{2}$.

Important values for the correction of the obtained spectral densities are spectral densities of the summed sensor noise and disturbances from the spacecraft, briefly called "background noise". This is obtained, with the help of time intervals of low magnetic field fluctuations in solar wind. Figure 4 shows the background noise as a function of frequency for Helios 1 and 2.

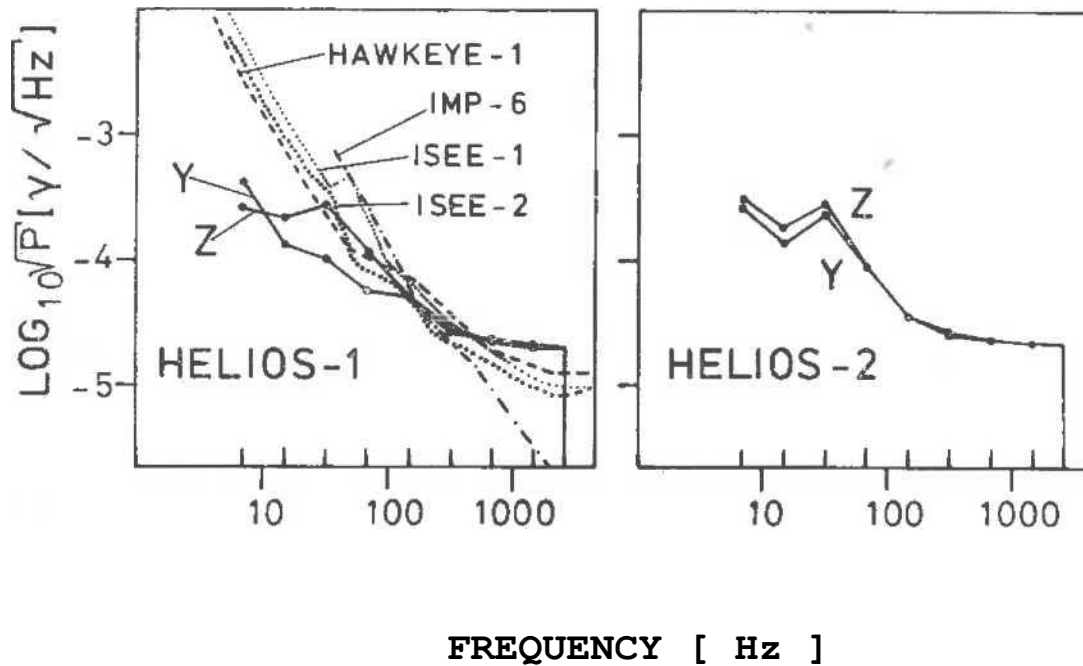


Fig.4:

Background noise of the E4 experiment in comparison with the other experiments for the measuring of high frequency magnetic fluctuations.

The maxima probably originate from stray fields from the solar cell arrays. For comparison, the noise values of other alternating magnetic field experiments are given. Long term studies of the background noise properties revealed that there was a $\pm 1\%$ constant value during the Helios mission. It was only at the end of the experiment that deviations of up to $\pm 10\%$ occurred during periods when temperatures were outside the specifications.

In addition to the spectral data described so far, the waveform data was transmitted from all three components during the time intervals of format 5 in a relatively low-frequency band. The format 6 transfer of the so-called "shock mode" will be discussed in section 4. The processing of the waveform data was also problem-free. Because of the time synchronous measurements, time allocation is simple. In order to achieve a high dynamic range with only a few bits per vector, a semi-logarithmic AD conversion with a relatively poor precision was chosen. For this reason, corrections for the slight misalignment of the three sensors are not necessary.

3.2 Routine Presentation of Reduced Data

The representation of the E4 data was very closely aligned with the E2 data processing, so section 2.2 will be referred to here.

The ADR bands have the form described here. The E4 data are the spectra of the Z and X/Y components in each case. For each record, peak values and time related records of mean values are grouped together. The data quality is either 0 (0 = good data) or 7 (7 = useless data).

For the mean value bands, the same applies as for the ADR-bands, however, no HKI, AOI, or CMD records are included. The waveform records are also omitted. Eight second mean value bands are generated by default. For comparison with the plasma data (E1), 40.5 second mean value bands are also available. In principle, bands with any mean length can be produced.

Plot program packets are available for displaying the data. By default, hour and day plots are created on microfilm, a large part of which is also available in "hardcopy" form. However, the hour plots had to be dispensed during times of low time resolution. There are 15 daily plots for all measurements. Plots with any time resolution can be created at any time. For the

direct output of the mean or peak values (or both together), there are programs for the production of *hard copies*. Apart from the E4 data, the hard copies contain all additional information.

4. Shock-mode

4.1 Working Principles

The physical background and design criteria of the Helios shock mode were described by Neubauer [1969]. A description of the shock mode was finally implemented in Helios 1 and Helios 2 and is described by Mussman et al. [1979]. Since the description of the shock mode data in 4.2 is not comprehensible without knowledge of the working principles, the working principles of the shock mode are discussed briefly.

Due to a few exceptions, limited to a 2048 bps data transfer rate for the real time data transmission of the Helios probes, the maximum time resolution of the E2 and E4 experiments is by no means fine enough to resolve structures of interest for plasma physics i.e. collision-less shock waves, tangential discontinuities, and rotational discontinuities etc. Each Helios spacecraft contains a 500 kbit core memory for the quick reading of short data intervals of particular interest, with a processing speed of 8kbps, 16 kbps, and 32 kbps. The E3 and E5 data can also be read. The memory content is regularly read slowly via the real time telemetry when sufficient transmission capacity is available.

The problem lies with the selection of the correct data intervals for processing in the core memory as well as the transmission to Earth. For this purpose, an event detector that responds to fast jumps due to high magnitudes of the magnetic field is used. The event detector in E2 calculates the relative change in magnetic field magnitudes at all times, e.g. indicated as $A(t)$. The respective calculated current value $A(t)$ will be compared with the maximum of all previous values since the shock

mode was initiated (with RESET). Only when all previous values of A are surpassed (when $A(t) > A_{\max}$), does the event detector output a signal for reading the memory, which requires overwriting the previous memory content.

In order to also detect the important part of an event preceding the detection of the most significant event to date, the memory is divided into three sections, A, B and C; which comprise 1/5, 1/5, and 3/5 of the memory content, respectively. The following strategy is then used: in one of the small memory parts, e.g. A, the time ordered data is constantly being processed and older data is overwritten so that for all points in time, all data between $t - T_A/4$ and t are stored. T_A is the total measured time for an event and can be selected by ground command. If an event is detected in the fashion described above, the memory in part C is processed until it is full. The event detected can then be found in part A with $T_A/4$, and in part C with $3T_A/4$. The constant writing and overwriting is continued in part B, until a more significant event is detected. Parts A and B contain the "precursor" at all times, t , of the most significant event to date and the last $T_s/4$ seconds.

After an interval that is typically four hours, the memory content is transmitted and A_{\max} is set to zero. Then, the loop starts from the beginning.

During the Helios missions, the event detection logic proved to be very good. A variety of time intervals with fine structure of interest were obtained with high data transmission rates during the primary missions of Helios 1 and Helios 2. The shock-mode data from E2 and E4 were sent to us from the GSOC through EDR bands.

4.2 Processing of Shock-Mode Data

As previously mentioned, the memory readings of the format 6 data from experiments 2 and 4 is contained in the normal data stream of the real-time formats. The processing of the EDR bands in experiment 2 is included in the format 6 data, and was carried out using separate program sections of the processing system for the flux gate probe data.

One particular difficulty of the data reduction was achieving the correct temporal allocation for the processed experimental data frames, which could be found in different areas of the memory; A, B, or C. During the analysis of different readings of the flux gate probe data, it was found that jumps in the angles associated with the fixed vectors occurred in shock-mode format 6, the magnetic field measurements started with 4, 8, or 16 vectors per spacecraft rotation; these also occurred within the defined memory parts, A, B or C, suggesting a source of error before or at the start of the EDR processing. A reconstruction of some erroneous readings could be achieved, through the implementation of special routines which were adapted for these errors.

Simultaneous with the flux gate probe processing, the results of which were written separately from the real time form data to a special "shock memory file", a copy of the chronologically assembled E4 data frames is in the compressed block diagram of the EDR-data. During the E2 processing (see section 2), this shock file, which could record some memory readings, was written on a "shock band".

In a second step, the band handled the E4 data blocks with separate routines and copied the already finished E2 data. This routine processing of the high resolution waveform data and maximum spectral values are in a similar form as in Format 5 of the E4 real time data (which also contains waveform data). The

result was the final "shock-ADR", which contains the memory readings for E2 and E4 in a physically interpretable form.

The absolute time allocation of the format 6 data (the times contained on EDR bands are memory reading times) could not be carried out automatically and required the flux gate probe data to be on hand for comparison with the real time data. For this purpose, a routine graphical representation of the format 6 flux gate probe data was required. All readings were plotted in their unaveraged form as either a component or as an angle magnitude representation. These standard plots served as the basis for the search for the "events" contained in the shock memory, which also had to be present in the real time data. The routine hour plots of the standard processing (see section 2.2) proved to be a comparative basis. In most cases, a time allocation could be found since a sudden, characteristic change in direction or magnitude of the magnetic field vectors took place.

Due to the huge abundance of data, special plot programs were developed for the waveform data, which was suitable for interactive operation on a graphic screen.

With the aid of these [plot] programs, the memory readings of the waveform data could be examined and special events with selectable time resolution could be viewed. In addition, these routines offered the possibility to apply filters of a suitable bandwidth to the waveforms and to compute performance spectra of certain, short time intervals. The interactive examination of the search coil magnetometer data proved itself in the scientific evaluation, since in this way, many short-time wave events could be found in the temporally high-resolution data.

The E2 event detector on Helios 1 was no longer usable after the "flipper" failed, as described in the introduction. In addition, it was decided that the format 6 data would only be transmitted to earth when the highest data rates were available. The primary

mission of both Helios spacecraft showed a large number of surprising events which are discussed in section 6.7 and briefly in 6.8.

5. Data Exchange with Other Groups

Most of the physical problems presented in the scientific objectives for Helios require close collaboration between the different groups of experiments for both spacecraft. This cooperation consists of scientific discussions between the groups and the exchange of appropriate data. In agreement with what was said in the introduction, the exchange of data between the plasma experiment (E1) and the flux gate probe experiment is mutually beneficial. The evaluated data bands from E2 and E1 are routinely compiled in Garching, Germany so that it can be available to both experimental groups. For various purposes, specially evaluated data was exchanged, for example data with high time resolution was exchanged for data with shorter intervals.

While for many scientific sub-projects, the exchange of previously evaluated data is adequate; e.g. between E1 and E2, the magnetic field data are of great importance in the evaluation of three dimensional distribution functions of charged particles measured by E1, E6, E7 and E8. The magnetic field direction is used in the plasma neutral system as the direction by which velocity distributions are axially symmetric. The gyrotropy of the plasma particles can be used both directly in the routine evaluation of ions and electrons and also for control of the particles. Corresponding magnetic field data for this purpose and for other purposes were made available to the E6, E7, and E8 experimental groups.

For the physical investigations of the search coil experiment (E4), the exchange with the E5 experiment, which measures high frequency electric fields, is of particular importance. In order

to define the propagating properties of plasma as well as its absorption or instability, detailed plasma data is necessary.

Aside from the data exchange between the Helios experiments, the data exchange with other spaceflight missions such as those that carry out ground measurements of Earth's environment or solar observations is particularly useful for answering questions about the macroscopic dynamics of solar wind. For such data exchange projects, direct contact between the interested groups has proved to be particularly useful. As an example, we point out the Helios-Voyager workshop in 1978. Data from the Helios 1 and Helios 2 interplanetary probes, IMP7 and IMP8 satellites, and the Voyager 1 and Voyager 2 space probes from the time interval between September and December 1977 was discussed. In the time interval shortly after the launch of Voyager 1 and 2, the spacecraft identified a unique array of observation stations in the interplanetary medium between 0.3 AU and more than 1.6 AU. Some of the particularly outstanding results can be found in a paper by Burlaga et al. [1980].

Furthermore, the large number of physical problems relating to the interplanetary medium, of space plasma physics, and of solar-terrestrial relations (whose solution enables the Helios mission), is so great that they cannot all be solved by the scientists in one experimental group. For this reason, data exchange with other groups who do not have access to the satellite data is very important. Up until now, data exchange has been carried out by direct contact between the groups involved. Recipients of such data have been Dr. Moussas and Dr. Geranios, both from Athens, Greece, and Dr. Mckenna-Lawlor from Maynooth, Ireland.

Finally, the transfer of data into the World Data Center A for satellites and rocket data (WDC-A is identical to NSSDC) begun at the Goddard Space Flight Center in Greenbelt, USA. 8-second average value bands from E4 were sent to the NSSDC. The E2 data

transfer is in preparation.

6. Scientific Evaluation

6.1 General Information

Since the routine data processing has been running satisfactorily for several years, work has increasingly shifted from routine data processing to scientific evaluation during the course of the project, which serves as the actual mission objective. According to the time spent by Helios staff, it is now about 80% finished. Because of the continually arriving interesting new data from the solar activity maximum, an adequate conclusion is only useful after a few years when there is an abundance of material. The staff required for the data analysis was essentially paid for by funds from the BMFT and the state of Lower Saxony, which is also shown in figure 1. Dr. Behannon from NASA-GSFC, winner of the Alexander von Humbolt Foundation, worked on the Helios data for one year [Behannon et al. 1981; Behannon and Neubauer, 1981]. Finally, accompanying theoretical work was partially carried out by the DFG [Riesebieter and Neubauer, 1978; Reisebieter and Neubauer, 1979].

In the scientific topics of the evaluation, questions about "kinetic structure of disturbances in the solar wind," waves, and discontinuities were dealt with first. Thus, sections 6.4, 6.5, 6.6, and 6.7 have already been examined to a certain depth, where as sections 6.3 and 6.8 have just begun to be investigated. 6.2 is in between. Because of the abundance of material already published, only a brief, condensed insight into the scientific results of E2 and E4 on board Helios can be given below.

For a better understanding, we also point out that the magnetic field units are given in nanotesla (nT) in the SI system and γ

in the electromagnetic CGS system; both correspond to 10^{-5} Gauss.

6.2 Macrostructure of the Interplanetary Magnetic Field

The solar wind plasma held within the interplanetary magnetic field (IMF), shows measurable variations are detected at all time scales, which are due to a large number of extremely complex plasma processes. Fluctuations occur starting with the 11-year period of quasiperiodic solar spot cycles or even with slower variations; the fluctuations that occur go to very high frequencies. From the Helios search coil magnetometer, waves up to approximately 1000 Hz were observed. In this section, we will discuss the macrostructure of the interplanetary magnetic field, i.e. variations with time scales of more than about 12 hours.

Numerous measurements before the Helios mission made mostly at 1 AU had shown that the magnetic field variations in this range of time scales, under quiet conditions, are approximately periodic with the solar rotation period. During a solar rotation period (synodic rotation period is about 27 days), characteristic variations of the magnetic field vector occur due to the slipstream caused by this rotation. The most prominent phenomenon is the sectoral structure of the interplanetary magnetic fields i.e. the periodic occurrence of two or more sectors with alternating polarity during several solar rotations. The number of sectors per rotation of the sun as well as the distinctness of this phenomenon, varies according to the time of the sunspot cycle. In connection, we mention that the Helios mission, starting with Helios 1, began in sun spot cycle 20. The minimum relative number of sunspots at the beginning of cycle 21 occurred in 1976, the maximum of cycle 21 occurred around the turn of the year 1979/1980. The "periodicity" due to the rotation of the sun must also be described as quasi-periodic, since small and large changes occur between sun rotations. In addition to these variations, violent disturbances of the interplanetary medium occur as a result of solar

eruptions with associated shock waves, which lead to long-term changes in the electrical and sector structure. These events are mainly dealt with in section 6.3.

According to the ideas developed in the last three decades, the sun's magnetic field, drawn from the upper layers of the solar atmosphere, is the reason for the high conductivity of the solar wind plasma; the solar wind generally comes from open field lines. The most prominent areas of open field lines on the sun are the so called coronal holes, which were under intensive surveillance especially during the Skylab mission. From all these ideas, it follows that the interplanetary magnetic field is a complicated function of the distance, r , from the sun, the heliographic longitude, λ , the latitude, β , and, the time. The latitude range detected by Helios is $-7^{\circ} 15'$ and $+7^{\circ} 15'$ and is given by the inclination of the solar equator about the ecliptic, which is simultaneous with the orbital plane of Helios. This complicated dependence is sometimes moderated by the quasi-periodicity with solar rotation.

As early as 1958, the simplest model of the interplanetary magnetic field was developed by Parker, which starts with spherical symmetry or axial symmetry. A decrease in the radial component, B_r , of the interplanetary magnetic field, with r^{-2} , and the transverse components, with r^{-1} , at a constant solar wind speed is a function of the distance, r . We also note that these principles are theoretically valid under much more general conditions, if we limit ourselves to the dependencies along a given field line. The first simple step in testing the legitimacy of these principles was done with the help of the magnetic field data obtained during part of the primary mission of Helios 1 i.e. From 12/10/74 to the 1st perihelion on 03/15/1975. For an approach of the $r^{-\alpha}$ type, the corresponding regression analysis for the solar equatorial components

$B_{XEQ} = -B_r$, $B_{YEQ} = -B_\phi$, $B_{ZEQ} = -B_\theta$ was performed using daily mean values.

$$|B_{XEQ}| = 2.55 \text{ nT} \times r^{-2.0} \quad (8a)$$

$$|B_{YEQ}| = 2.26 \text{ nT} \times r^{-1.0} \quad (8b)$$

And for the magnitude, $F = |B|$

$$F = 5.33 \text{ nT} \times r^{-1.6} \quad (8c)$$

The distance, r , is measured in AU. As an example, figure 5 shows the results for $|B_{XEQ}|$ according to Musmann, Neubauer and Lammers [1977], compared with other observations. The accordance between 8a, 8b and the theoretical dependencies is excellent but may be somewhat misleading because of the dependence of the magnetic fields of λ and eventually β .

The next logical step is the investigation of the dependence of the interplanetary magnetic field on longitude, λ , and latitude, β , in addition to r . Because of the clear signature in the measured data and the source freedom of the magnetic field, the examination of sector structure is particularly suitable as a first step in this direction. Figure 6 shows the course of Helios 1, which had a synodic period of 27 days in a rotating coordinate system with polarities for half days, or, whole days when closer to the sun during the primary mission (Neubauer, 1978). The polarity is positive for an outward field and negative for an inward directed field. Polarity changes lasting at least three hours are marked by black triangles. This results in somewhat disturbed two-sector structures, or four-sector structures in which two sectors are only weakly developed. The polarity changes that took place on January 8 are associated with a shock wave stream and do correspond to the usual image of the sector structure. In contrast to data taken at 1 AU, the Archimedean spiral structure of the magnetic field can be shown directly from the measured data from Helios

(previously also by Mariner 10), and is indicated by the dashed line.

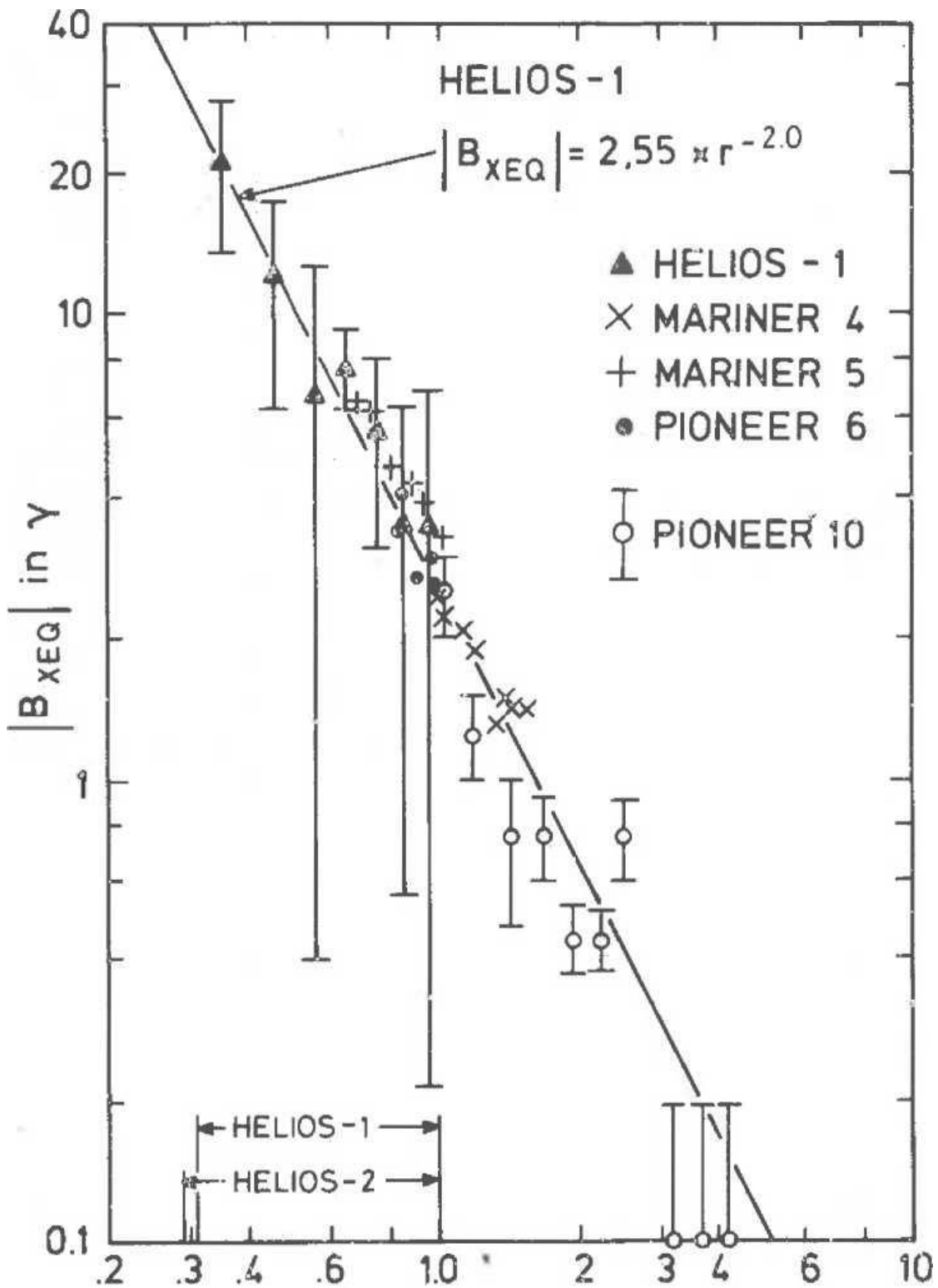


Figure 5:

Mean value, $|B_{XEQ}|$, after measurements of Helios 1 in comparison with other missions. The result of the regression is also shown.

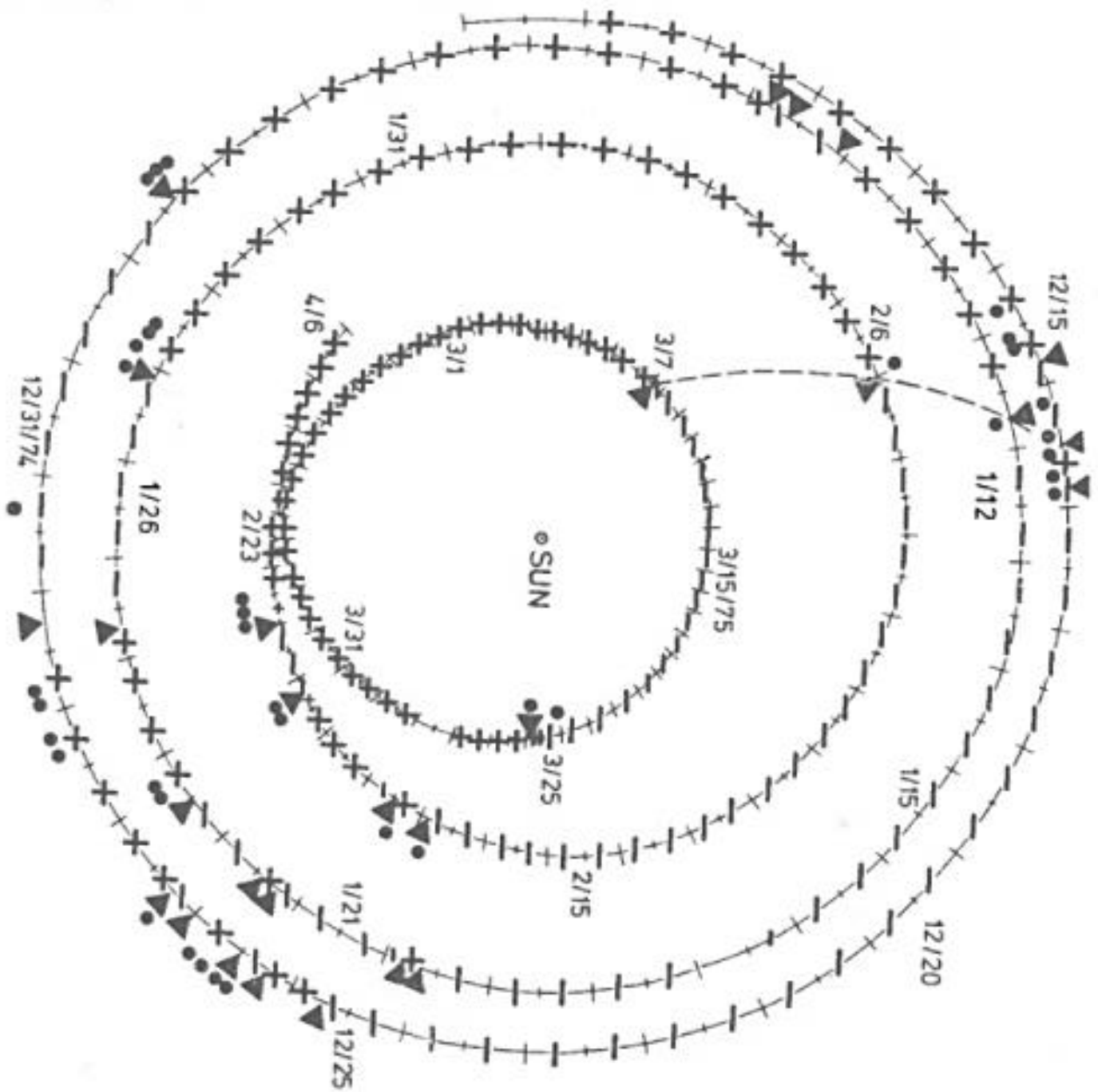


Figure 6:

Sector structure during Helios 1's primary mission in the solar rotating system.

Since the entire latitudinal range is traversed within the measurement interval, the possibility exists that the dependency of r and λ is corrupted by the dependence on β (the heliographic latitude) in this representation. Since sector boundaries, from a three dimensional perspective, must be derived from surfaces that have negative and positive polarities, the question of the orientation of these surfaces at the observation position of Helios arises. If the planes are meridional, the dependency on latitude does not matter. This leads us to the general question of the orientation of these current sheets, which represent the sector boundaries in three dimensions. On the other hand, Rosenberg et al. [1974] concluded from the strong dependence on the latitude of relative frequency of the polarities at 1 AU on a current sheet, that it is practically around the solar equator and is only slightly corrugated. The use of statistical effects goes by the name "Dominant Polarity Effect". This image was from Smith et al. [1978] by means of data confirmed by pioneer 11 slightly outside 4 AU. The model developed by Svalgaard and Wilcox and derived from sun observations, countered the "ballerina model" with a very steep current sheet. This view was somewhat modified later [Svalgaard et al., 1974].

Our study of the sector boundaries began with the attempt to use Helios-1 data to triangulate the current sheets. Here, successive observations of a sector boundary are used at intervals of one solar rotation. For sector transitions that occurred on the 17-19th of February, 1975, and on the 25th of March, 1975, there was a tilt between 29° and 65° from the solar equator, which leaves both possibilities open [Neubauer, 1978]. In a very detailed study, Behannon used the E2 data obtained from the primary mission of Helios-1 to study each sector boundary in detail. [Behannon and Neubauer, 1981; Behannon et al., 1981]. The sector boundaries are usually not characterized by a simple directional discontinuity, but in a complicated

manner with several partial discontinuities.

The discontinuous changes are made by well defined tangential discontinuities. Figure 3 shows an example of a complicated sector transition that occurred on December 26, 1974. In addition to a large number of other results, it was revealed with the help of analysis of wake turbulence. In the minimum variance model, the inclination of the individual discontinuities is substantially steeper than that of the ballerina model. Although the current sheet contains local ripples and grooves, this does not necessarily contradict the ballerina model. In a study concerning the "Dominant Polarity Effect" using E2 magnetic field data for the period of October 12, 1975 - 1980 (which is as of yet still unpublished), a current layer with a small latitudinal extension was observed, which must also be provided with many grooves and ripples, according to the results described above.

Similar studies were carried out for the Helios 2 primary mission in early 1976 from the E3 magnetometer group on Helios.

A different strategy for investigating the physics of the solar wind and its embedded magnetic field consists of the development of a three dimensional magneto-hydrodynamic model, and the comparison of the predictions of this model with in-situ plasma and magnetic field observations made by Helios [Riesebieter, 1977]. In a further study, comparisons were made with Faraday rotation observations made on Helios [Riesebieter and Neubauer, 1978]. The theoretical model devised by Dr. Howard from the Mt. Wilson Observatory began with magnetic field observations along the line of sight. These observations were extrapolated using potential theory methods for a source area of up to 2.5 solar radii. For this purpose, an algorithm was developed [Riesebieter and Neubauer, 1979], which is more efficient than that developed by Altschuler et al. [1977] and Adams and Pneuman [1976]. The magnetic field was assumed to be radial from the source area up

to 30 solar radii. The MHD equations were solved along the magnetic field lines, and plausible plasma parameters of 1.1 solar radii were assumed. The MHD equations were solved with all three components from 30 solar radii and outward. The model begins with the most realistic and plausible treatment among currently known models of the three dimensional current problem in a given photospheric magnetic field. The comparison between the model calculations and the observations from Helios 1 during its primary mission revealed a strong agreement with regard to the relative variations. The high measured solar wind speed could not be reproduced, as in previous models. The predicted magnetic fields turned out to be far too small. From the strong agreement between the Faraday rotation measurements and the reliability of the in situ measurements, it is possible to ascertain that the potential model is not correct in the vicinity of the sun and/or that the photospheric magnetic field measurements do not correspond to the true values. This discrepancy also occurred with simpler models based on a current-free spherical shell between the photosphere and the source surface. With these model calculations the discrepancy between observations and theoretical predictions could be reduced but not eliminated. As the above statements show, the E2 data combined with the E1 plasma data, could be used to obtain new substantial results. However in this domain, the data analysis is only just beginning. More precise investigations of the magnetic field in high speed streams are necessary. Furthermore, the study of the sector structure from periods of high and low solar activity needs to be continued. The possibility of gaining ascertations closer than the perihelion distance should also be pursued.

6.3 Disturbances of the Interplanetary Medium by Shock Waves

The most spectacular disturbances of the interplanetary medium are caused by shock waves. These are spatially spreading discontinuities in the plasma and correspond to the thermodynamic state variables: density, pressure, temperature, the velocity vector, and the magnetic field. They arise when the solar wind strikes an obstacle (like a planet), or after a solar eruption occurs; compression waves at high amplitudes are divided, and fast and slow solar winds interact.

With the aid of the two space probes Helios 1 and 2, it is possible to conduct shock wave observations near the sun (from 0.3 AU). Because of the temporarily small angular distance between the satellites, the same shock wave can often be observed from both satellites. By using the observation data of other satellites, e.g. the IMP satellite in Earth's vicinity, as well as the Pioneer and Voyager space probes investigating the outer solar system, shock waves can be traced over a large range in the radial direction.

The occurrence of shock waves is closely correlated with general solar activity; they are observed more frequently at times of great solar activity.

Table 1 shows the frequencies of shock wave observations for Helios 1 and 2 per quarter-year up to 1979.

Table 1

The current evaluation status of the shock wave frequency observations

	1975				1976				1977				1978				1979			
Helios 1	2	0	0	1	0	0	1	1	5	3	5	2	5	11	3	10	4	5	?	?
Helios 2	-	-	-	-	2	1	0	0	5	2	1	7	8	11	3	5	13	8	1	2

The time limit corresponds to the current evaluation status. In these time periods Helios-1 observed 58 shock waves and Helios-2 observed 69 shock waves; in nineteen cases, the same shock wave was measured by both satellites. Table 1 shows an increase in the shock wave frequency as time increases. This corresponds to the increased solar activity, the maximum is assumed to be around the end of 1979 or beginning of 1980.

In Table 2, the observed shock waves are ordered by frequency according to the distance from the sun in AU, which the relevant satellite recorded during the observation.

This frequency distribution, viewed from statistical fluctuations, essentially represents the variation in their duration with different distance intervals. It also gives an overview of the existing observation material. Individual shock wave events will now be discussed in the following sections.

Table 2

Shock wave frequency at different distance intervals (in AU).

	0.3-0.4	.4-.5	.5-.6	.6-.7	.7-.8	.8-.9	.9-1.
Helios 1	10	5	6	7	4	10	16
Helios 2	13	10	2	13	5	5	21
Sums	23	15	8	20	9	15	37

For the first time, the Helios mission offers the opportunity to systematically examine shock waves near the sun. Fig. 7 shows as an example the observation of a shock wave made by Helios 2 at a distance of 0.298 AU.

The proton density, N_p , proton temperature, T_p , proton velocity v , the velocity angle of elevation, Θ_v , the kinetic energy current density, j_{EK} , and the magnetic field with its direction expressed by the azimuth angle, ϕ_B , in the ecliptic ($\phi_B = 0^\circ$ corresponds to the Sun), the elevation angle, Θ_B , ($\Theta_B > 0$ for vectors above the ecliptic) and the magnetic field magnitude, B , are listed from bottom to top. The plasma parameters N_p , T_p , and v , were measured by experiment E1 at the Max Planck Institute in Garching and Lindau. A rise in the parameters N_p , T_p , j_{EK} , v , and B at 20:22 UT on April 20, 1977 showed the arrival of a fast magneto-acoustic shock wave on the spacecraft. Table 3 shows their properties.

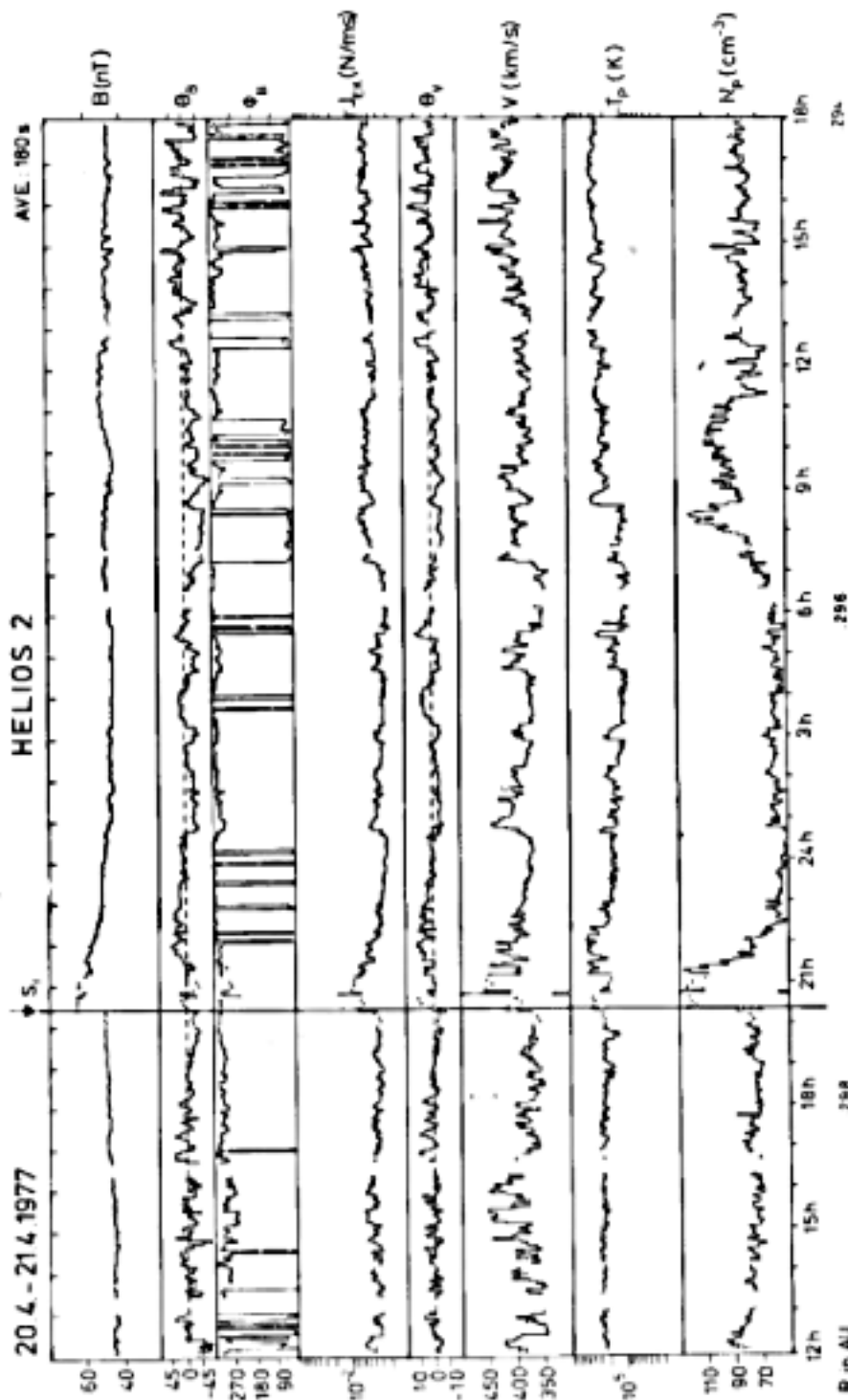


Figure 7:

Shock wave from April 20, 1997; (represented by S_f) an explanation of the parameters is given in the text.

With the aid of observational data, the normal of the shock front to $\phi_N = 215^\circ$, $\theta_N = +45^\circ$, as well as a shock wave velocity, V_s , of 382 km/s in the normal direction, was determined by known methods [Lepping et al., 1971; Amraham-Shrauner et al., 1976].

Table 3

Properties of the shock wave from April 20, 1977, 20:22 UT (1 = state before, 2 = state after the shock wave).

	B (nT)	V (km/s)	N_p (cm^{-3})	T_p (K)	V_s (km/s)	Normals	
						ϕ_n	θ_n
1	48.3	393	69.6	235200	382	215 ^o	+45 ^o
2	74.6	418	125.4	401400			

Under the assumption that the normal to the shock front had not changed during propagation, a mean travel time from the sun to the observer of 18.8 hours was calculated. This is in agreement with a flare, which took place on April 10th, observed at 1:13 UT, at S20 and W22 on the sun and can be regarded as the cause of the shock.

The course of the stream behind the shock front is characterized by an approximately two-hour compression region, followed by a pronounced rarefaction region. After twelve hours, the disturbance in the interplanetary medium from the shock wave ended; density and temperature once again assumed values which correspond to those before the shock front occurred. The temporal sequence of the shock wave event is similar to that predicted by theoretical calculations for the propagation of shock waves (Hundhausen and Gentry, 1969).

Typical for shock waves near the sun, is a brief magnetic field compression, which in this case only took two hours.

In Figure 8, the frequency of directional discontinuities of the magnetic field is also indicated for the same shock wave (upper part of image). In order to ensure statistical reliability, directional discontinuities with a spreading angle, $\omega > 20^\circ$ have also been recorded.

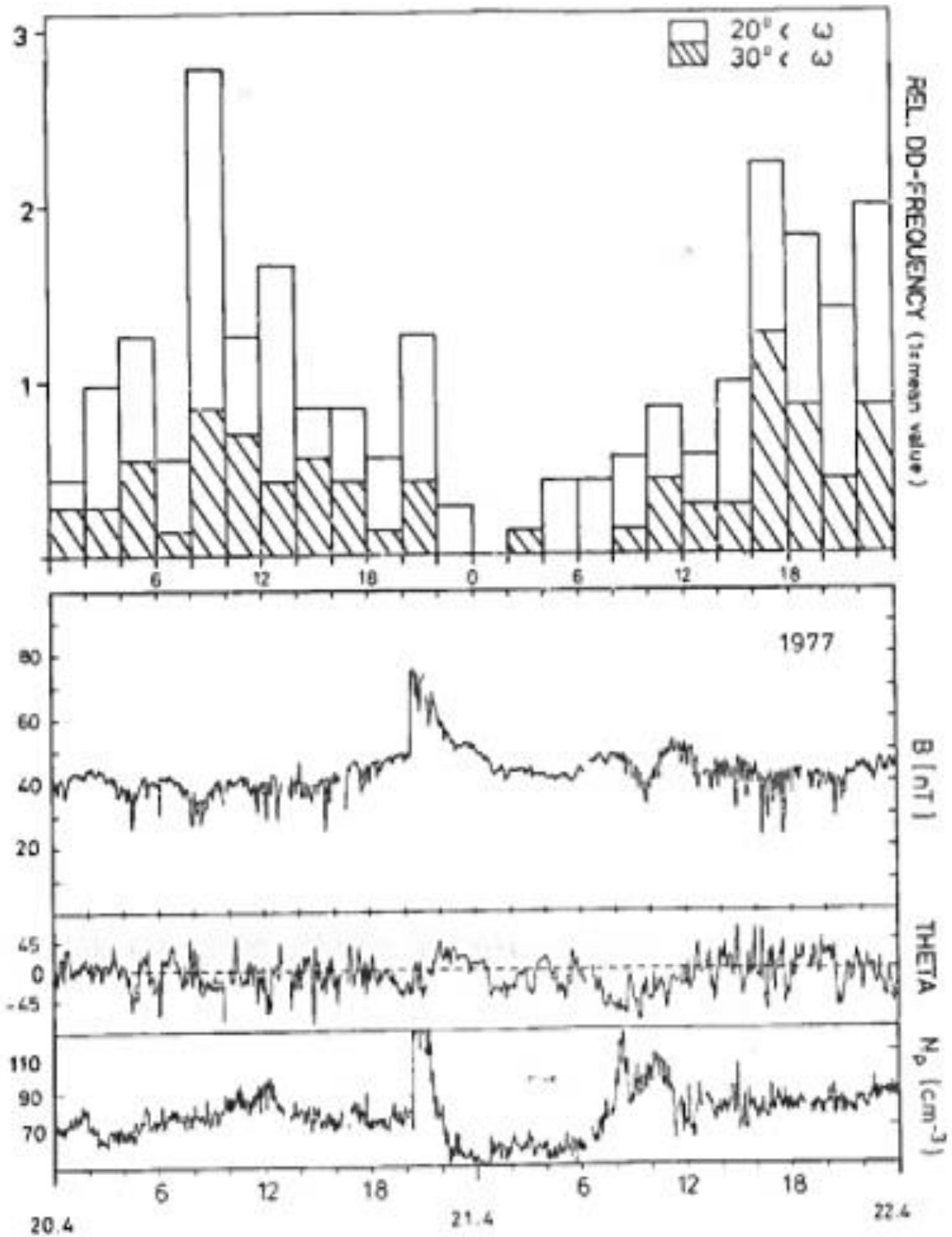


Fig.8:

Frequency distribution of directional discontinuities with $\omega > 20^\circ$ and $\omega > 30^\circ$, normalized to the mean value of the observed shock wave on April 20th, 1977.

A decrease in the frequency in the rarefaction region and the increase in the compression region is clearly seen. This behavior is also often observed in other shockwave events and can be explained, as follows: directional discontinuities do not propagate (tangential discontinuities), or propagate very little (rotational discontinuities), against the solar wind. During the passage through the shock wave, the spatial distance between successive discontinuities is reduced, and together with the increased plasma speed, leads to a higher frequency of condensed plasma after the shock wave. The following minimum of the frequency of directional discontinuities can be explained by the fact that the plasma, originally filled with the same number density of discontinuities, has greatly expanded. Another possibility is that the normal is in an unfavorable location (almost orthogonal to the current velocity) that the discontinuities are too difficult to observe.

A favorable constellation of the satellites Helios 2, IMP7, IMP8 (earth satellites), Voyager 1, and Voyager 2 at the end of 1977 between 0.6 AU and 1.6 AU made it possible to follow the radial propagation of disturbances from the sun over a large distance range [Burlaga et al., 1980]. In addition to the shockwaves produced by flares, there was a special interest in a co-rotating high-velocity current. Corresponding data were examined in a workshop between the Helios and Voyager experimenters. In the lower part of Figure 9, the spatial arrangement of the satellites with their relative time intervals is shown.

Furthermore, observations of the magnitude of the high-speed stream by Helios 1, Helios 2, IMP 7, IMP8, Voyager 1, Voyager 2, in the form shown, center around the time of arrival of the "stream interfaces" (marked by the vertical line).

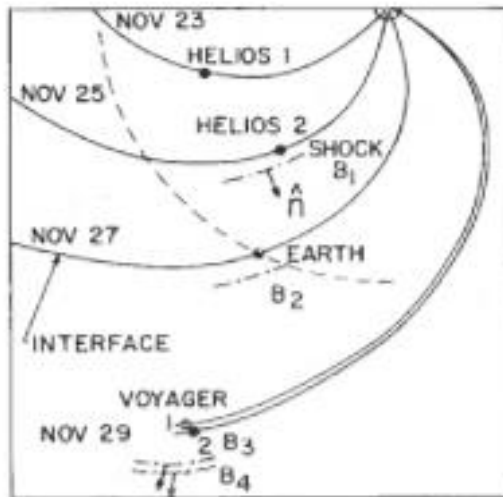
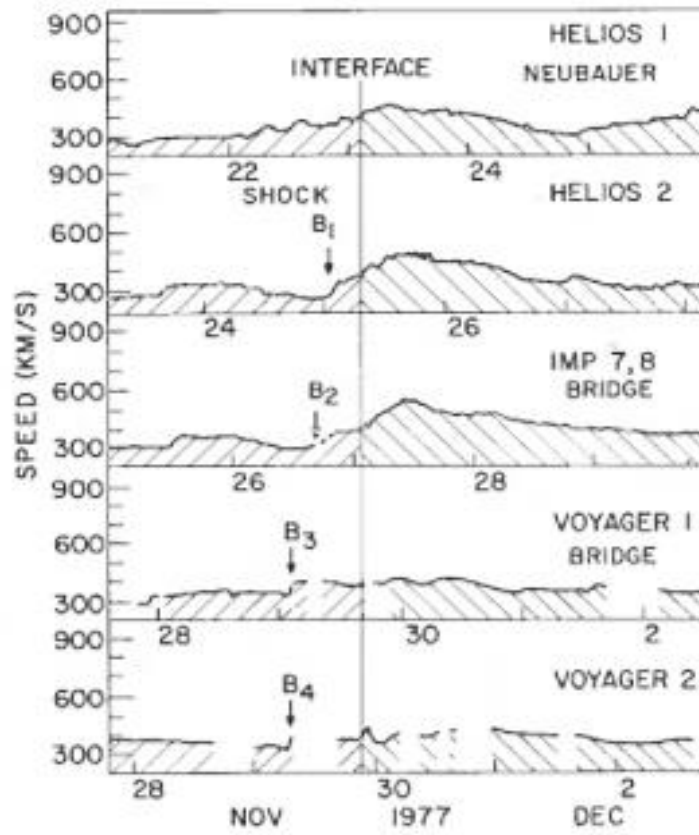


Figure 9:

Velocity profile (centered about the "stream interface") for Helios 1, 2, IMP 7, 8, Voyager 1, 2, and their position relative to each other

The "stream interface," is understood to mean the abrupt simultaneous drop in density and rise in temperature before the rise in velocity of a "stream" [Belcher et al., 1971, Burlaga, 1974, 1975]. The 2-day time interval for the successive observations of "stream interfaces" for the mentioned satellites corresponds to the expectations for a co-rotating "high speed stream" with $v = 400$ km/s. In fact, a coronal hole has also been identified as a source of this stream.

This dynamic development of these stream interfaces is of importance (Figures 9 and 10). Helios 1 and 2 observed similar profiles of velocity, proton density, and proton temperature as a function of time. The observations of IMP 7 and 8 also fit into the picture of the co-rotating stream. On the other hand, the Voyager 1 and 2 data seem to be missing, or at least, much slower, although these space probes also observed the "stream interface". An explanation for this is that during the development of the stream, two compression waves formed, which moved with respect to the stream interfaces, both to and away from the sun. At the same time, the wave moving toward the sun was slowed and weakened, while the other compression wave developed into a shock wave (Shock $B_1 - B_4$ in Figs. 9 and 10)

The shock wave observations from Helios 2, IMP 8, Voyager 1, and Voyager 2 yielded shock wave normals consistent with a co-rotating shock wave driven by the following "high speed stream". Surprisingly, the shock wave was already observed at 0.6 AU (Helios 2), i.e. within 1 AU, which is very rare. The fact that Helios 1 did not observe a shock wave before the "high speed stream" shows that it was co-rotating and not stationary. This co-rotation may result from a time-dependent stream profile of the coronal hole which was the source of the stream.

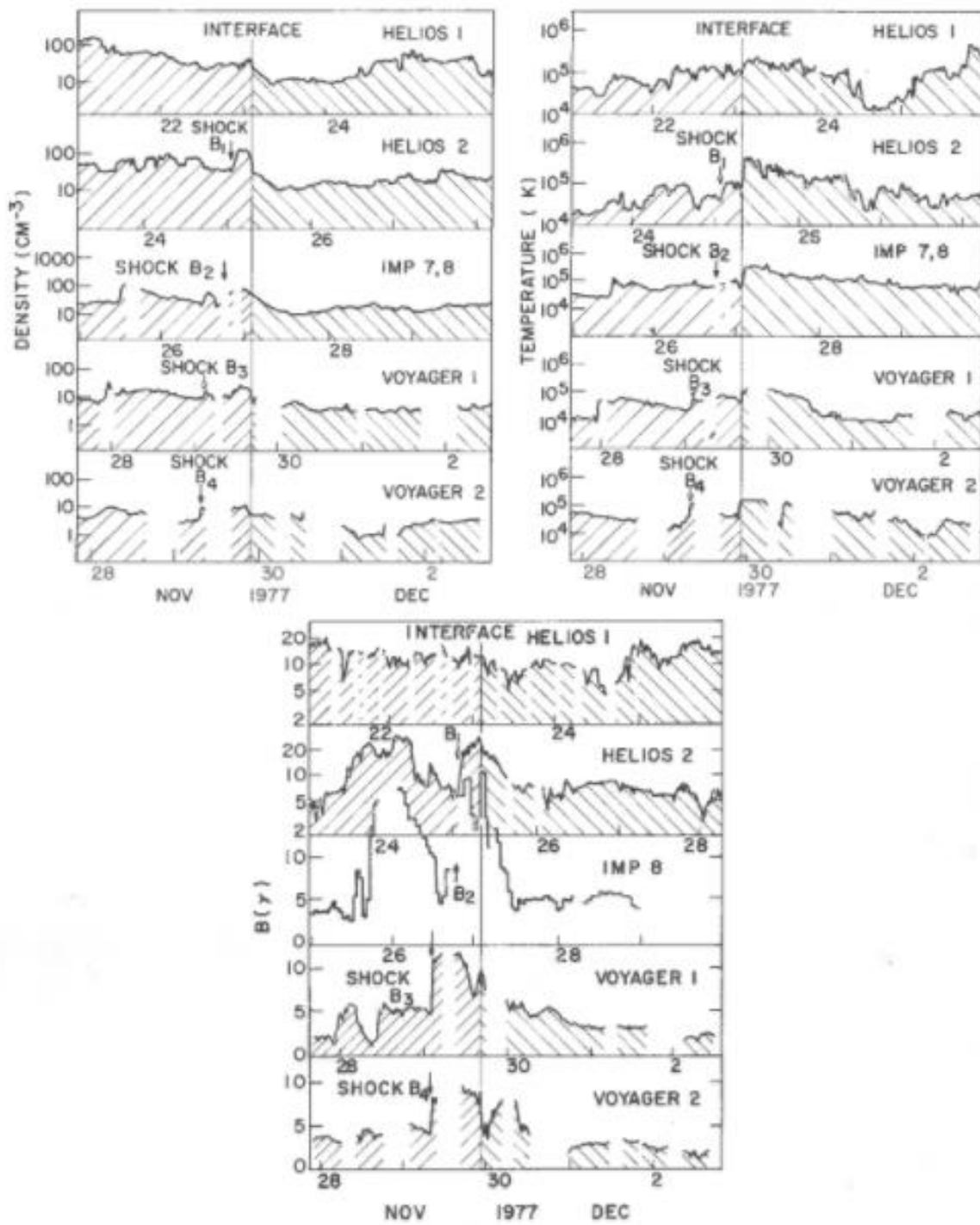


Figure 10:

Density, temperature, and magnetic field paths of high speed streams centered about the "stream interface"

In fact, there are small differences in the velocity profile as well as in the other data for Helios 1 and 2, as shown in Fig. 9. These differences in the plasma parameters for Helios 1 and 2 could be the reason for the fact that the plasma environment around Helios 1 did not fulfill the conditions that are associated with the formation of a shock wave.

The statistical results and case studies presented above illustrate the value of the Helios data for the investigation of shock waves in a previously inaccessible region of space. In the future, propagation properties of most of the observed shock waves and the associated magneto-hydrodynamic currents will be investigated more closely, by increasing the use of solar observations in order to define initial conditions for the observed disturbances.

6.4 MHD Waves

The average spiral configuration of the interplanetary magnetic field is superimposed with constant fluctuations. These fluctuations have periods from fractions of milliseconds up to several days. The magneto-hydrodynamic span extends from the proton-gyroperiod to longer periods. In general the observed fluctuations are complex and result from various physical processes. A share of which are Alfvénic fluctuations, which according to previous in situ observations with Mariner 5 (for example), were present during more than one third of the observation period. Alfvénic fluctuations are characterized by a high correlation between fluctuations of the plasma velocity and the magnetic field. They are important for several reasons: they scatter cosmic radiation, and influence heat flow and geomagnetic activity. They may also contain information about the fundamental acceleration mechanism of the solar wind. They

are the best example of directly measured astrophysical plasma turbulence.

Due to the correlation mentioned above, plasma and magnetic field data are necessary for investigating Alfvénic fluctuations. These possibilities are provided by both Helios spacecraft in a convenient way. For the investigation, "merge tapes" were used; which simultaneously contained 40.5 s-mean values from the magnetic field (experiment 2) and plasma parameters (experiment 1). There were fundamental studies on their propagation from 0.29 AU to 1.0 AU. Since for this investigation a complete, high resolution data overlap is required, the evaluation is limited to measurements taken during the primary missions of both satellites. The results so far can therefore only be regarded as representative for solar minimum conditions.

For the global investigation of the occurrence of Alfvénic fluctuations, we calculate the correlation between magnetic field fluctuations, δb , and solar wind velocity fluctuations, δv , (Denskat et al. 1981a). If a correlation has a correlation coefficient greater than 0.6, it was found that during the solar rotation at aphelion for Helios 2 (Figure 11), Alfvénic fluctuations are present during 75% of the observational period. These are not arbitrarily distributed, but are essentially limited to the central parts and decaying edges of high-speed streams. As the normalized standard deviations of the magnetic field components, the magnetic field magnitude, and the density show, there is also wave activity in slower solar wind and in the rising edges of high speed streams. There are indications that the latter is generated, at least in part, locally from the impingement of fast on slow plasma. These fluctuations as well as those in the slow solar wind show few Alfvénic characteristics. It is possible that Alfvénic wave activity also occurs in slow solar wind plasma [Marsch et al., 1981a].

HELIOS-2

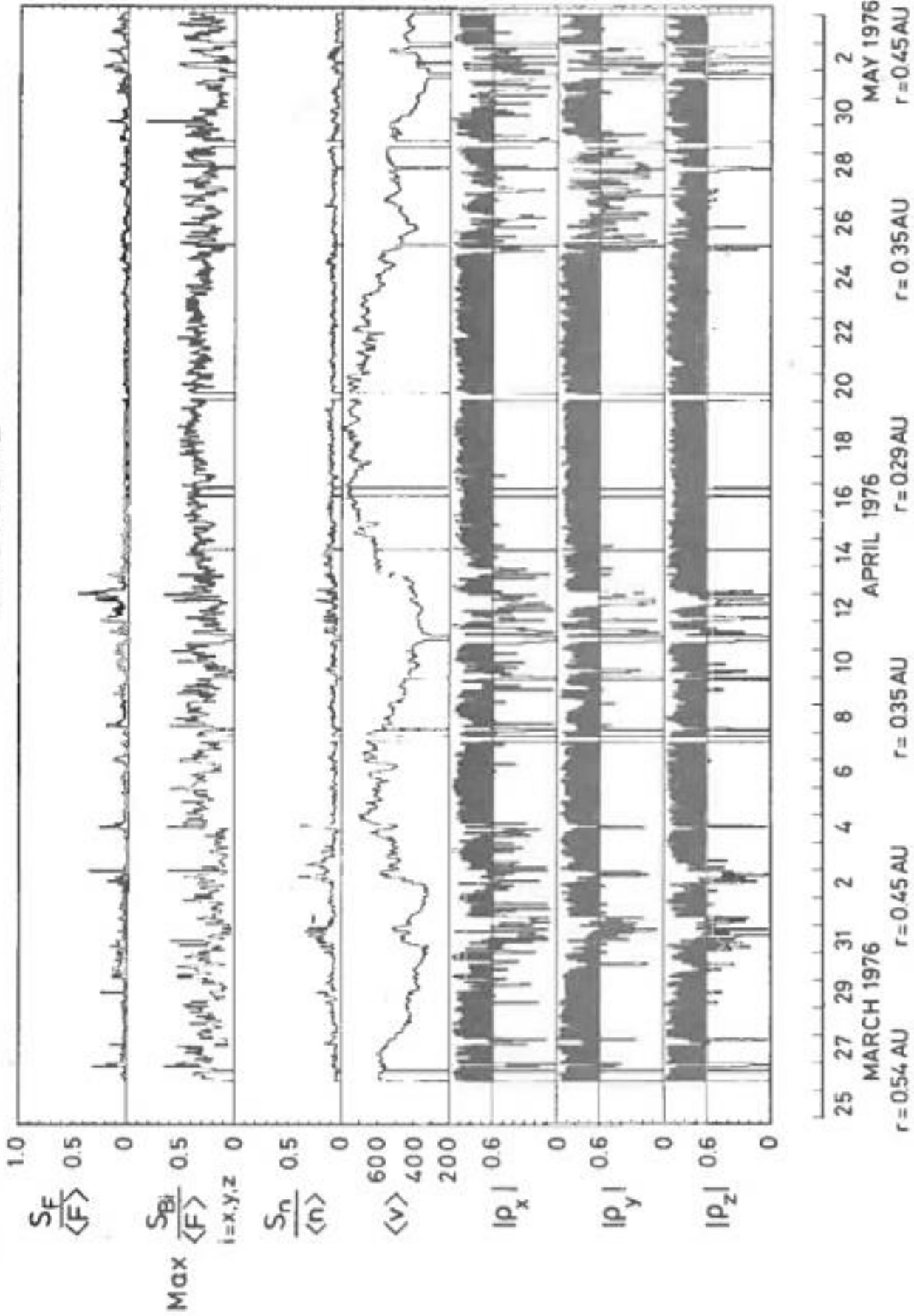


Figure 11: General characteristics of the measured MHD-fluctuations in connection with the velocity profile at solar distances between 0.98 AU and 0.91 AU for Helios 2. The seven boxes contain (from bottom to top) for each calculation for one hour, the normal standard deviation of the magnetic field magnitudes, magnetic field components, density, average solar wind speed, and the absolute value of the correlation coefficients between δv_x and δb_x for the three vector components.

The nature of the correlation, whether in phase or in counter phase, together with the direction of the interplanetary magnetic field, indicates the propagation direction of the Alfvénic fluctuations. For the period shown, all Alfvénic fluctuations in the central parts and decaying edges of high-speed streams propagate outward from the sun. The same behavior is shown during the perihelion phase, where the percentage frequency of Alfvénic fluctuations is about the same. If a generation mechanism is not found in the flowing solar wind up to 0.29 AU, for Alfvénic fluctuations with a propagation direction, it can only be concluded that the Alfvénic fluctuations must have been produced within the Alfvénic critical radius (about 10 to 20 solar radii), since only Alfvénic fluctuations with an inward propagation direction can actually spread to the sun. Alfvénic fluctuations generated further outside, would flow backwards past the spacecraft due to the faster solar wind, and therefore had to be observed.

As shown in Fig. 12, not only is the frequency of occurrence of Alfvénic fluctuations at 0.3 and 1.0 AU approximately the same, the normalized fluctuation amplitudes of the directional fluctuations also remain approximately the same. Slight differences in the frequency distribution for the perihelion and aphelion phases, as well as between Helios 1 and Helios 2, are probably caused by time variations, since the differences are not shown to be systematic. As an explanation for the differences, the dependency on solar latitudes should be considered.

The distributions of the normalized magnetic field magnitude fluctuations, which are shown in Figure 12, indicate a different behavior of the magnetic field magnitude. Both satellite systems show systematic differences for the perihelion and aphelion phases. The distribution of the frequency distribution at aphelion indicates a local generation of compressive wave modes

in the solar wind plasma, which lead to increased magnetic field fluctuations. Furthermore, static structures can contribute to

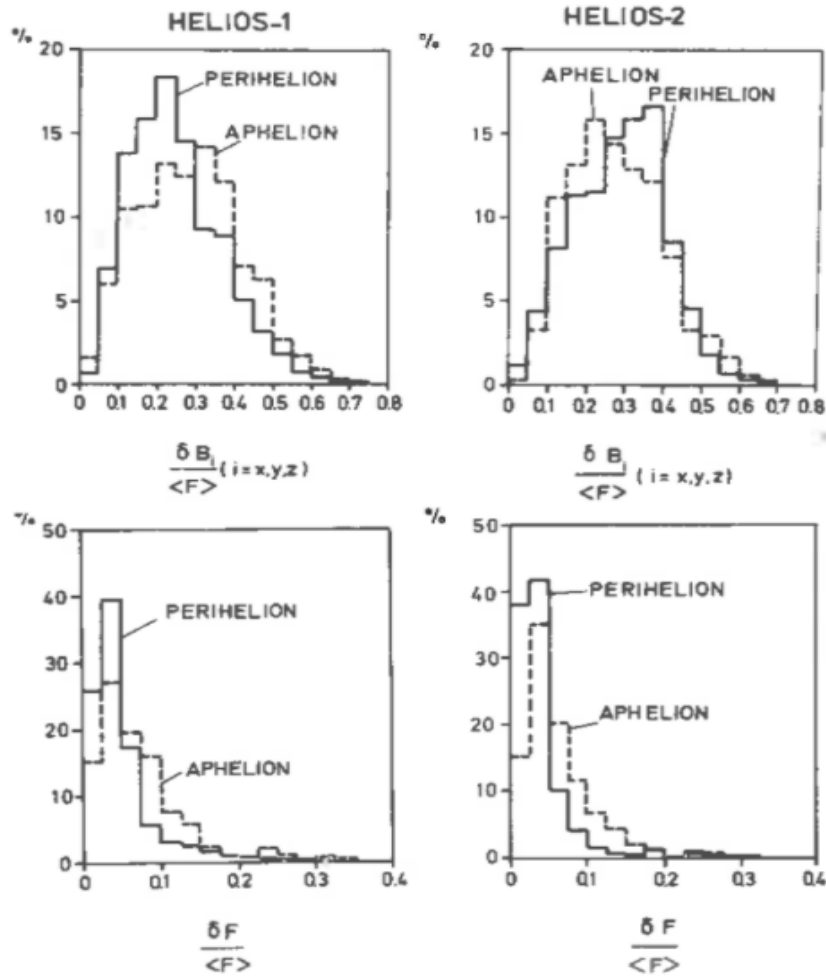


Figure 12:

Distribution of the standard deviation of magnetic field vector components and magnitudes normalized with the average magnetic field magnitudes over one-hour intervals. For both the magnetic field vector components and magnitudes, the largest of the three standard deviations were used for the distribution. For the calculations, time periods of a solar rotation were used. The time interval for aphelion is between a solar distance of 0.90 AU and 0.98 AU; for perihelion, it is between 0.31 AU (Helios 1) or 0.29 AU (Helios 2) and 0.40 AU.

the measured distributions. As little is known about the development of these static structures in the solar wind from 0.29 to 1.0 AU, they may contribute to varying degrees in the observed magnitude fluctuations at perihelion and aphelion.

Particularly in the inner solar system, Alfvénic fluctuations are of interest because they possibly propel the solar wind. Figure 13 shows the radial dependence of the radial Alfvén wave energy flow relative to the radial solar wind energy flow for the primary mission of Helios 1 and Helios 2.

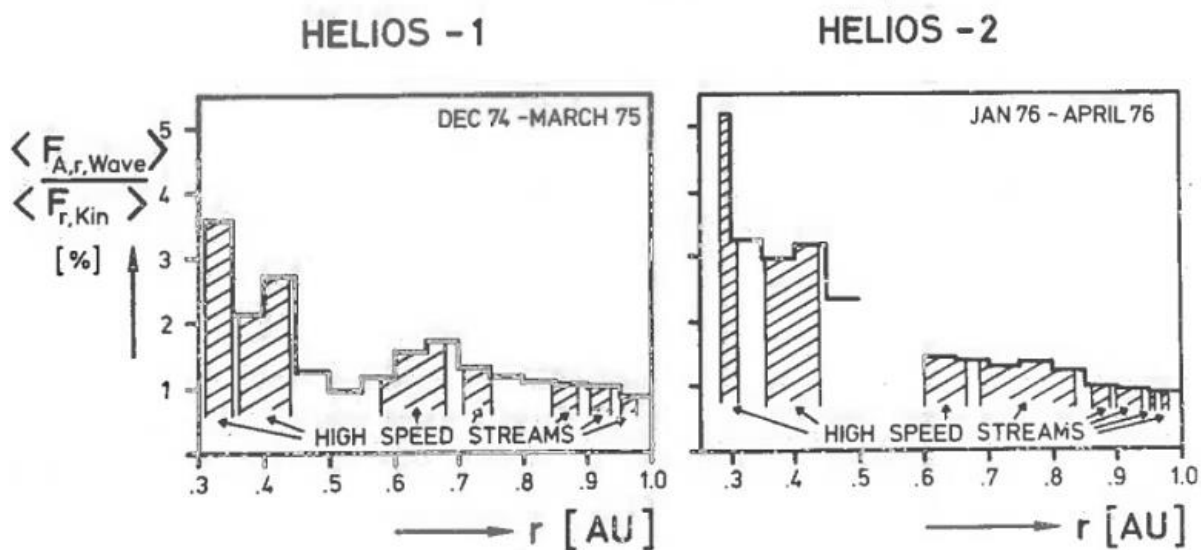


Figure 13:

The dependency on solar distance of the relationship between radial Alfvén wave energy flow and kinetic radial solar wind flow. The Energy flows were at first calculated at one-hour intervals and then averaged over many days.

For this purpose, the observed Alfvénic fluctuations and their Alfvén waves, for which theoretical formulas for the calculation of the energy flow are available, at least at small amplitudes, were used. In general, a higher relative proportion of wave energy flow is present when closer to the sun, up to 5% at

perihelion of Helios 2 at 0.29 AU. The relative share of the Alfvén wave energy flow decreases from the outside in, indicating the waves underwent damping as they propagated in the solar wind plasma. The investigations described have not yet been differentiated with respect to different wavelengths. The contribution of different wavelengths to the total fluctuations and also the different possible characteristics of fluctuations at different wavelengths will be investigated. The investigated wave period is from 80s to 11.5 hours. It is selected in such a way that the influence of ion gyro periods and large-scale solar wind structure is kept as low as possible. In the period mentioned above, the power spectra of the magnetic field components and their magnitudes were computed using the magnetic field data from the primary mission of Helios 1 and 2 (Denskat and Neubauer, 1980). Figure 14 shows spectra obtained at different solar distances. The amplitudes of the spectral densities at greater solar distances are smaller than the background magnetic field which was measured to be 42 nT at 0.29 AU and 6 nT at 0.97 AU. Furthermore, the differential decay of the spectra decreases as the frequency range increases. This is flatter near the sun and becomes steeper farther out. This is a systematic effect, as will be shown below. If we assume that the spectral density $P(f)$ is proportional to $f^{-\alpha}$, we can calculate the spectral exponent α between 0.9 and 1.1 at 0.29 AU, and between 1.5 and 1.7 at 0.97 AU.

Figure 15 shows the distribution of the spectral exponents for the 3 orthogonal components and the magnitude for different distance ranges.

HELIOS-2

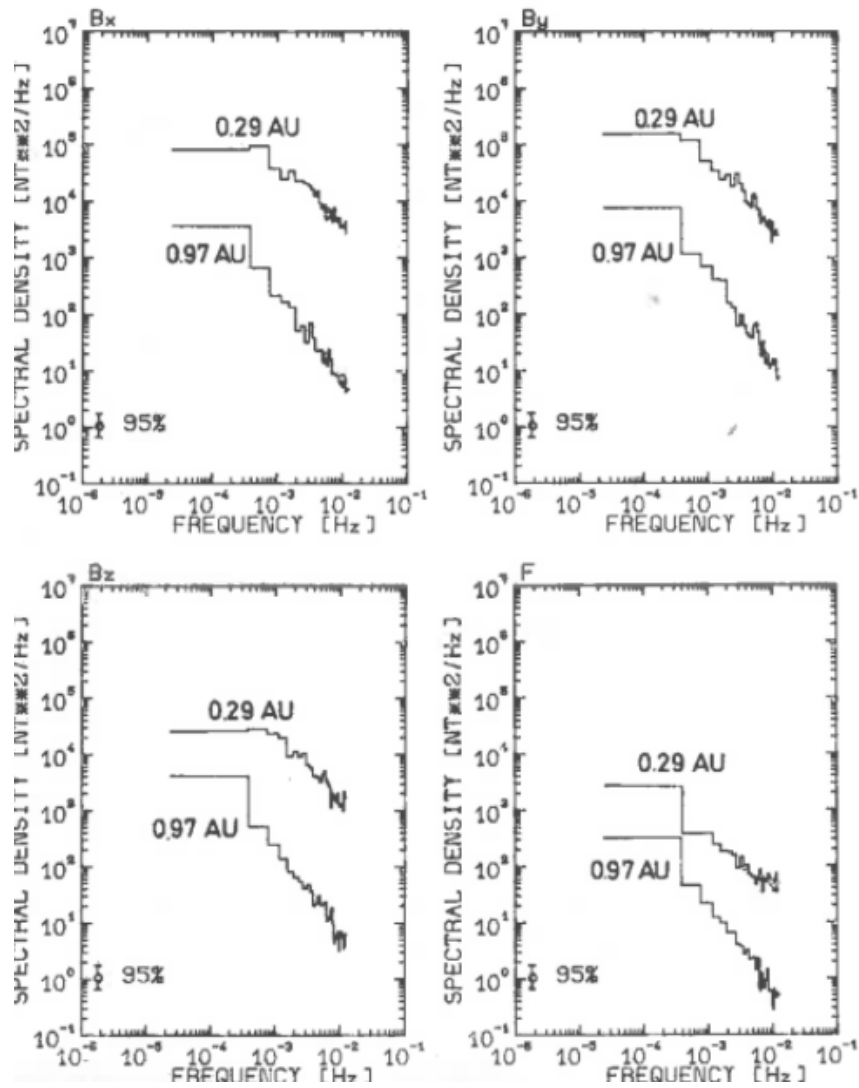


Figure 14:

Spectral densities of the magnetic field (vector components and magnitude) at different solar distances. The spectra come from 40s magnetic field average values.

HELIOS - 2

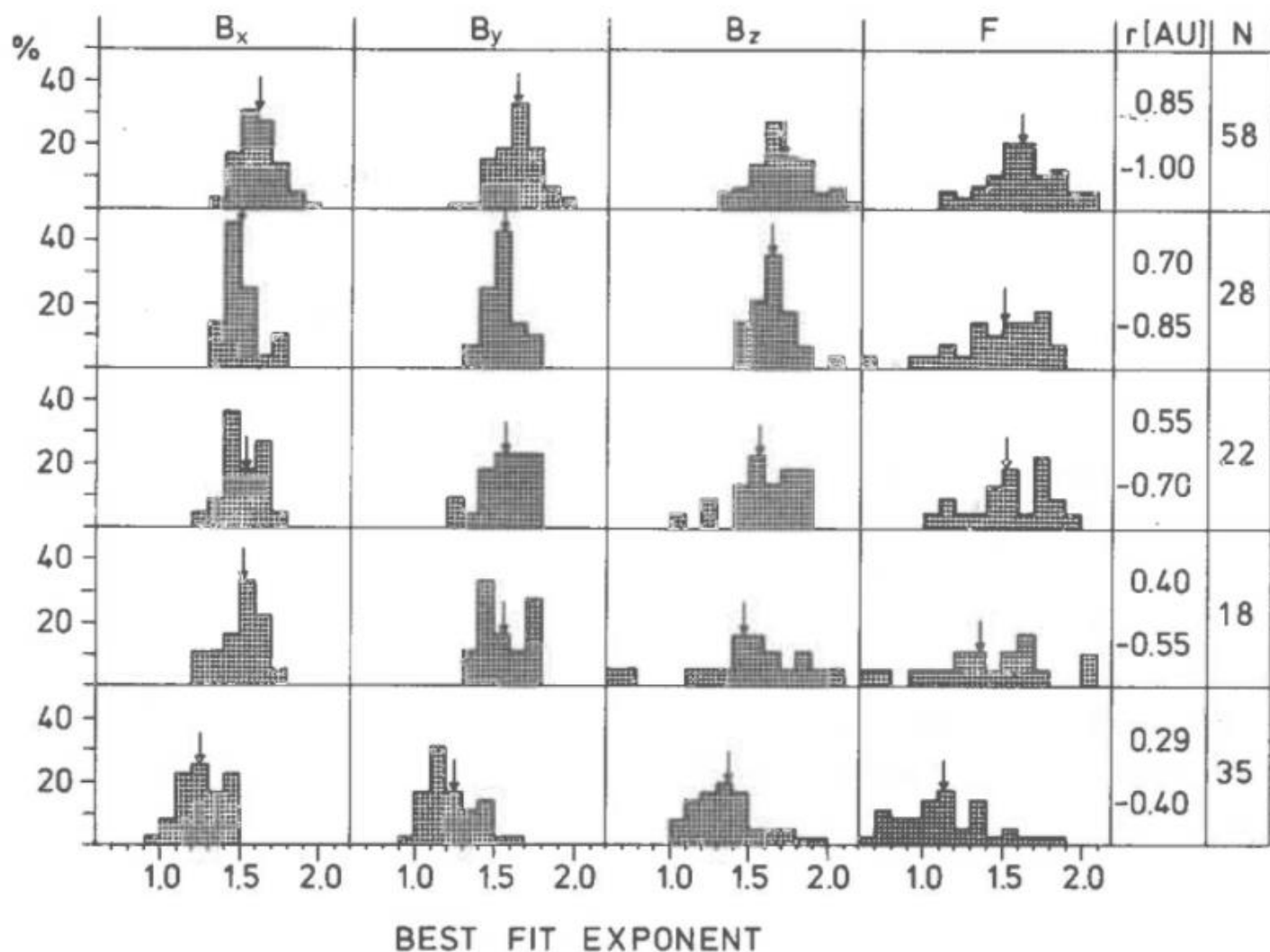


Figure 15:

Distribution of the spectral exponents α ($P \sim f^{-\alpha}$) according to the least (error) squares method for five different distance intervals between 0.29 AU and 1.0 AU for vector components and magnitudes. N gives the number of calculated spectra in each distance interval. Arrows indicate the average value in each distribution.

The change in the distributions shows that the spectra do not continuously get steeper from 0.29 to 1 AU, but that the steepening occurs mainly within 0.40 AU; further outside 0.4 AU,

the changes are small. Helios 1 produced a similar result during the primary mission, although the spectra at 0.3 AU are not quite as flat. It can safely be assumed that there is a steepening of the spectra from 0.29 AU to 1 AU, however, influences due to temporal variations and latitudinal dependence cannot be ruled out. Furthermore, the path of the spectra is dependent on the structure of the solar wind. At all solar distances, the spectra are the steepest in regions of slower solar wind velocities. In the rising edges of high-speed streams there are steeper as well as flatter spectra than in the corresponding center parts and decaying edges of the high-speed streams. The reason for this is probably due to the steepening of the rising edges towards the sun, as observed by the Helios plasma experiment (E1).

The radial dependence of the spectral density is shown in Figure 16 for some frequency channels. Apart from time and stream structure dependent variations, there is a clear difference in the radial dependence between high and low frequency ranges. The latter fall significantly less strongly. There are three possible explanations: 1) the high-frequency ranges are damped more strongly than the low-frequency components 2) low-frequency ranges are generated 3) there is an energy exchange from high-frequency to low-frequency waves.

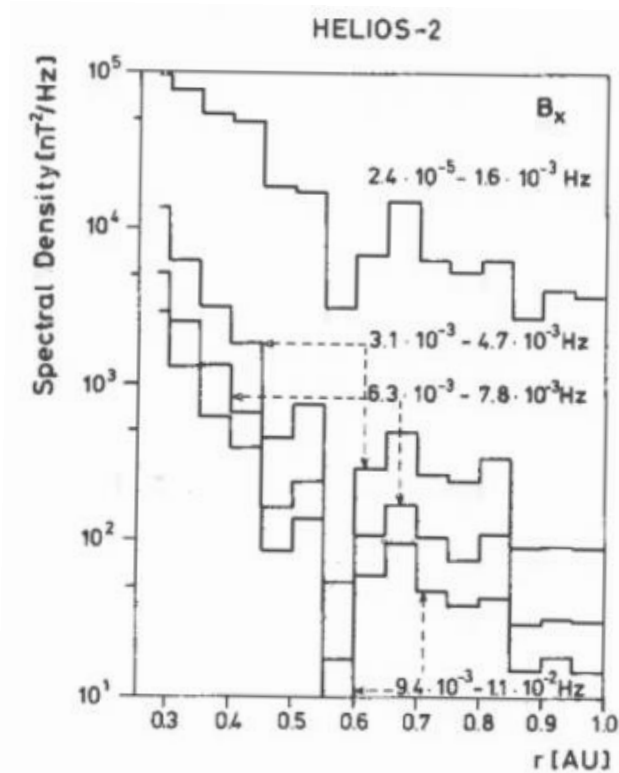


Figure 16:

Spectral densities of the magnetic field components as a function of the distance to the sun. 161 spectra were used for the calculation.

As can be seen in Figure 12, the directional fluctuations have quite large amplitudes (RMS wave amplitudes are typically 0.3-0.4 of the background magnetic field). If they are purely transverse fluctuations, they must be circularly polarized since the magnetic field must remain constant for Alfvénic fluctuations. However, as shown in Figure 17, the fluctuations are parallel and orthogonal to the background magnetic field and are correlated with a phase of 180° . Such correlation is typically observed in the central portion and the decaying edges of high speed streams at solar distances between 0.29 and 1.0 AU. For Alfvénic fluctuations of large amplitudes, the wave magnetic field is spherical. This applies to all observed periods between 80s to 11.5h.

With the Helios magnetic field data, power spectra over a wide frequency range of more than 7 orders of magnitude (from 2×10^{-5} Hz to 470 Hz) were calculated with the data of the magnetic field experiments E2 and E4 [Denskat et al., 1981b]. Figure 18 shows the time of these spectra in transition between fast and slow solar wind. While in the range of compressed plasmas before the high-speed stream, the spectra have strong variation in their individual frequency ranges, and show a very constant course in the central part of the high-speed stream. The fluctuations observed by Helios in this frequency range can be regarded as an interesting example of astrophysical plasma turbulence.

The Alfvén wave studies are to be concluded with the investigation of the propagation between Helios 1 and Helios 2 and of the dependence on the solar activity cycle. Then, the presence of other wave modes should be quantitatively analyzed.

HELIOS-2

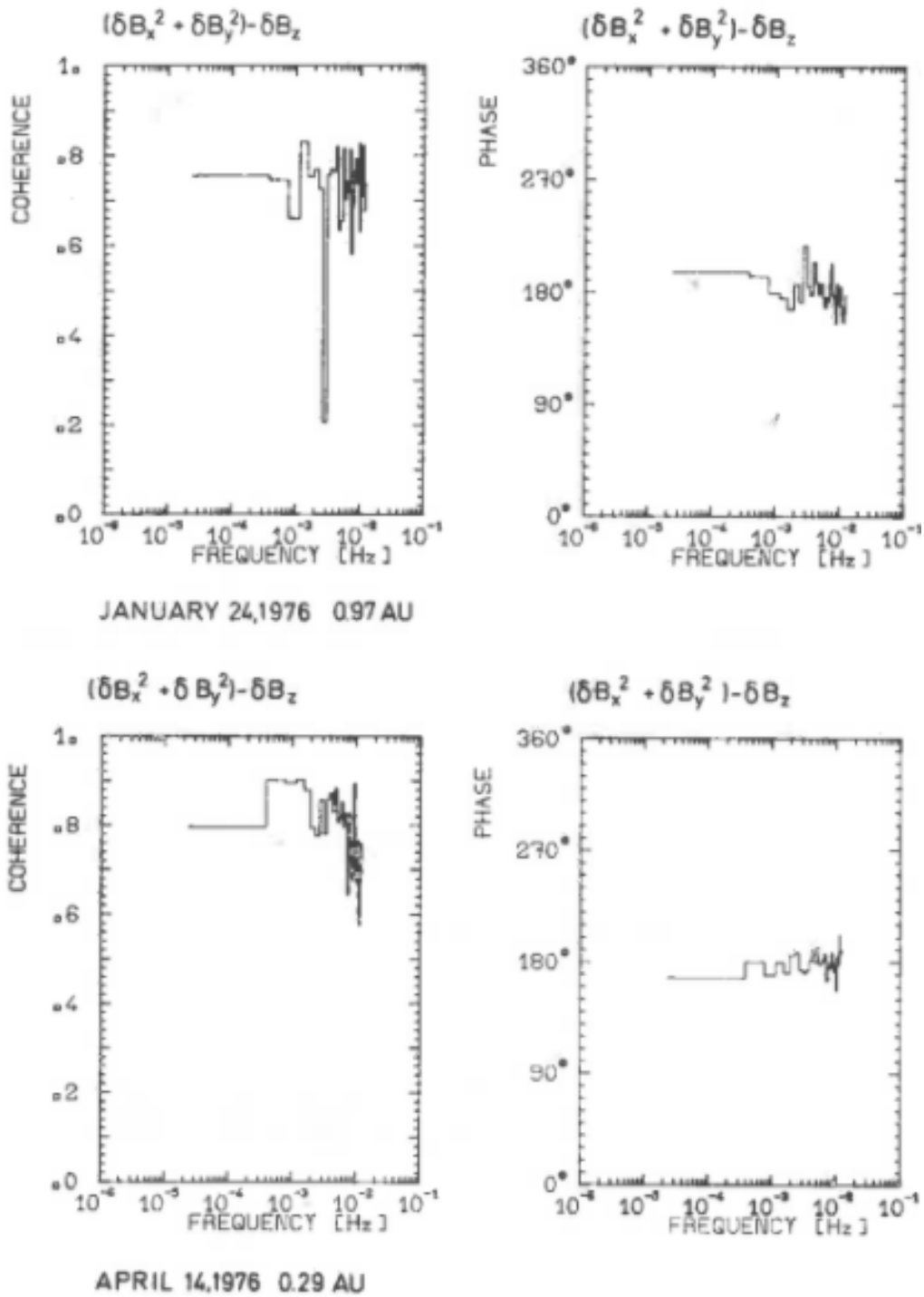


Figure 17:

Two typical examples of the coherence and phase between magnetic field fluctuations perpendicular and parallel to the average magnetic field at different distances from the sun.

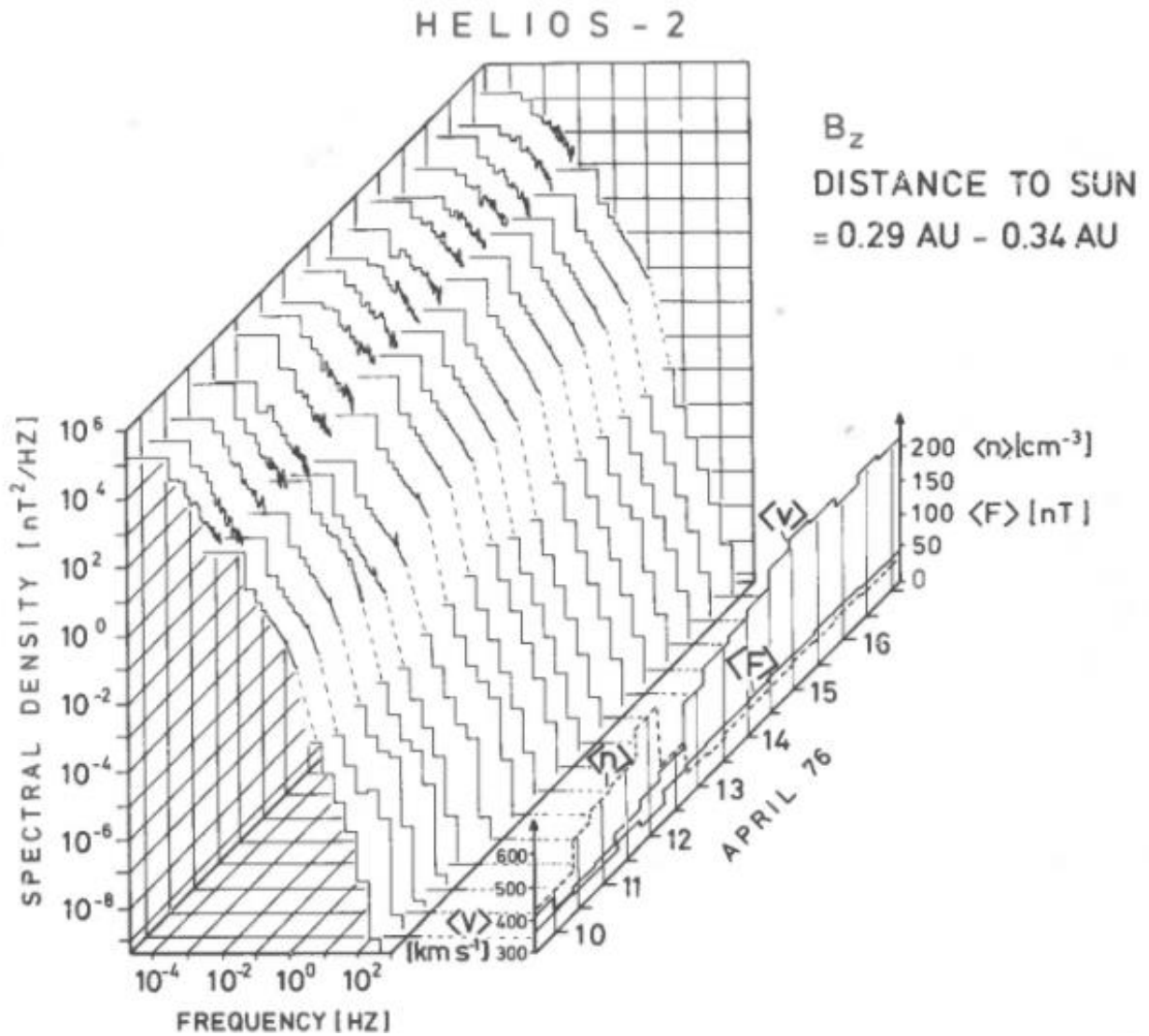


Figure 18:

Time sequence results of the magnetic field spectral densities of a vector component on the transition path from slow solar wind to a high-speed stream. Additionally, average values of the solar wind speed and proton density of the magnetic field magnitude are given.

6.5 High-Frequency Wave Fields in "Whistler Mode" Range

In each plasma, there are some characteristic frequencies shown by the waves that exist within. The gyro and plasma frequencies of the particles exist in the thin magnetoplasma of the solar wind. For example, waves can exist in the "cold" plasma approximation only in the range from greater than 0 Hz up to the electron gyrofrequency and approximately above the electron plasma frequency. In the range between the electron gyrofrequency and approximately the electron plasma frequency, no waves for the "cold" plasma approximation can be found. If the complicated, but precise, "warm" plasma approximation is used, the electrostatic "Bernstein mode" occurs. Waves with frequencies well below the proton gyrofrequency are generally referred to as MHD waves. They have been dealt with in Section 6.4; except for Figure 18, which covers the entire spectral range magnetically susceptible to Helios. The high-frequency magnetic field fluctuations measured by E4 will now be investigated.

The measurements with the search coil magnetometer E4 show constant wave activity between the proton gyrofrequency and the electron gyrofrequency. In Figure 19, the vertical lines indicate the most common frequency range of the waves measured during the 3-hour interval. The upper limit of the widest occurring field. The spectra generally increase to 220 Hz; 470 Hz has also been observed for some cases. The plasma experiments indicate the intervals in which the proton velocity is above 450 km/s using a black line. The upper limit of the widest, occurring spectrum is marked in the same interval.

In the range from 1 AU down to 0.75 AU, the "noise" of the waves usually extends up to 10 Hz. Even wider noise spectra of up to 47 Hz also occur. Below 0.75 AU, the width of the spectra follows the increase of the gyro frequencies and thus the static magnetic.

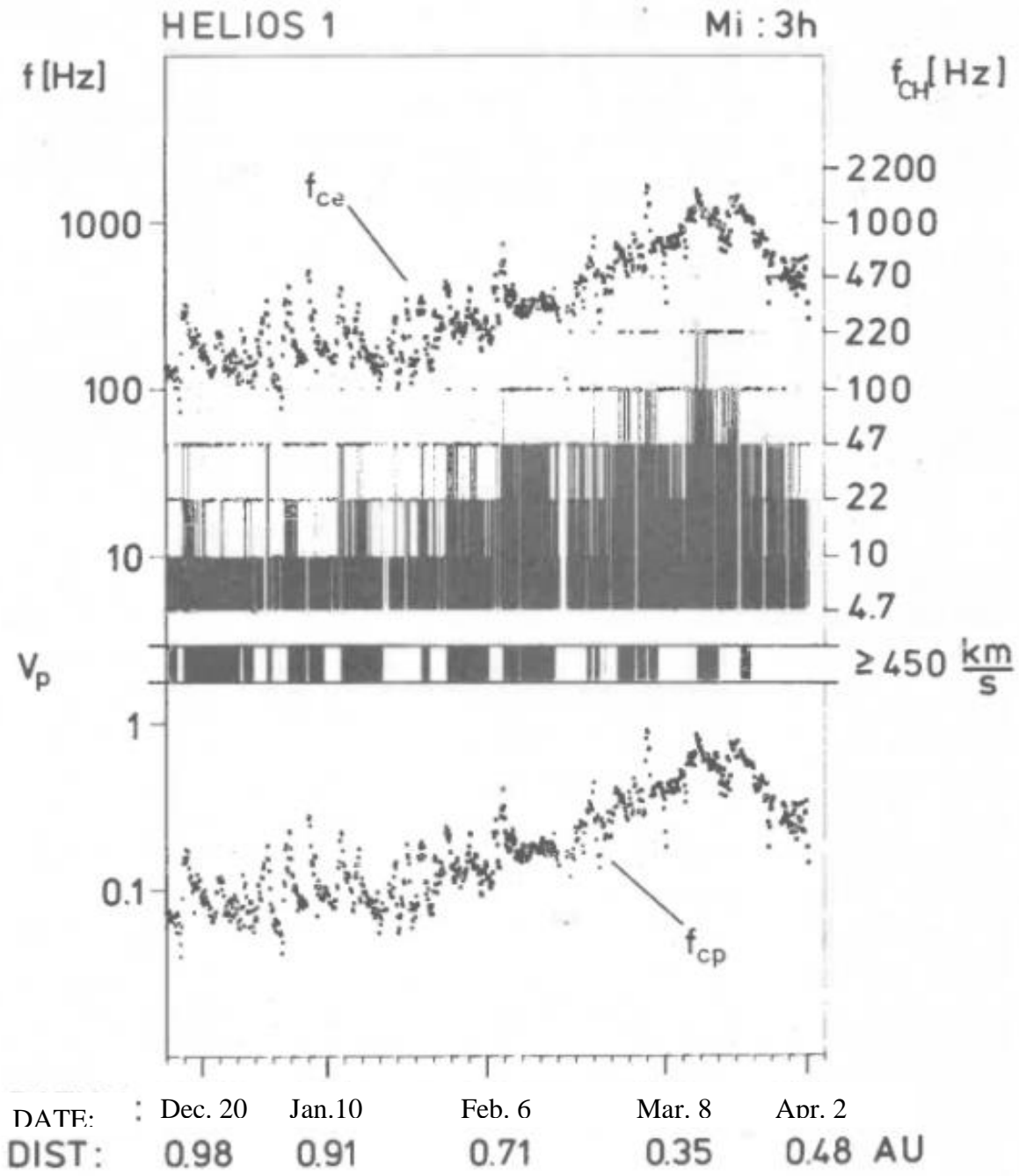


Figure 19:

Width of measured frequency spectrum in the limit f_{CH} in particular for a single band pass filter. The electron gyrofrequency f_{ce} and the proton gyrofrequency f_{cp} are from the fluxgate probe measurements, and the proton speed V_p is from the plasma experiment. For further explanation, refer to the text.

It can be seen that the width of the wave spectra rises significantly with higher frequencies at the beginning of a high-speed stream. In general, there are often strong and rapid changes in wave activity. The local electron gyro frequency has as of yet not been reached. The frequencies are usually much lower.

In this frequency range, the measured magnetic noise can be caused by several wave types. According to the theory of plasma waves, some candidates considered are: the ion cyclotron wave, the magnetic wave - and its high-frequency continuation, and the so-called whistler mode. The whistler mode is the most important type, since it can occur in the entire frequency range from approximately the lower hybrid frequency to the electron gyro frequency. However, the ion cyclotron waves and magnetosonic waves can provide a contribution in the lower frequency ranges for high doppler shifts, particularly in the plasma near the perihelion. For the whistler mode as a dominant component, some evaluations from the wave channel are also relevant. They provide the polarization suitable for the whistler mode for the measured waves [Barnstorf, 1980].

Apart from the plasma waves, static structures could also be a cause of the magnetic noise. As the solar wind passes the satellites, such structures can contribute to the noise level to the extent of a few times the electron gyro radius [Neubauer et al., 1977b]. In their kinetic theory, Lemaire and Burlaga [1976] have described electron structures of this order of magnitude. However, a direct measurement with a particle experiment is not possible with any current experiment due to the small extent of these structures.

In order to discuss the influence these structures have, the plasma experiment and the E2 magnetometer measurements were used to find time intervals, in which the angle, δ , between the magnetic field vector and the solar wind velocity

vector, covered the largest area possible within a few hours. In addition, the time intervals were selected in such a way that values such as magnetic field magnitude B , density, and temperature could be held as constant as possible, and no increased wave emissions were included in the discontinuities. Let us now assume that the measured spectra vary at these intervals only because they are seen by an observer under a variable aspect angle δ ! This is equivalent to the assumption of local generation. Furthermore, the quadratic spectrum can be obtained by passing static structures, and it has a gradient of $P_{st}^\circ \sim f^{-2\alpha}$ for $\delta = 90^\circ$. The following formula applies for the quadratic spectra at other angles δ and fixed frequency

$$P_{st}(\delta) = P_{st}^\circ |\sin^{2\alpha-2}\delta|$$

For example, when $\alpha = 3/2$, we have $P_{st}(\delta) = P_{st}^\circ |\sin\delta|$. Figure 20 shows the measured spectral densities together with the theoretical curve for $\alpha = 3/2$ a 5° grid. Observations and theory are roughly compatible between 30° and 150° .

The existence of spectral densities even for small angles proves that the static structures can indeed contribute, however a large proportion of the measured magnetic fluctuations must be caused by waves.

The low energy density of the fluctuations in this frequency range was already known from previous measurements (for example, see measurements from the IMP and OGO satellites). The two Helios probes were able to provide comprehensive measurements of magnetic fluctuations in interplanetary space between the proton and electron gyrofrequency due to the very low self-noise of their electronics. The slow-varying component of the spectral density shows a continuous decrease in the frequency. When the satellites move towards

the sun, the spectral densities increase significantly in each frequency channel.

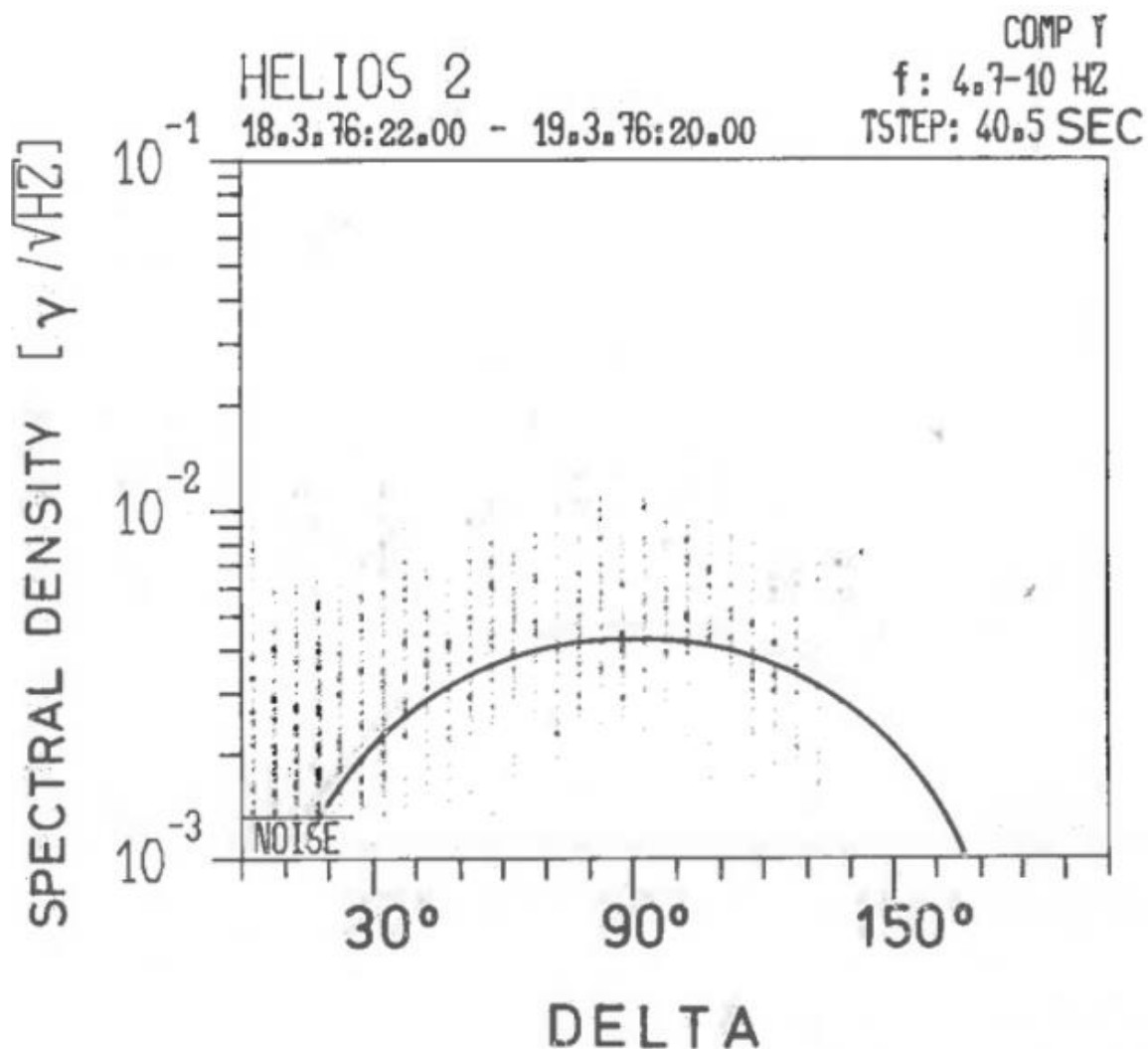


Figure 20:

Spectral densities with dependence on angle δ between the magnetic field and the solar velocity vector. For information about the curve, refer to the text.

The increase is at least one order of magnitude for each case. (A detailed discussion can be found in: Beinroth and Neubauer, 1981). This suggests that the free energy that feeds these fluctuations increases significantly closer to the sun. Figure 21 shows the result of an investigation for

all frequencies collectively. According to the logarithmic power law: $\log P = \text{constant} - 2\alpha \log f$, and assuming a monotonic decrease of the spectral density, \sqrt{P} (measured in $\gamma/\sqrt{\text{Hz}}$) with the frequency f , the spectral index α can be determined with linear regression. The associated total energy W is also shown. Since the large-scale overall situation of the solar wind plasma for the respective solar rotations changes only insignificantly, the increase in the energy density is solely a consequence of approaching the sun. On the other hand, the distance shows no perceivable influence on the spectral index.

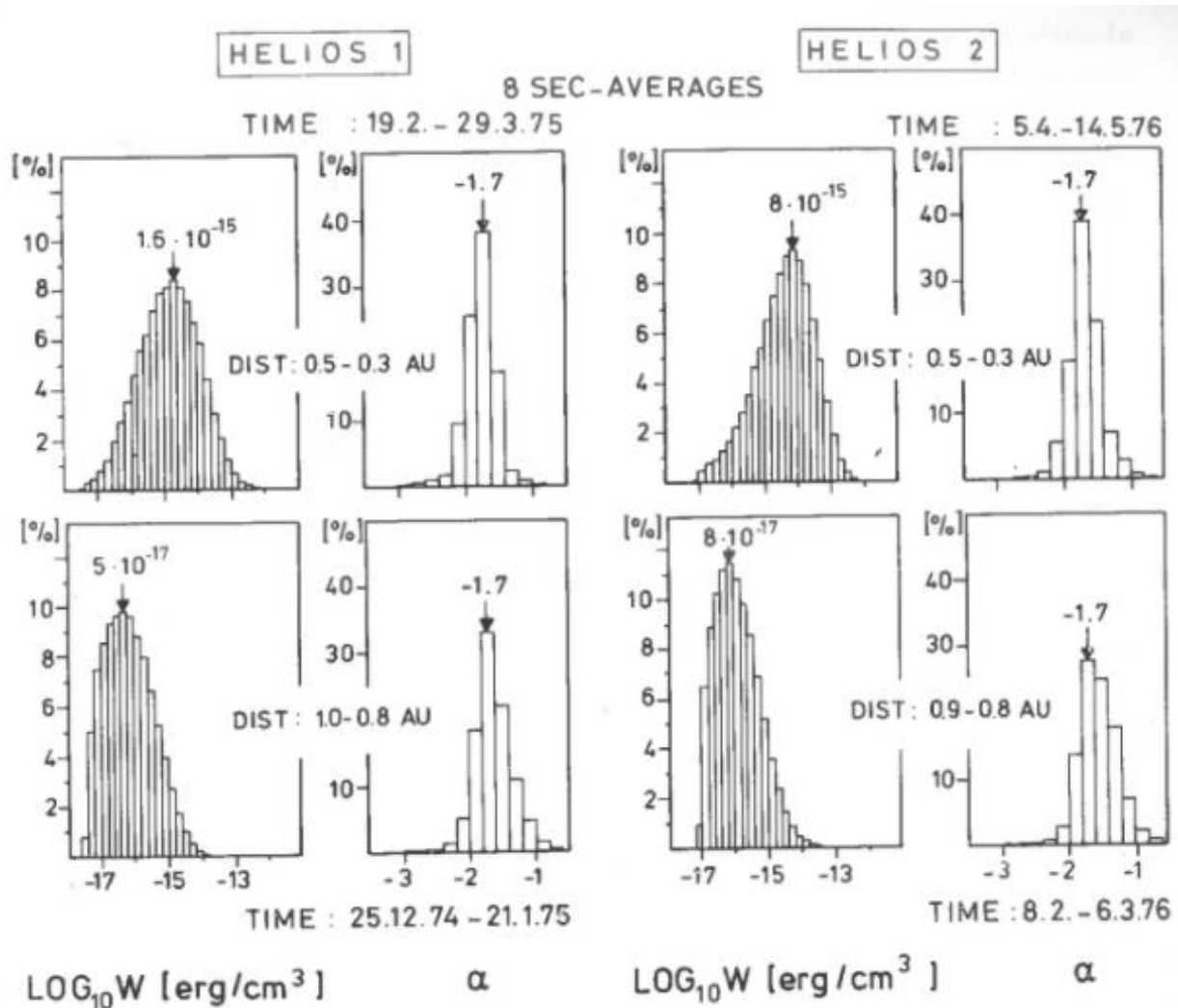


Figure 21:

8 second average value histogram of the total energy density W and the spectral indexes α for an entire solar rotation at two different distance intervals. Here $\sqrt{P} \sim f^{-\alpha}$ is assumed.

In the search for the damping and excitation mechanisms of these fluctuations, it is necessary to assume properties which, regardless of the solar distance at the time of measurement, act uniformly on broader frequency ranges over instrument noise. The extraordinary similarity of the histograms of Helios 1 and 2 is remarkable; the time interval between the measurements shown is over 1 year! The

uniformity of the solar wind during the sunspot minimum is very clear.

However, the approximation of the drop in the spectrum by the simple power law does not reflect the real image in the entire frequency range. The power law applies in the range of small frequencies. The analysis of 8 frequency channels shows higher deviations occur at higher frequencies. Figure 22 shows histograms of the drop-in spectrum around the center to center frequency of the channels.

The histograms from the region at the distance of the earth's orbit indicate a decrease of most spectra $\alpha = -1.5$ for frequencies up to 22 Hz. Above this, the spectra are usually quicker to steepen. When the satellite reaches perihelion, the range of the α spectra, has expanded from -1.5 to 100 Hz. The spectra will then become steeper.

With help from the plasma experiment E1, the correlation of the wave activity with some other plasma parameters can be investigated. Figure 19 shows the increase in frequencies when a high-speed stream is used. After a few hours, the frequencies fall back to the normal level. In Figure 23a the spectral densities are plotted against the proton velocity for the period between aphelion and perihelion for Helios 1. Proton speeds for the time period between aphelion and perihelion for Helios 1 are included. The mean of the measured data taken over a day means that only very large-scale events in the solar wind are taken into account. The point cloud of the measured data shows no correlation between both parameters.

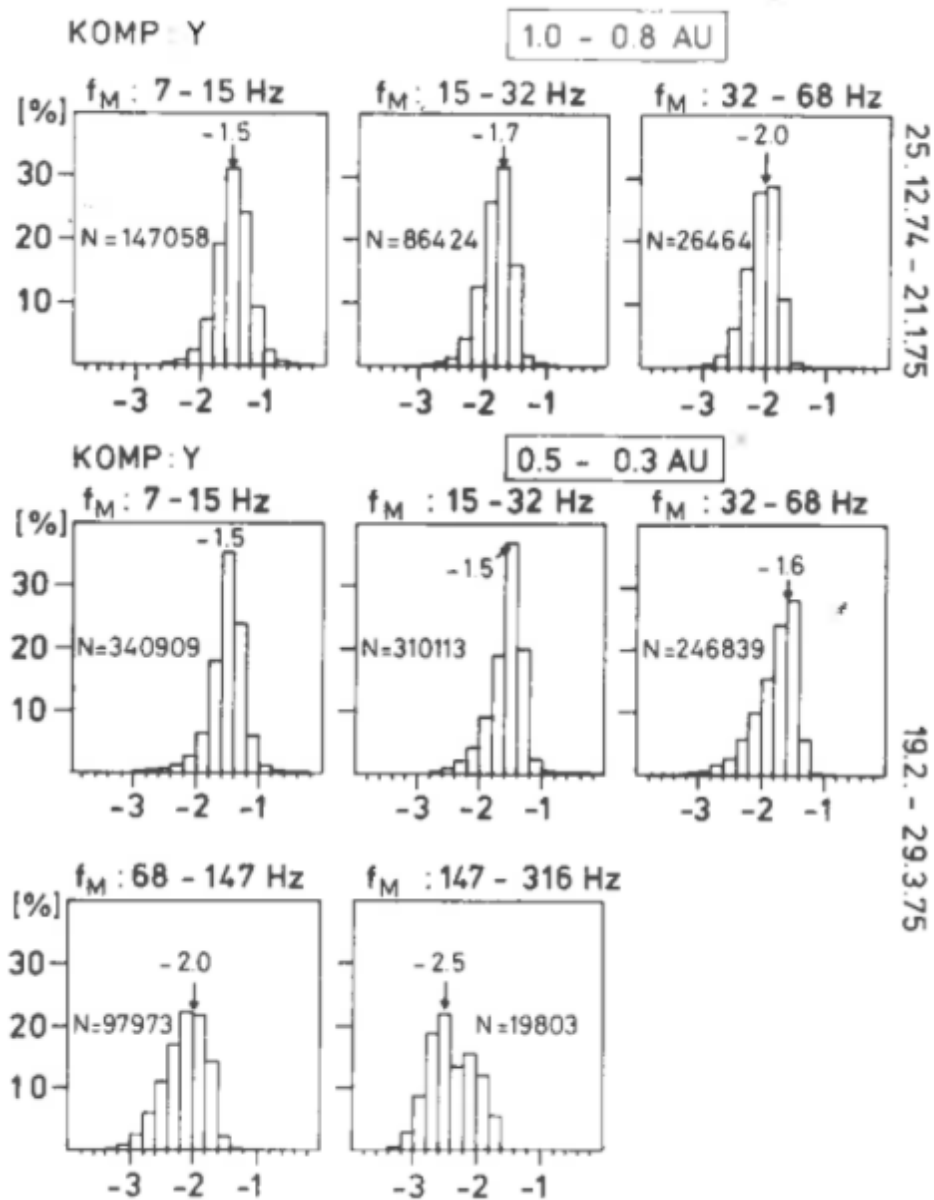


Figure 22:

8-second histograms of the drop in the spectrum of the center frequency f_M to the center frequency for Helios 1. The time period is the same as in figure 21.

HELIOS-1
 KOMP: Y
 f : 4.7 - 10 Hz
 AVER: 1 DAY
 TIME : 12.12.74 8.4.75

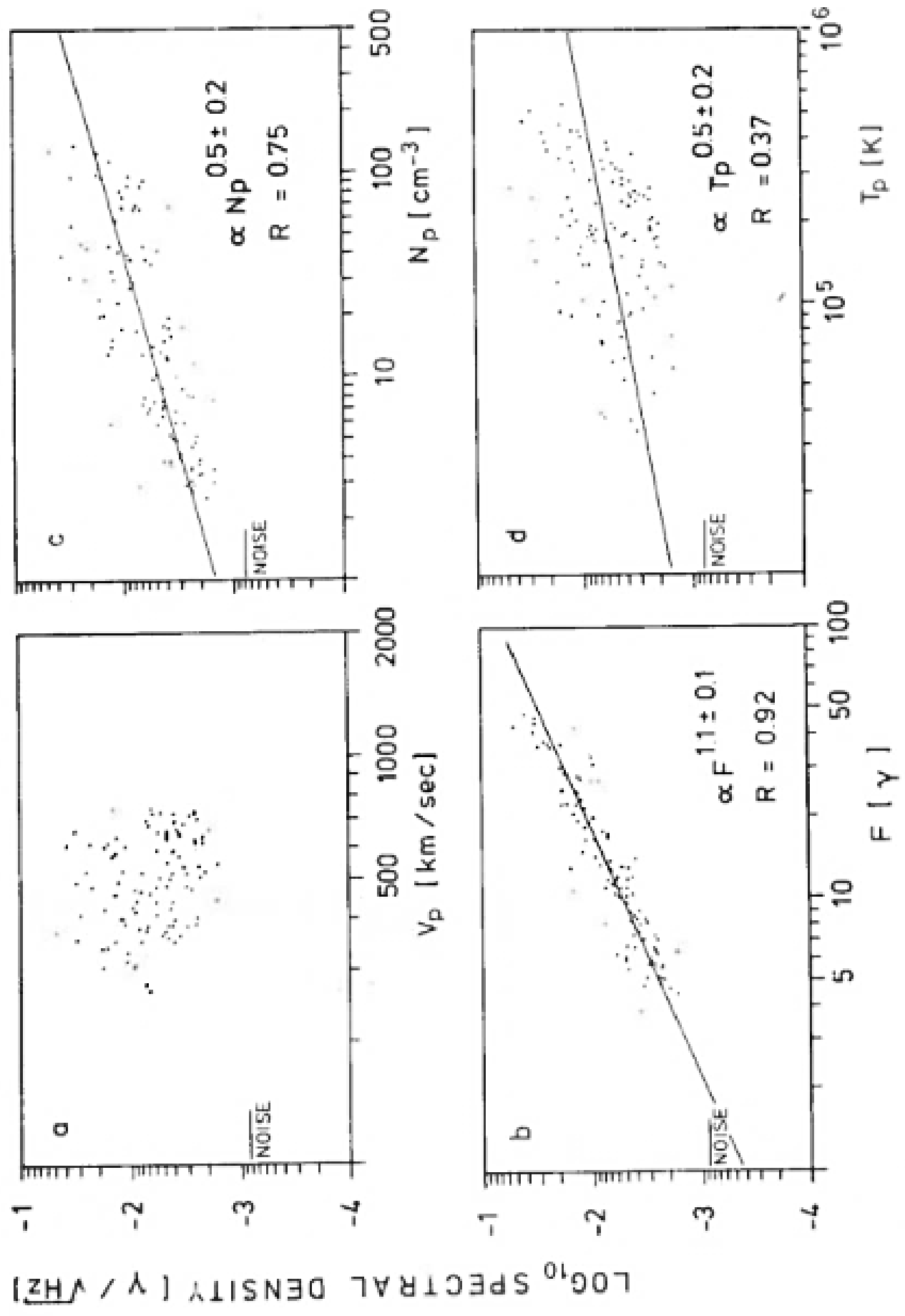


Figure 23: Correlation analysis of the daily average values of spectral densities with a) Proton speed V_p , b) the magnetic field F , c) the proton density, d) the proton temperature. The correlation coefficient, R , is also given.

The correlation of the average values of spectral density \sqrt{P} is high in comparison (see figure 23b). $\sqrt{P} \sim F$ is a good approximation. A direct influence on the static magnetic field into the measured values can be excluded, since such influences are prevented sufficiently by the frequency filters. The correlation with the proton densities, N_p , is slightly less pronounced; it is roughly: $\sqrt{P} \sim N_p^{0.5}$. The calculated correlation with the proton temperature T_p is not as significant. These studies were repeated with spectral densities from other frequency channels as long as they were above the noise. There were no other significant results. If the correlation analyses are extended to small time scales, the images for magnetic fields and proton densities change more as the time scales become smaller. Within time intervals of hours or fractions thereof, there are usually no significant correlations for the appropriately adapted mean values of these variables. In certain sections, the correlation between spectral densities and magnetic field or proton densities is very high. The investigation of the magnetic field showed, in some cases, intervals with high negative correlation for days. The conditions under which these small-scale correlations are exhibited are illustrated by the discussion of Figure 24 below. The relationship between the spectral densities, magnetic field, and proton densities on a large scale is a consequence of the dependence these parameters have on the distance to the sun.

Figure 24 illustrates the dependence of the magnetic fluctuations on the macrostructure of the solar wind plasma. In an earlier investigation, events which revolve with the sun and are therefore repeated in every rotation, were discussed (Neubauer et al., 1977a). A more detailed analysis has now shown that because of the high-velocity streams in the solar wind plasma, the wave activities in the covered frequency range vary in a characteristic manner. The high-speed stream spans the days

between the 17th and 25th of December. In the low velocity range before its mission, magnetic fluctuations displayed only minor activity. As the compression zone approaches, the

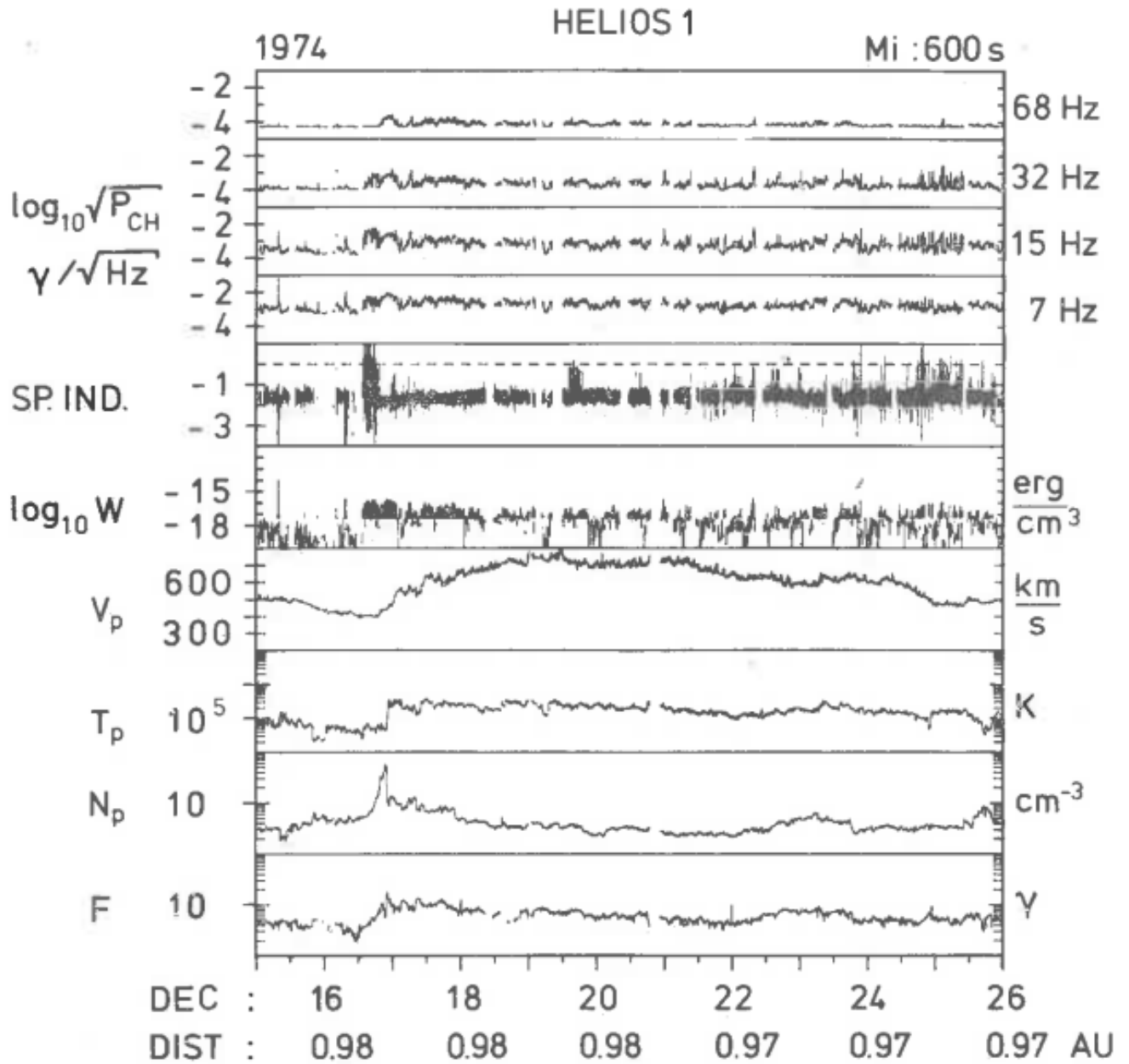


Figure 24:

10-minute averages of wave fields and some plasma parameters near 1 AU. The boxes show (from bottom to top): the static magnetic field F , Proton density N_p , Proton temperature T_p , Proton speed V_p , total energy of the magnetic fluctuation W (extended lines represent

values above $2 \cdot 10^{-17} \text{ erg/cm}^3$ to the limit, and the spectral densities P_{CH} of the 4 channels between 4.5 Hz and 100 Hz.

amplitudes increase strongly and higher frequencies with increasing magnetic field are detected. The large variations of the spectral indexes from one spectrum to another is evidence of the extremely turbulent conditions in this region. The largest energy densities of these waves are found symmetrically around the boundary layer between colder and warmer plasma, the so-called "stream interface". In high speed regions, the amplitudes remain relatively high, but no longer reach the level of activity that occurs at the boundary layer. After passing through the velocity maximum, the energy densities decay slowly. The "peaks" in the spectral densities of the frequency channels around 15 and 32 Hz are typical of the decreasing velocity region at the end of a stream. It is here that individual emissions are several minutes. The calculated spectral index does not describe the real spectra in these events because they do not fall monotonously in short emissions. In the region around 0.3 AU, high-velocity streams closely follow each other. Nothing in the magnetic fluctuations changes from the following:

-low activity in low velocity regions - highest amplitudes and strong broadening of the spectra in the transition layer ("stream interface") - high energy densities during the high-speed phase - decaying energy densities, interrupted by individual "emission peaks" towards the end of the high-speed stream. This sequence was demonstrated in all stationary plasma regions. In the investigation of high-frequency wave fields in "whistler mode", the analysis of the dependence on the solar activity is of particular interest for the future. In addition, the possible excitation or damping mechanism of the waves is to be found with the aid of three-dimensional distribution functions of the ions and electrons.

6.6 Discontinuities in the Interplanetary Plasma

One of the surprising discoveries in the early exploration of the solar wind was the discontinuous structure of the interplanetary medium. Together with that discussed in section 6.4, the Alfvénic fluctuations dominate the discontinuities, i.e. discontinuities in the magnetic field and the plasma parameters at time scales of 12 hours and below. Of the five types of discontinuities possible in magneto-hydrodynamics, there are theoretically four types in the solar wind that have actually been observed. First of all, there are the rare yet spectacular fast shock waves, which have already been partially discussed. In addition, slow shock waves also occasionally occur. tangential discontinuities (TDs) and rotational discontinuities (RDs) are the most frequent types of discontinuities observed. Both groups together also experience directional discontinuities (DDs). If we count all the DDs with spreading angles $\omega = \angle \underline{B}_1, \underline{B}_2 > 30^\circ$, the result is about 1-2 DDs per hour at 1 AU. \underline{B}_1 is the magnetic field before and \underline{B}_2 is the magnetic field after the discontinuities occurred. Early studies yielded many statistical features of the discontinuities mainly at 1 AU, but the initial results were obtained using insufficient observation data, such as too little time resolution in the magnetic field data and partly missing plasma data, which gave controversial results.

The Helios data is remarkable for two reasons. First, the properties can be examined as a function of the distance from the sun. Secondly, plasma data is practically always available, in particular to be able to distinguish between TDs and RDs.

In this subsection, analyses of all the properties of the DDs will be examined, which relate to the frequency of RDs and TDs, orientation, some jumping properties, amplitude, and polarization of the RDs. The fine structure of the transition is

dealt with in Section 6.7. Some of the results can be found in Neubauer and Barnstorf [1981], most of which was found by Barnstorf [1980]. The results presented here were obtained with the aid of the data from the fluxgate probe experiment, E2, and the plasma data, E1.

The first step is to investigate the frequency of the discontinuities as a function of the distance, r , from the sun. Table 4 shows this result. The time intervals during the primary mission of Helios 1 were chosen so that they correspond to approximately complete solar rotations.

Table 4

Frequency of directional discontinuities with $\omega > 15^\circ$.

Time Interval	Distance Interval in AU	Avg. number per hour	Corrected Number per hour
1.1.75 - 26.1.75	0.950 - 0.806	4.1	4.1
27.1.75 - 24.2.75	0.806 - 0.496	4.2	4.8
25.2.75 - 3.4.75	0.496 - 0.309	3.8	5.6

The value of events counted directly per unit of time above the minimum spreading angle of 15° is reduced by the fact that the speed of the spacecraft is so high at perihelion that it results in reduced counting rates. The number is only physically meaningful when corrected for this effect per unit of time. The frequency increased slightly when approaching the sun which is in close agreement with the results of Mariner 10. To measure variations in the stream structure's frequency, we chose complete solar rotations without the influence of errors. However, effects on the width cannot be ruled out.

For all solar distances, the frequency of the DDs with a spreading angle between 30° and 180° decrease monotonously. A special feature of the longitudinal dependency investigation was

discovered with the help of the Helios data. More DDs were found to have positive rather than negative magnetic sectors, they occur in a statistically significant manner with a spreading angle of 90° . It should be noted that positive sectors during the primary mission of Helios 1 originated from the northern hemisphere of the sun. Further analysis shows that the asymmetry results from more RDs with $\omega \approx 90^\circ$ in positive sectors. Figure 25 shows an example of the asymmetry in the polarity of the DDs.

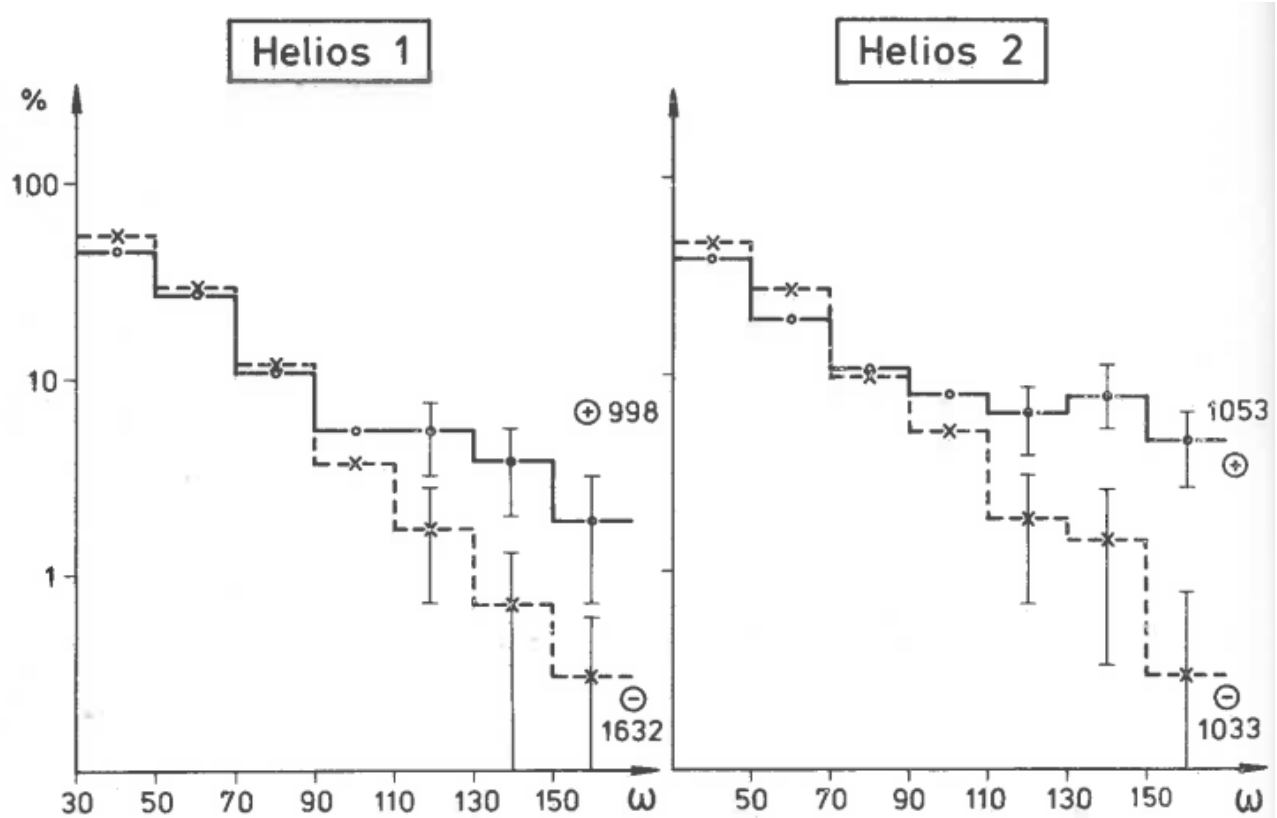


Figure 25:

Distribution of the spreading angle ω of the directional discontinuities for positive and negative sectors

A detailed study of the characteristics of the discontinuities, in particular, type identification, are made possible by the minimum variance analysis (MVA) from Sonnerup and Cahill (1967).

It is necessary that the experiment is provided with a high time resolution in order to resolve very thin (but natural for a finite depth) discontinuities. This is given for Helios at higher data rates with up to 4 magnetic field vectors per second from E2. For the MVA, the selection of analysis intervals is done with the help of data plots and is best carried out on a monitor, the analysis of many of these events is very labor intensive. The minimum variance analysis gives the normal direction, \underline{n} , to the local plane boundary layer between the two different magnetoplasma states on both sides of the discontinuity. Now the magnetic field component B_n in the direction of \underline{n} for TDs is given by $B_n \equiv 0$. RD's are given by $B_n \neq 0$. Figure 26 shows the distribution of B_n/B_0 with the mean magnetic field magnitude B_0 for 1427 discontinuities from Helios' primary missions. The bimodal distribution points to the division of the DDs into TDs and RDs. Due to the inevitable errors of the observations and the MVA at small values of B_n/B_0 a distinction between TDs and RDs is not possible. For RDs, between the velocity and magnetic field jumps, certain relations are seen, which can be tested with the aid of the plasma and magnetic field data. For RDs in an isotropic plasma the following equation applies:

$$\underline{v}_2 - \underline{v}_1 = \pm (\underline{B}_2 - \underline{B}_1) / \sqrt{\mu_0 \rho_0}$$

In the case of the anisotropies which are common in the solar wind, the relation must at least be approximately fulfilled for RD. ρ_0 is the average mass density. The plus or minus sign depends on whether the direction of propagation of the RD's magnetic field had an acute or obtuse angle. There is no such relationship for TDs.

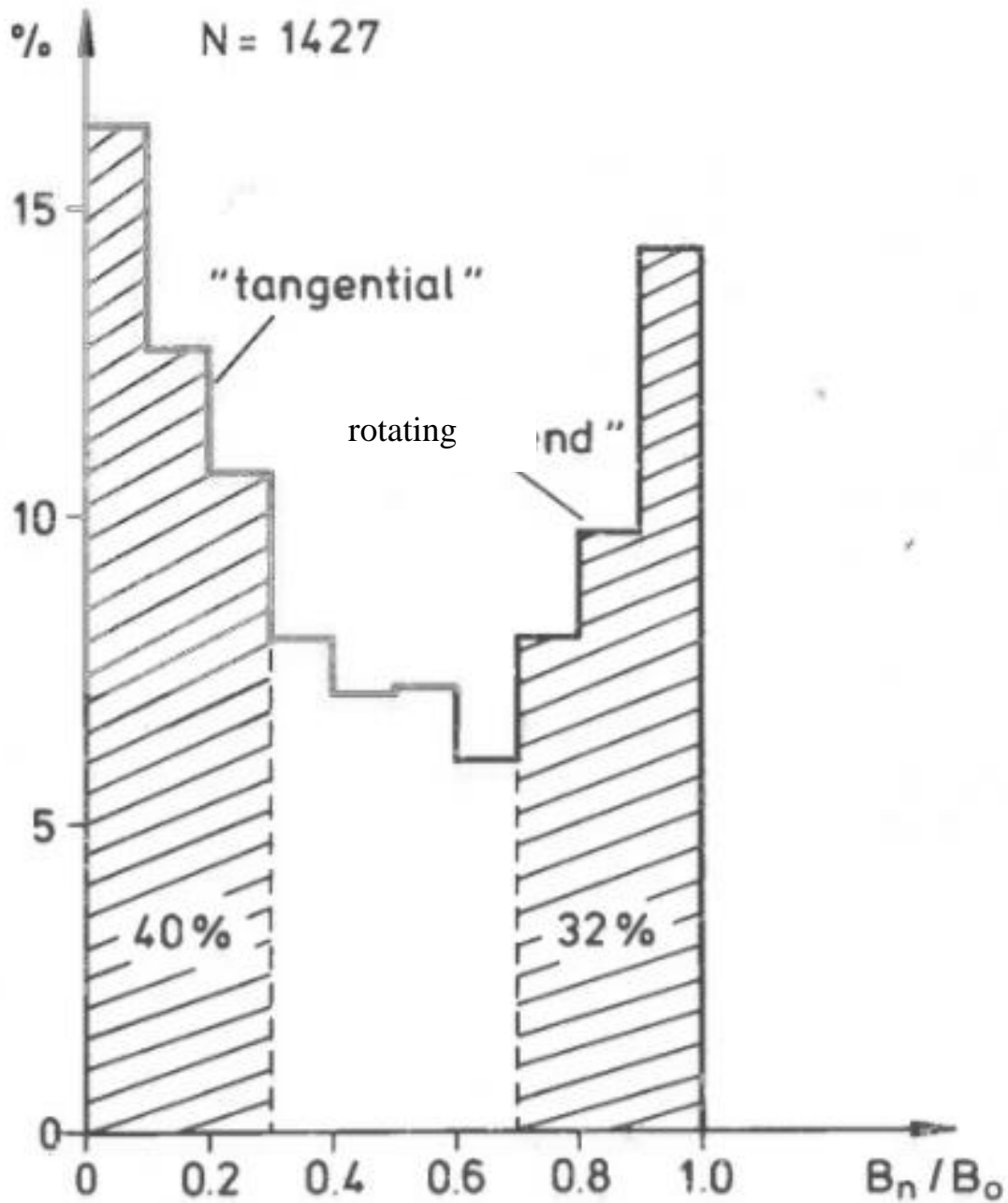


Figure 26:

Distribution of the parameters $\frac{B_n}{B} \geq 0$ from the Minimum Variance Analysis (MVA) for 1427 discontinuities.

The MVA results [Barnstorf, 1980] together with the above relationship for RDs show first that all DDs have a ratio of 2 between the TD frequency and RD frequency. Considering the dependence on distance, a slight increase in the RDs results when closer to the sun. In solar wind stream structure, RDs are

relatively frequent in high speed regions. We must point out, however, that the criteria used still discriminate somewhat against the RDs. The normal directions, \underline{n} , are somewhat perpendicular to the mean spiral direction of the TDs, and parallel to the RDs.

In graphical representations of the magnetic field from several hours to one hour, the DDs appear to be practically discontinuous. The high time resolution of experiment E2 at high data rates mainly in telemetry FORMAT 1, together with variance analysis at known solar speeds, enables the thickness of a "discontinuity" to be determined. TD structures have been discussed theoretically [Lemaire and Burlaga, 1976]. Depending on the nature of the transition, the size of TD must be at least one ion gyro radius or one electron gyro radius. The latter case requires very special conditions for the transition. Figure 27 shows the statistical results for the frequency by size for TDs and RDs. The results are given in km and in ionic gyro radii. It is interesting, that very small sizes only occur to a limited extent. The thickness of the TDs in ionic gyro radii is practically constant while the thickness of the RDs in ionic gyro radii increases noticeably outwards.

Finally, we consider an interesting peculiarity in the rotational discontinuities. The rotation or polarization of the rotating magnetic field vectors in the case of magneto-hydrodynamic observation is arbitrary, i.e. clockwise and counterclockwise rotation, gyro rotation, and "ionic" or "electronic" polarization are all completely equivalent. When the thickness of the RDs approaches the thermal ion gyro radius, the MHD description and waves in the R mode and L mode are no longer applicable, and it is to be expected that small mainly sizes occur in electronically polarized RDs. The frequency distribution in Figure 28 confirms this expectation.

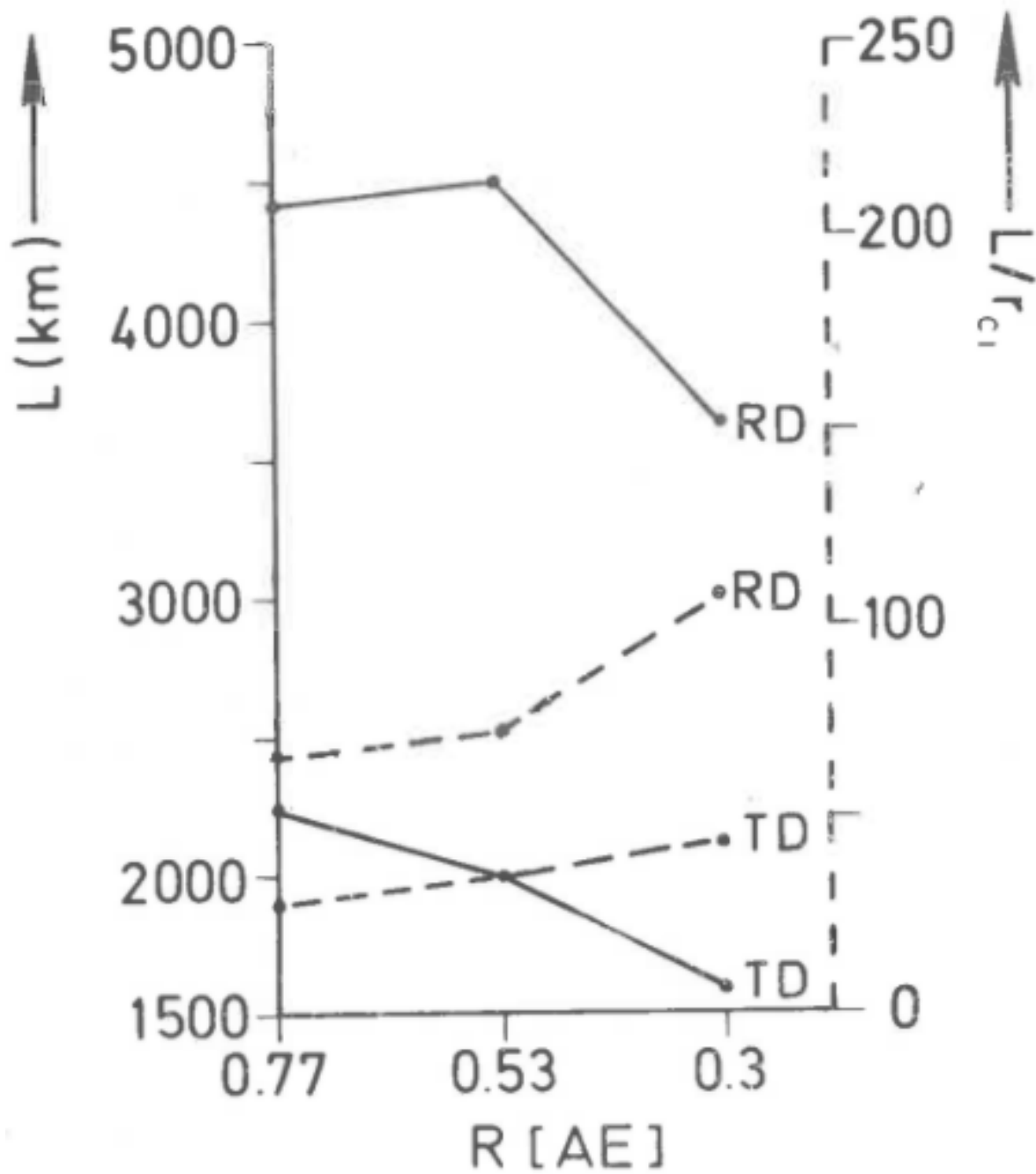


Figure 27:

Average thickness for rotational and tangential discontinuities for distance intervals 0.3-0.53 AU, 0.53-0.77 AU, and 0.77-1.0 AU.

In addition to further investigations using the Helios data, theoretical studies are necessary to understand the evolution of the statistical properties of RDs and TDs from 0.3 AU to 1.0 AU, and to investigate their origin. A question of interest that arose from studying the data is about the variation in the solar cycle. In order to better understand the differences between the TDs and RDs, static outputs should result from changes in the plasma parameters (which have not yet been treated), as well as a consideration of exact kinetic properties in the plasma such as anisotropy.

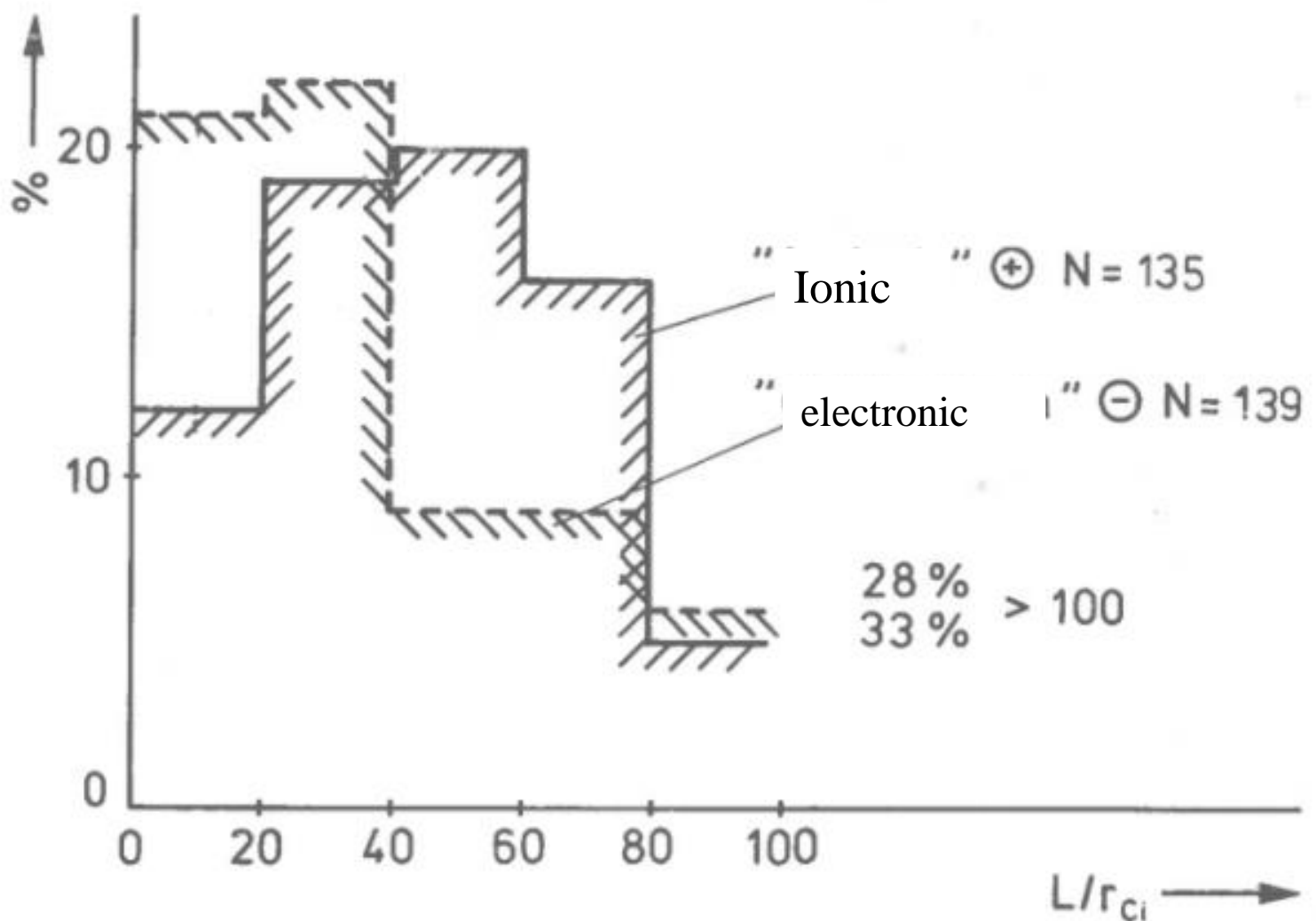


Figure 28:

Frequency distribution for the rotational discontinuities with "ionic" and "electronic" polarization

Particular subgroups are particularly important in the TDs e.g. TDs with great velocity changes.

6.7 Fine Structure of Discontinuities

In Section 6.6, we have dealt with the most important class of DDs, without being interested in the details of the transition between states on both sides of the "discontinuities". However, these transitions are important for various reasons. First, because of the very thin transitions for instabilities with corresponding wave generation can be considered, e.g. in the whistler mode, come into question. Possible plasma variations cannot be solved by the plasma experiment E1. Apart from these plasma-physical interests, the evolution of the TDs and RDs can be found in investigating the transitions. References to the fundamental process of the field lines merging are also important.

The magnetic field transitions are best represented as hodographs. The path of the tip of the magnetic field vector is represented in the plane perpendicular to the normal, \underline{n} . \underline{n} can be obtained by MVA. An example of a Hodograph of a TD is shown in Figure 29. Component B(3) in the normal direction is very small. The Hodograph shown is very regular. Many DDs also show very complicated hodographs.

The behavior of the high-frequency magnetic field fluctuations in and around the discontinuities measured by the search coil magnetometer E4 is very revealing. We can roughly distinguish between two behavioral patterns [Neubauer et al., 1977a; Barnstorf, 1980; Neubauer and Barnstorf, 1981]. The wave fields sustain discontinuities in some of the DDs. This can be explained by the fact that either the discontinuity represents a wave-reflecting "wall" or that there is a difference in the equilibrium level of locally generated waves between both sides

[of the discontinuity]. Figure 30 shows an example of a "waveguide".

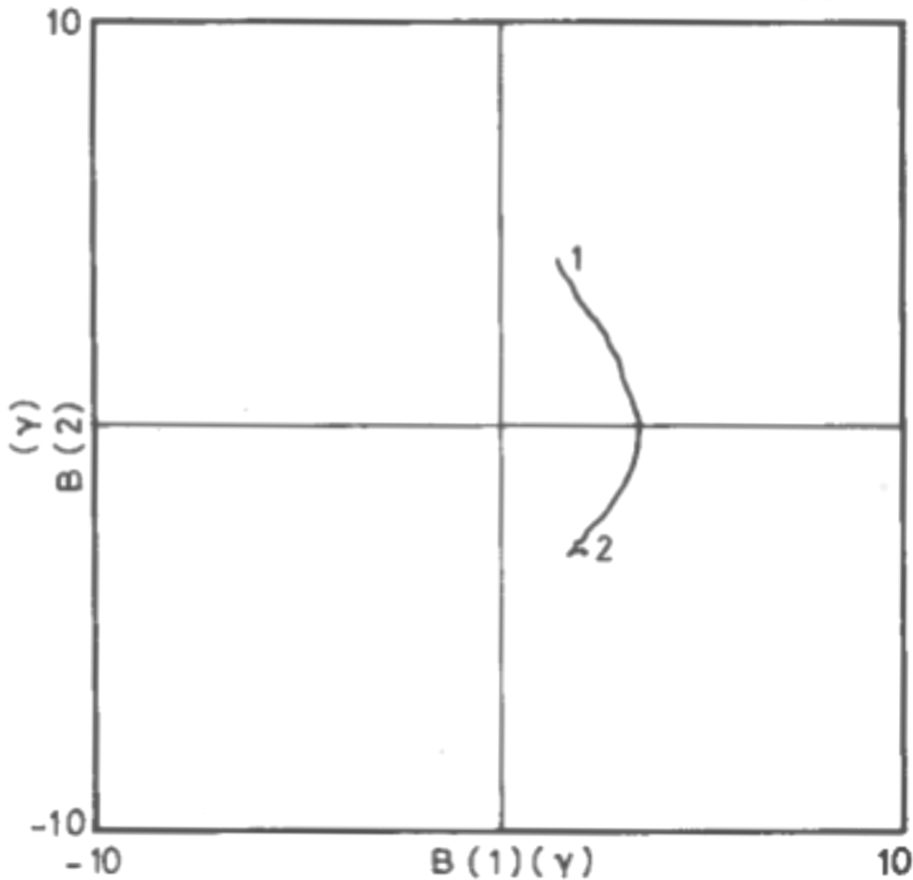


Figure 29:

Hodograph of tangential discontinuities from December 25, 1974 at 7h 19m 50s.

Another large number of the DDs show that the transition maxima of the fluctuations suggest the formation of a transitional layer of discontinuities. Important candidates for this source of waves are stream-induced instabilities. The simplest conditions are present when the magnetic field magnitude B is constant. We then have to deal with field lines parallel to streams. Figure 31 shows the size for the tangential discontinuity shown in Fig. 29,

$$M_{jII} = \frac{|v_i - v_e|}{V_A}$$

where \underline{v}_i and \underline{v}_e are the velocity vectors of the ions and electrons, and V_A is the Alfvén velocity of the electron. The components in the MVA coordinate system are also shown. At the maximum M_{jII} , the relative velocity between protons and electrons is 80% of the Alfvén velocity.

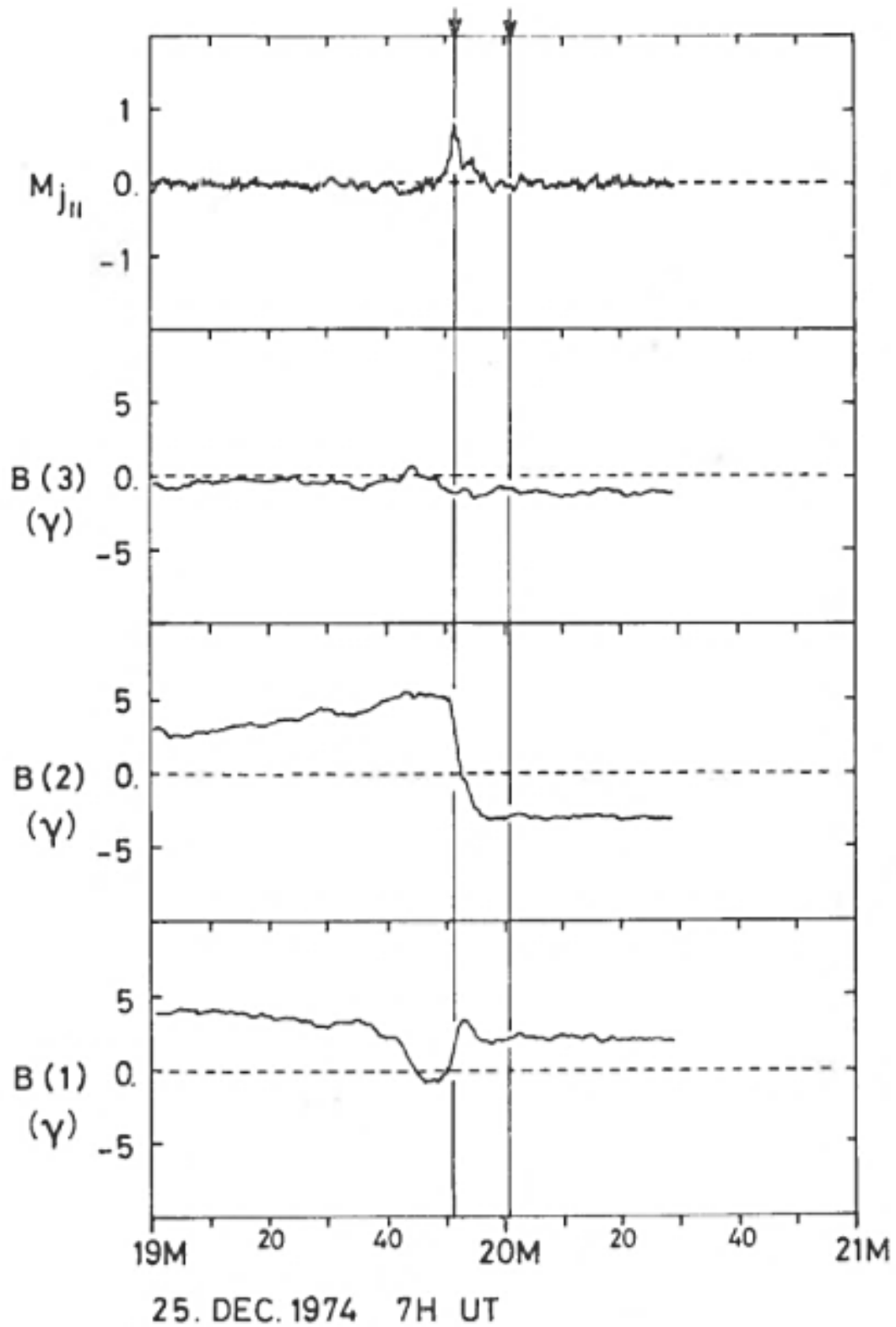


Figure 31:

Alfvénic current Mach number M_{jII} and the magnetic field components in the main system of the Minimum Variance Analysis for the TD in fig. 29.

A wave activity maximum occurred simultaneous with the maximum of M_{jII} , as Figure 32 shows. This result and similar results in other cases confirm the role of stream induced instabilities. It has also been shown that the density of the free kinetic energy in the relative motion of electrons and ions is statistically equal to the energy density of the magnetic field fluctuations [Barnstorf, 1980].

The spectral densities \sqrt{P} of the maxima are sometimes more than an order of magnitude over the environmental spectral densities. If the spectra are investigated more precisely, the spectral density decreases monotonously by the power law $\sqrt{P} \sim f^{-\alpha}$ with a mean $\alpha = 1.75$. In many cases, monotonic spectra with pronounced peaks can be observed.

The vast majority of spectra of magnetic fluctuations in the interplanetary medium show a monotonous decrease in the frequency and practically simultaneous variations in all channels of the search coil magnetometer experiment E4. This somewhat "amorphous" image of the spectra is misleading and is a result of the very good but still inadequate temporal resolution of the spectral data. The memory readings of the shock mode (section 4), largely contain transitions of DDs with relatively strong magnetic field variations, and often show relatively short narrow-band wave trains; they can be interpreted as waves in the whistler mode. In many such cases, the determination of the direction of the \underline{k} -vectors is made possible by a combination of minimum variance analysis, polarization observations, and the use of the plasma dispersion relations.

Figures 33 and 34 show an example of such a wave train in the region of very strong magnetic field gradients of a discontinuity, through which strong variations in B and minor variations in the angles ϕ and θ occur. [Barnstorf, 1980]. Figure 33 shows the magnetic field variations of the E2 experiment, the real-time spectral densities from E4, and the shock mode data from E4 in the waveform channel. The latter includes a time interval of only 14 seconds. Figure 34 shows the waveform data in the MVA system, the spectrum of the waveform data and their hodographs.

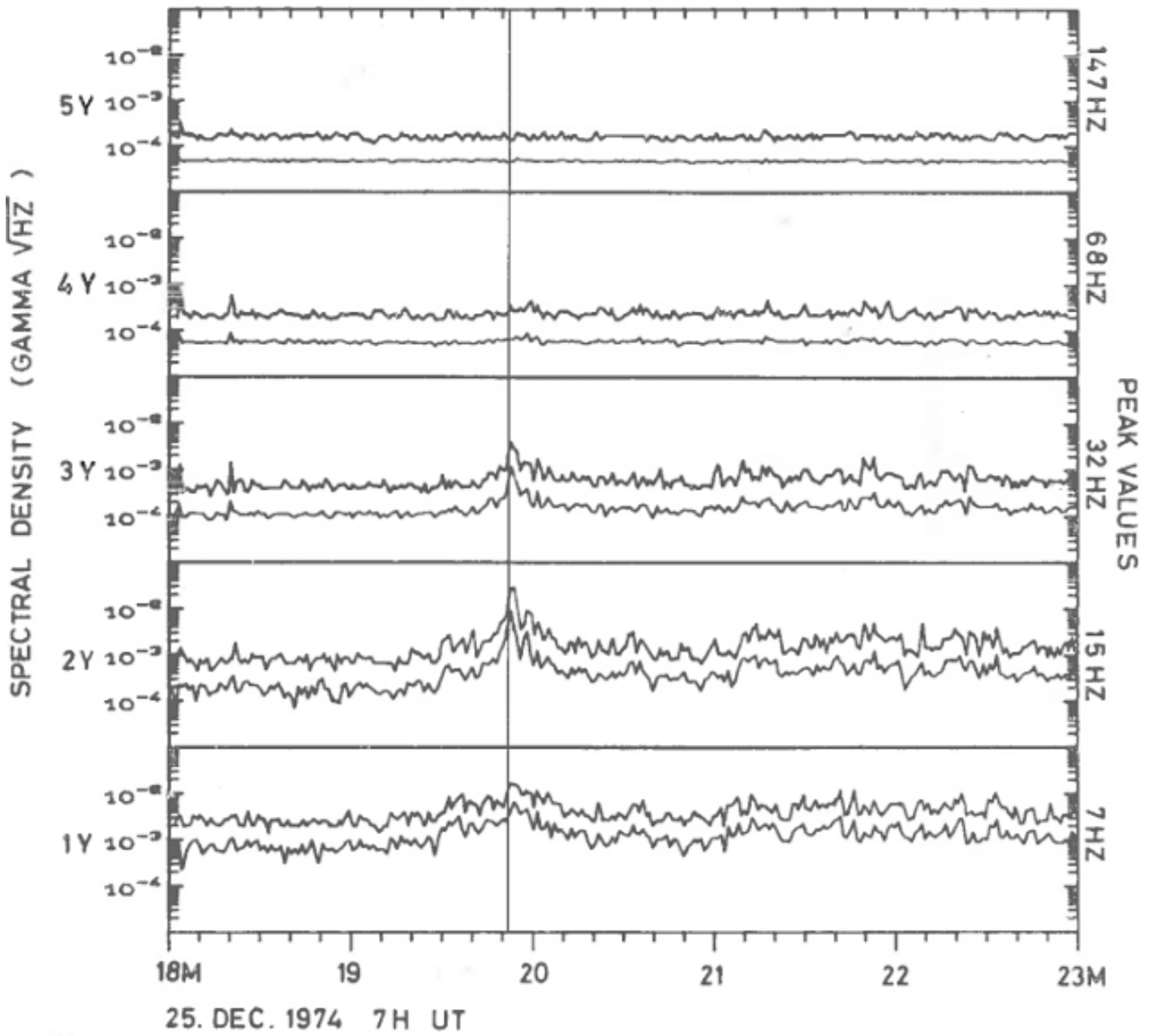


Figure 32:
 Magnetic fluctuation spectrum of the TD from figures 29 and 31.

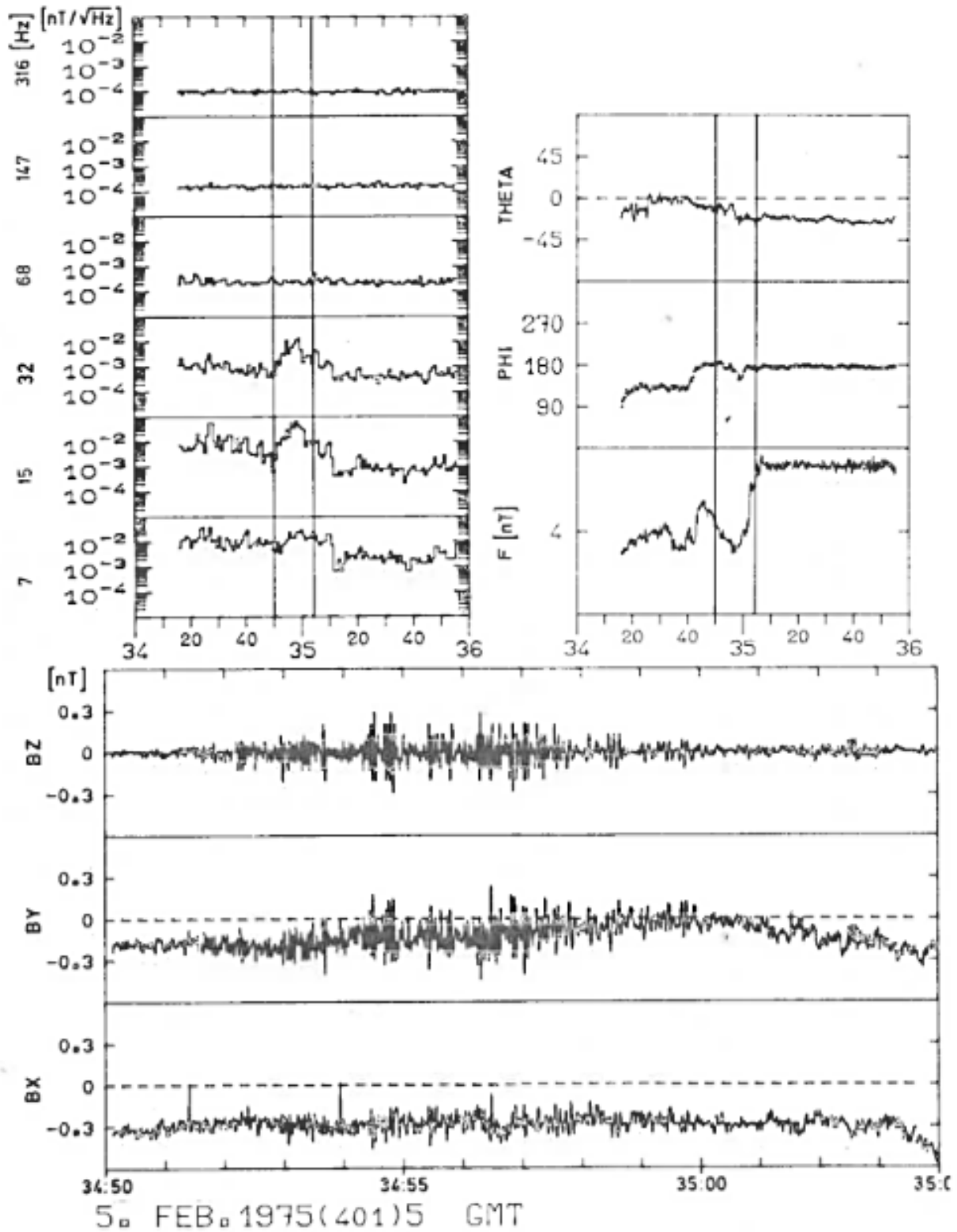
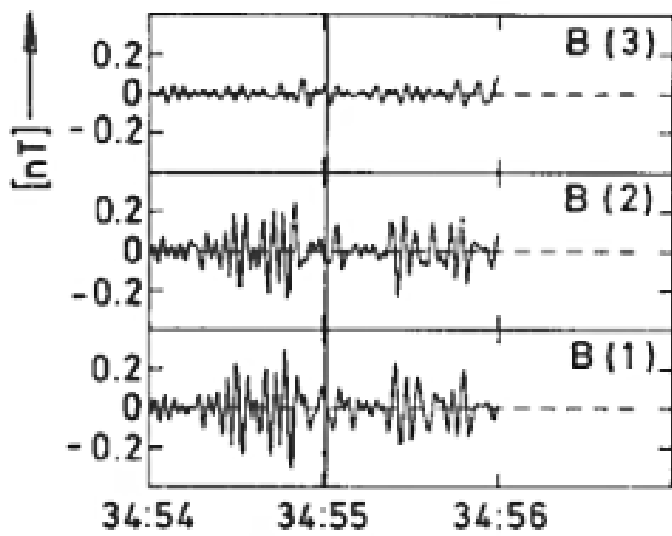


Figure 33:

Wave observations at the field gradients of a discontinuity in the quantity F (top right). Spectral data for one minute (top left) and wave form data for 10 seconds (bottom) are illustrated.



401:04:34:54

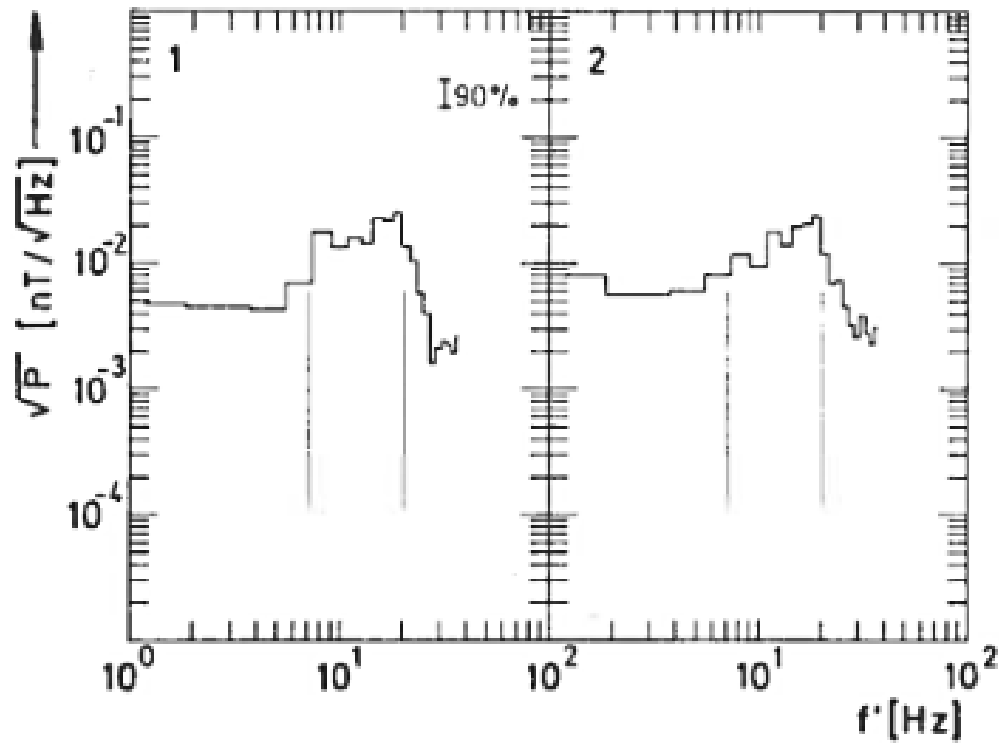
$f_z' = 19\text{Hz}$ $f_z = 7\text{Hz}$

$\theta = 33^\circ$ $f_{ce} = 93\text{Hz}$

$\alpha = 26^\circ$

$V_{sw} = 560\text{ km/sec}$

$n = 6.2\text{ cm}^{-3}$



401: 4 : 34: 54.000

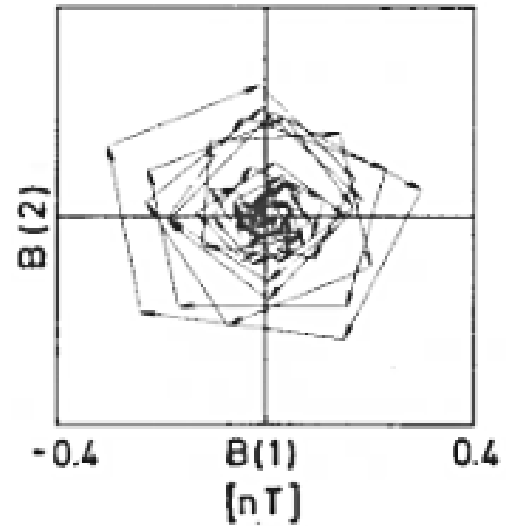


Figure 34: Analysis of wave observations from fig 33.

The latter indicates nearly circular polarization. The results of the physical evaluation of the wave train are also shown. A central frequency of $f_z' = 19$ Hz was measured in the Helios reference system. This frequency was produced by the Doppler shift of the frequency in the plasma rest system of 7 Hz. The wave propagated at an angle of 33° from the magnetic field. This and other examples emphasize the importance of waveform data for the analysis of plasma waves.

Despite the abundance of results already obtained, further research is needed in this area. In addition to the dependence on distance on the solar activity cycle, potential dependencies on the distance to the sun should also be examined. Is there an asymmetry between left and right circular polarized thin RDs with respect to the wave fields?

6.8 Fine Structure of Shock Waves

In Section 6.3, we dealt with rapid magneto-acoustic shock waves, which result in spectacular disturbances in the interplanetary medium which often continue for more than one day. We are interested in the large-scale plasma stream. The fine structure of the shock waves, i.e. the physical processes in the abrupt transition between two different magnetoplasma states, is an aspect of shock waves with a particular importance in plasma physics. In the case of shock waves, collision-dominated gas streams, dissipative processes, such as internal friction, heat conduction, and diffusion, all of which are determined by particle collisions that control the properties of the wave transition, other processes must also play a role in a magnetoplasma with long path lengths and have very large influence on the shock wave paths. For such collision-less shock waves, there are so called collective interactions (i.e. the two collisions of the classical shock wave theory are replaced by

the more ordered interactions, where instabilities are caused by waves).

Satellite observations of these collision-less shockwaves have the great advantage that, in the case of the occurring dimensions, the measuring probes do not distort the shock wave itself, as is readily apparent in the laboratory. In the interplanetary plasma, shock wave studies can be made on the basis of the bow shock waves made by the planets in the interplanetary medium, by corotation, or by solar eruptions generating interplanetary shock waves. The measurement coordinate system is completely different in both cases. The characteristic parameters of the shock waves are also very different. In the general case, these characteristic quantities are the plasma properties in the rest system of the undisturbed medium on the shock wave front: the magnetic field magnitude, the angle θ_1 of the magnetic field to the propagation direction, and the propagation velocity into the undisturbed medium on the front (index 1). Although it is somewhat simplified, we can use the following characterization: N_1 for the number density, $T_{p,1}$ and $T_{e,1}$, for the temperatures of the protons and electrons, B_1 the magnetic field magnitude, the angle θ_1 , and the propagation velocity, V_s . In a more compact form, the dimensionless magnitude, B , equals the ratio between plasma pressures and magnetic field pressures, T_{e1}/T_{p1} , θ_1 , and the fastest Mach number $M_{f,1}$, $M_{f,1} = 1$ for extremely weak shock waves. For a more detailed consideration, more plasma values are important.

The Helios mission data gives the opportunity to investigate shock waves between 0.3 and 1.0 AU over at least six years. The large range of variation of the parameters T_{e1}/T_{p1} , β_1 , etc. allows for the investigation of medium strength shock waves. Data intervals at very high data rates from Helios are of particular interest. The time resolution is particularly significant for the plasma data and completely insufficient for the shock waves

studies. However spectral data for the magnetic and electric fields (E4 and E5) were obtained. Although the relevant investigations are only at the beginning, some examples will be presented here.

Figure 35 shows the magnetic field variations of the shock wave, observed on January 6, 1975 at 20h 44m 6s as well as the magnetic spectral data [Neubauer et al., 1977a]. The shock wave was almost orthogonal, i.e. $\theta_1 \approx 90^\circ$. All data are averaged over 8 seconds. The propagation velocity with respect to Helios was 625 km/s. It is shown that the sharp transition is connected with an increase of the wave amplitudes by an order of magnitude, \sqrt{P} , or two orders of magnitude, P , respectively. At high frequencies, a sharp maximum is shown in the spectral densities.

Figure 36 shows the high-resolution magnetic field variations (E2) and spectral data (E4) for the shock wave on January 8, 1975 at 0h 22m 09s [Neubauer et al., 1977b]. ξ is the distance from the shock wave in Alfvén gyro radii c/ω_{pi} . Figure 37 shows the spectra at three different times. The spectra show an interesting increase in the spectral density from the shock wave in the preceding region, in the actual transition to the "wake" of the shock wave. Particularly at magnitude F , there are peculiar coherent oscillations, which are also in agreement with theoretical ideas.

Finally, Figures 38 and 39 show the magnetic field variations (E2) and the magnetic spectral data (E4) of the shock wave from March 30, 1976 at 17h 44m [Gurnett et al., 1979]. The shock wave was spectacular because of the very low β_0 and very high T_{e1}/T_{p1} , which favors the excitation of ionic acoustic waves.

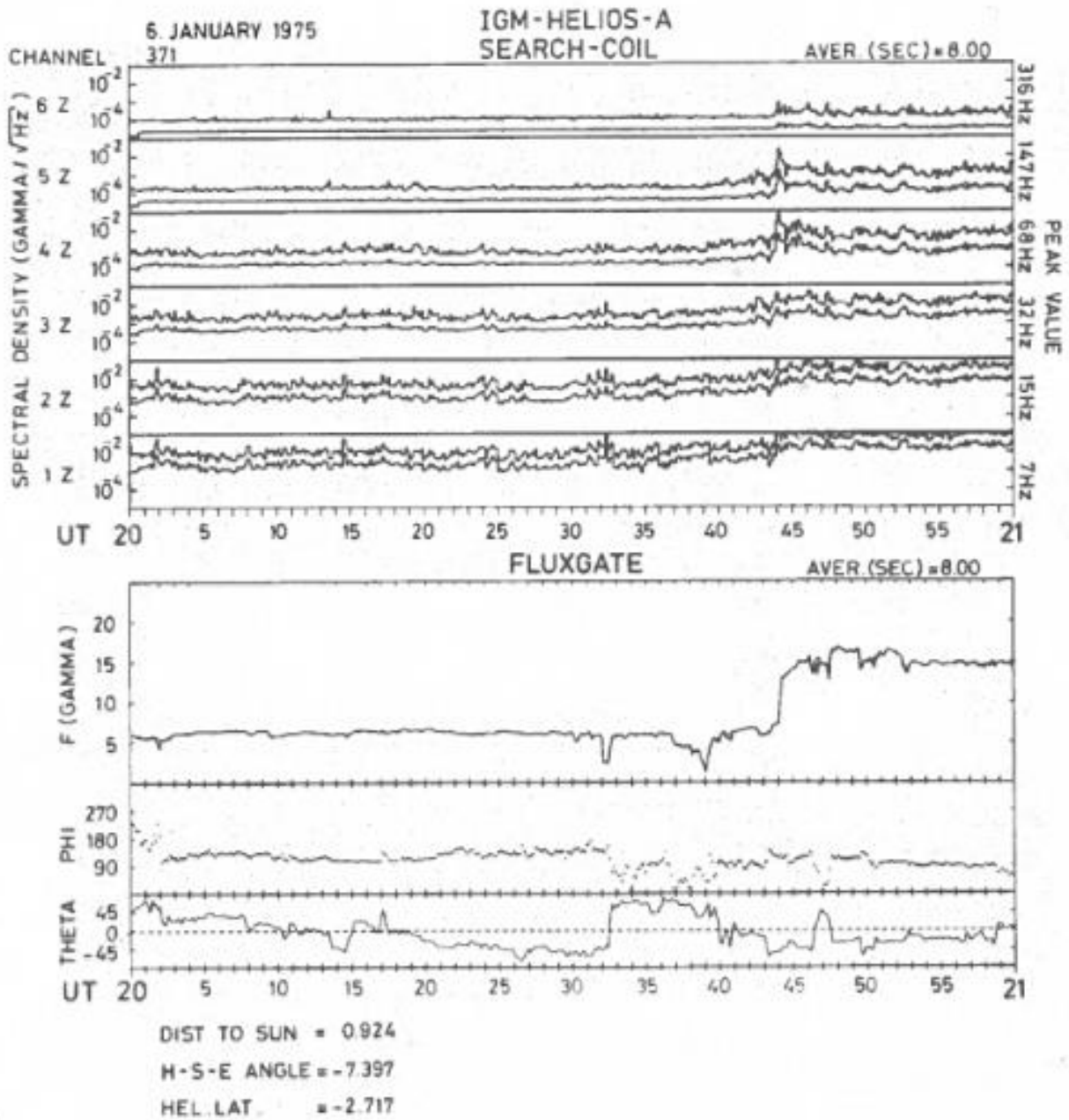


Figure 35:

Magnetic field variations (E2) and magnetic spectral densities (E4) for the shock wave that occurred on January 6, 1975 in 8 second mean values.

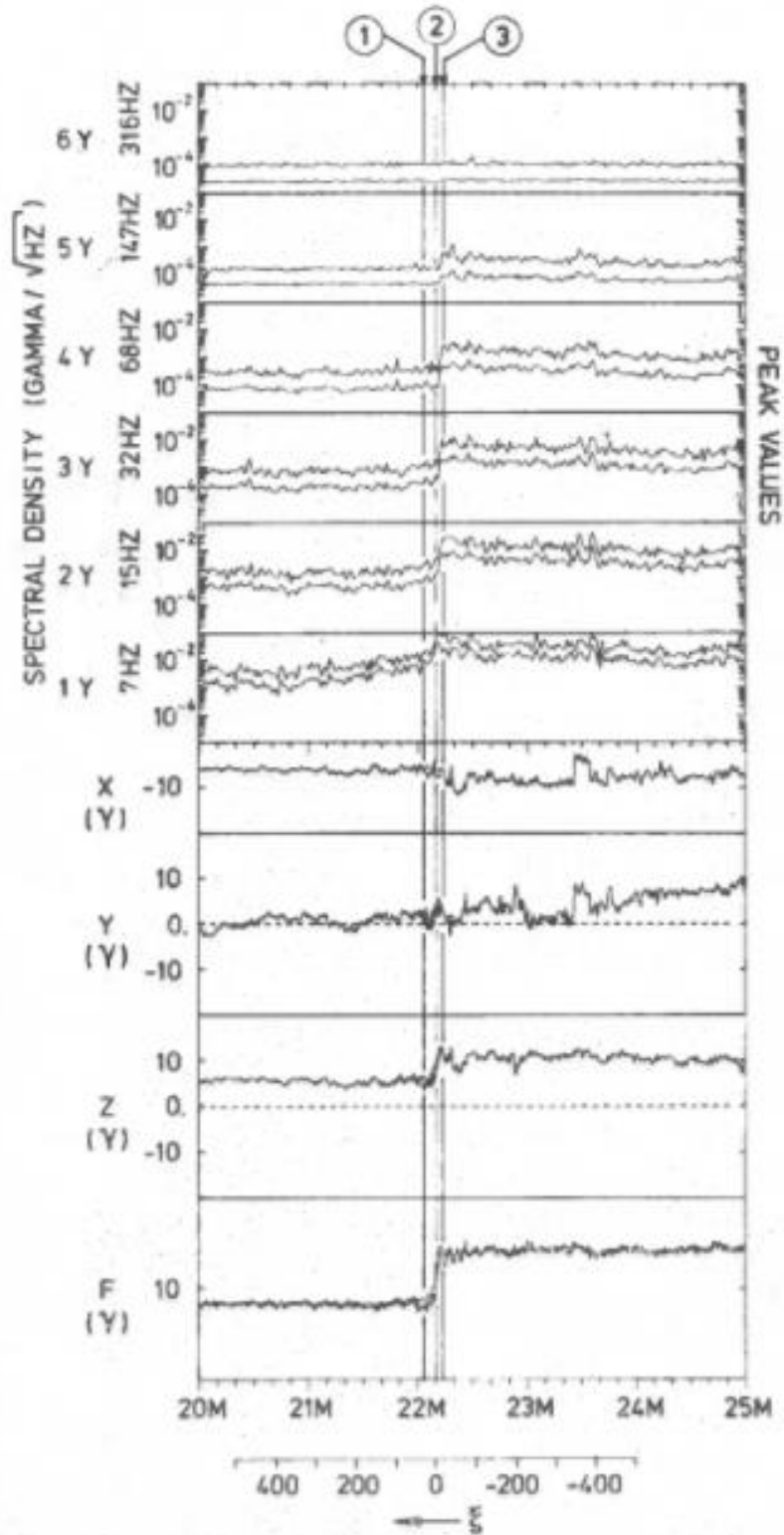


Figure 36:

Magnetic field variations (E2) and spectral data (E4) for the shock wave on Jan. 8, 1975 0h 22m 9s at the highest time resolution.

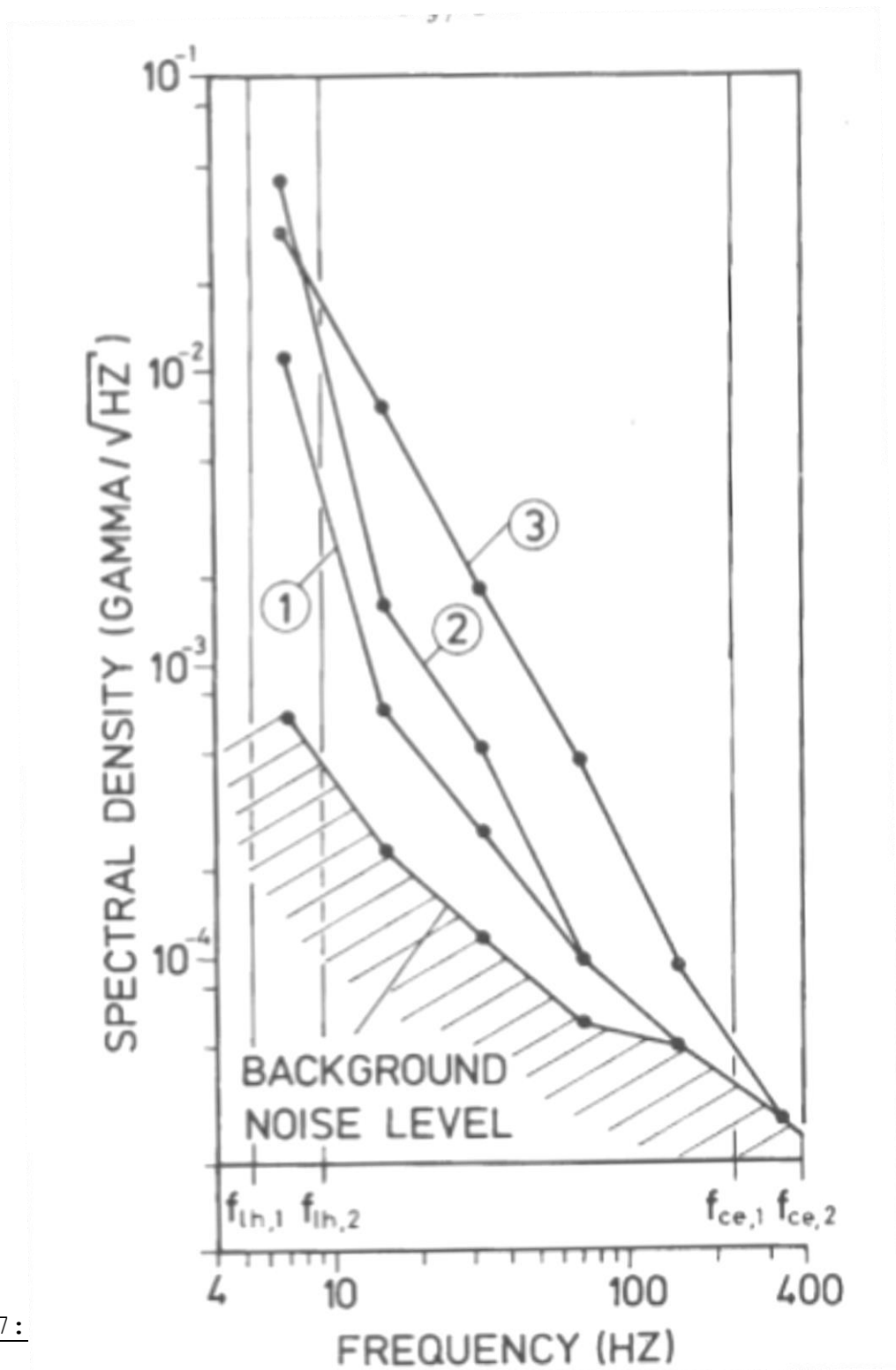


Figure 37:

Spectral densities as a function of the frequency for three different times (see fig. 26) for the shock wave that occurred on January 8, 1975. f_{1h} and f_{ce} are successive upper hybrid frequencies and electron

cyclotron frequencies.

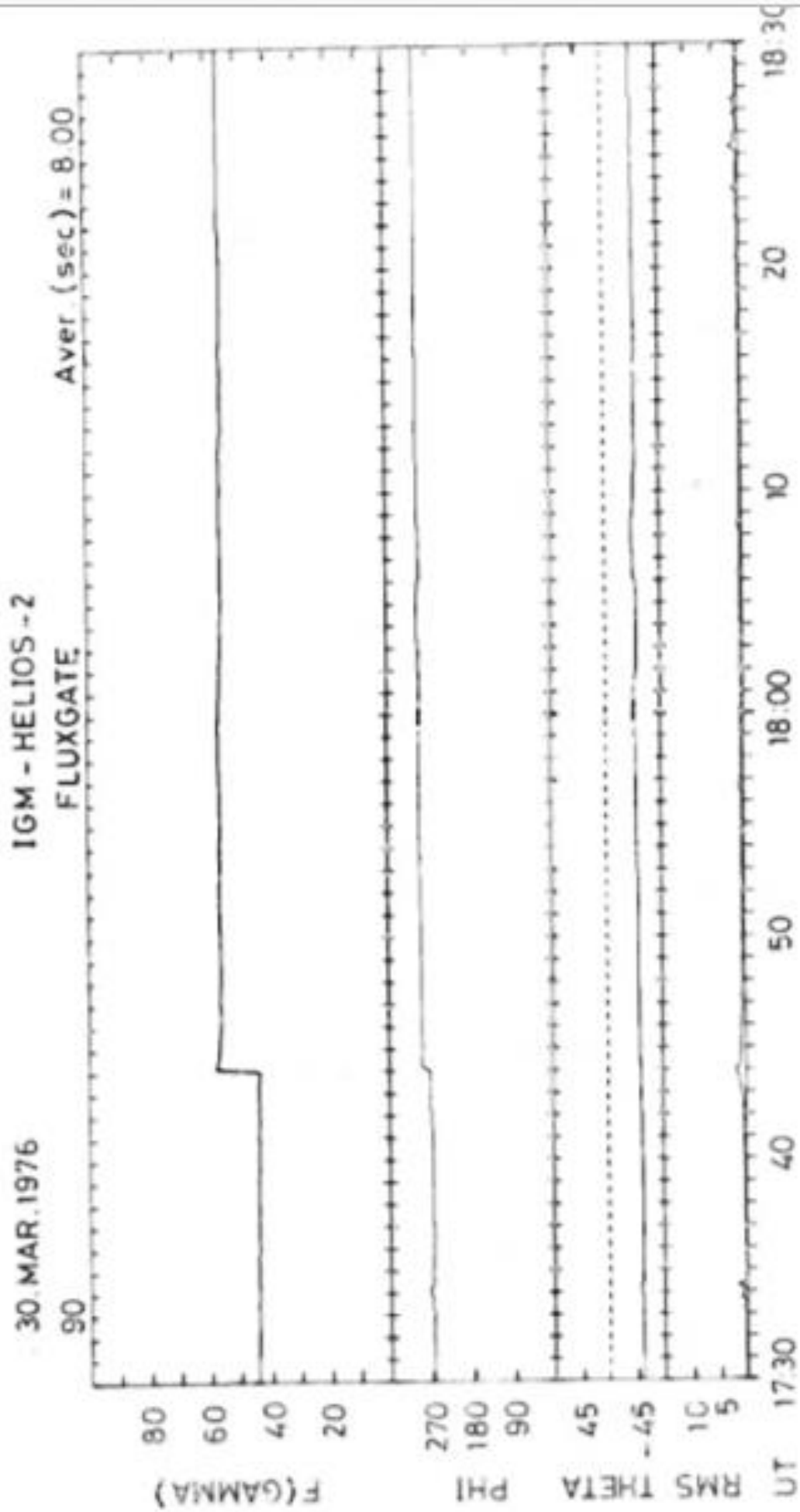
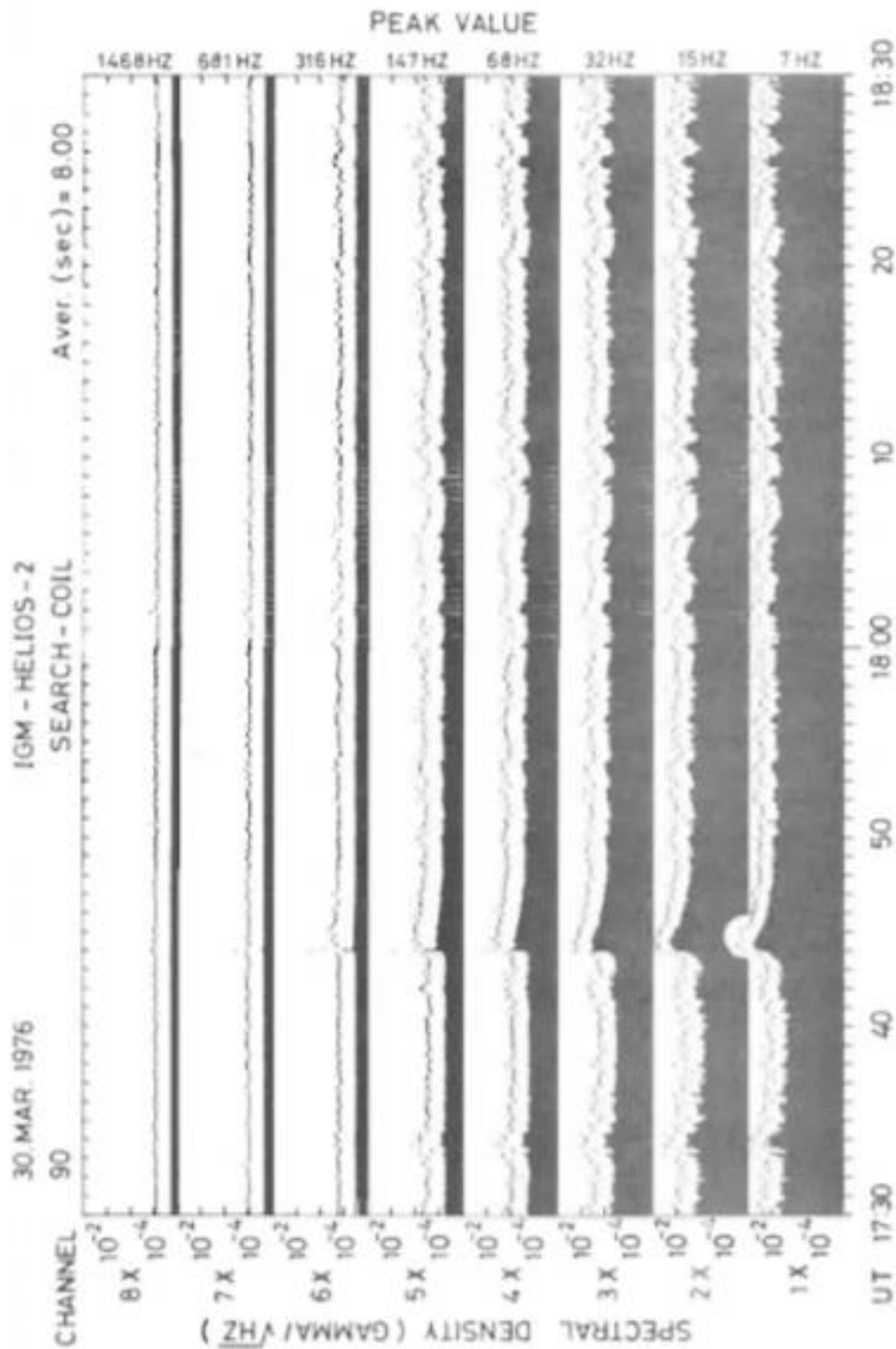


Figure 38: Magnetic field variations for the shockwave that occurred on March 30, 1976 at 17h 44m.



O. MARS 1976

Figure 39: Magnetic fluctuation spectrum (E4) from the shock wave that occurred on March 30, 1976 at 17h 44m.

The high fraction of α -particles in the plasma is remarkable. Even in the channel of 470 - 1000 Hz, measurable increases in magnetic fluctuations occurred. The shock wave is particularly suitable for more precise investigations since the plasma state before the shock wave was remarkably calm. The interpretation [Gurnett et al., 1979] showed that electron plasma oscillations and electrostatic ionic-acoustic turbulence occurred.

For a large number of shockwaves, a file has been created, the evaluation of which will allow for more accurate individual investigations, as well as extensive comparative studies.

7. Summary and Conclusion.

After the methodology behind the Helios data processing and its various problems, as well as the numerous scientific results has been explained in detail, some of the experiences are summarized here:

1. For the experiment put on board Helios 1 and 2 by the Institute of Geophysics and Meteorology at the Technical University of Braunschweig, the technical procedure for the data processing was be done in approximately one year for the search coil experiment (E4); for the fluxgate probe experiment (E2), it took approximately three years to run all configurations of the spacecraft telemetry system. The delay in E2's processing was not due to the experimenters but to unexpected problems with the thermal control in the experiment. The delay also led to an unfavorable ratio of the time it took for the routine processing and the time for the actual measurement for the E2 data. Aside from the problem with the thermal control for E2, the Helios probes carried out the experiments superbly.
2. The data from the E2 and E4 experiments have produced many

important and unexpected results on the physics of the interplanetary magnetic field. This is expressed in a number of publications, which are cited in the bibliography. The data from both experiments have played a role in studies from other experimental groups, which are only listed here in part. The results from the Helios data have contributed to the whole field of the physics of the interplanetary medium at an international level in the last years.

3. The data analysis showed that, despite the problems caused by constantly changing external conditions and a fluctuation of employees, given appropriate planning by the management institute, large scale projects could be undertaken by a university.
4. The availability of special computer systems is indispensable for processing satellite experiments with large amounts of data. Tasks of this scale are normally not manageable by a university computing center.
5. In the case of scientific evaluation, a suitable composition of the evaluation team is important. A ratio between scientists and programs of about 3:2 proved to be optimal for the E2 and E4 experiments.

Finally, it should be pointed out that, the Helios probes, with their unexpectedly long service lives, carried out their original mission objectives until reaching the solar maximum, and a new mission has been started without having to launch a new spacecraft. Since the still "live" Helios 1 offers the unique possibility of future successive missions (which are not to be expected in the foreseeable future), the possibilities for further scientific data evaluation is self-evident.

8. Acknowledgments:

We would like to thank all those who contributed to the success of the Helios data processing for the E2 and E4 experiment. At the Institute of Geophysics, the Institute's Director Prof. Dr. W. Kertz. The mathematical technical assistants and technical assistants Baumert, Brasch, Kaller, Stoll, Thuringy, Walter, and Wysocki, as well as the scientists of the Helios evaluation team who left during the mission: team Dipl.-phys. Lange and Dr. Lammers. Our own contributions to the data processing of the E2 and E4 experiments would not have been possible without the long-time, consistent work of the members of the Helios teams at the GSOC in the Oberpfaffenhofen and Weilheim as well as the members of DSN at NASA.

For the fruitful collaboration with the Plasma team (E1) and the Plasma Wave (E5), we would like to express our special thanks to Dr. Rosenbauer, Dr. Schwenn, Dr. Marsch, Dr. Mühlhäuser, Dr. Pilip, Prof. Gurnett, and Dr. Anderson.

Finally, we would like to express our gratitude to the Federal Ministry for Research and Technology and to the BPT of DFVLR for the financing and implementation.

Bibliography:

In the following bibliography, the members of the E2-E4 evaluation team's written publications are highlighted.

Abraham-Shrauder, B. and S.H. Yun, Interplanetary shocks seen by Ames plasma probes on Pioneer 6 and 7, *J. Geophys. Res.*, 81, 2097-2102, 1976.

Adams, J., and G.W. Pneuman, A new technique for the determination of coronal magnetic fields: A fixed mesh solution to Laplace's equation using line-of-sight boundary conditions, *Solar Physics*, 46, 185-203, 1976.

Altschuler, M.D., R.H. Levine, M. Stix, and J. Harvey, High resolution mapping of the magnetic field of the solar corona, *Solar Physics*, 51, 345-375, 1977.

/ Barnstorf, H., Current sheets in the interplanetary plasma, Doctoral dissertation, Institute for Geophysics and Meteorology at the Technical University of Braunschweig, July 1980.

/ Behannon, K.W., and F.M. Neubauer, Investigation of sector boundary fine structure between 0.3 and 1.0 AU, Proc. of the 4th solar wind conference, Burghausen, F.R.G. printed in Lecture Notes in Physics, Springer, 1981.

/ Behannon, K.W., F.M. Neubauer, and H. Barnstorf, Fine scale characteristics of interplanetary sector boundaries, *J. Geophys. Res.*, 86, 3273-3287, 1981.

/ Beinroth, H.J., and F.M. Neubauer, Properties of whistler mode shock waves between 0.3 and 1.0 AU from Helios observations, published in *J. Geophys. Res.*, 1981.

Belcher, J., and Davis Jr., Large-amplitude Alfvén waves in the interplanetary medium, 2, J. Geophys. Res., 76, 3534-3563, 1971.

Burlaga, L.F., Interplanetary stream interfaces, J. Geophys. Res., 79, 3717-3725, 1974.

Burlaga, L.F., R. Lepping, R. Weber, T. Armstrong, C. Goodrich, J. Sullivan, D. Gurnett, P. Kellogg, E. Keppler, F. Mariani, F. Neubauer, H. Rosenbauer, and R. Schwenn, Interplanetary particles and fields, November 22 to December 6, 1977: Helios, Voyager, and Imp observations between 0.6 and 1.6 AU, J. Geophys. Res., 85, 2227-2242, 1980.

Dehmel, G., F.M. Neubauer, D. Lukoschus, J. Wawretzko, E. Lammers, The search coil magnetometer experiment (E4), Space Travel Research, 19, Volume 5, 241-243, 1975.

/ Denskat, K.U., and F.M. Neubauer, Statistical properties of low-frequency magnetic field fluctuations in the solar wind from 0.29 to 1.0 AU during solar minimum conditions: Helios 1 and Helios 2, submitted to J. Geophys. Res., 1980.

/ Denskat, K.U., F.M. Neubauer, and R. Schwenn, Properties of "Alfvénic" fluctuations near the sun: Helios 1 and Helios 2, Proc. of the 4th Solar Wind Conference, Burghausen, F.R.G., printed in the Lecture Notes in Physics, Springer, 1981a.

/ Denskat, K.U., H.J. Beinroth, and F.M. Neubauer, Interplanetary magnetic field power spectra with frequencies from 2.4×10^{-5} Hz to 470 Hz from Helios observations during solar minimum conditions, in progress, 1981b.

- Gliem, F., G. Dehmel, G. Musmann, C. Türke, U. Krupstedt, R.P. Kugel, the computer onboard the Helios magnetometer experiments E2 and E4, *Space Travel Research*, 20, Volume 1, 16-19, 1976.
- Gurnett, D.A., F.M Neubauer, and R. Schwenn, Plasma wave turbulence associated with an interplanetary shock, *J. Geophys. Res.*, 84, 541-552, 1979.
- Hedgecock, P.C., A correlation technique for magnetometer zero level determination, *Space Sci. Instr.*, 1, 83-90, 1975.
- Hirschberg, J., The transport of flare plasma from the sun to the earth, *Planet. Space Sci.*, 16, 309-319, 1968.
- Hirschberg J., A Alksne, D.S. Colburn, S.J. Bame, and A.J. Hundhausen, Observation of a solar flare induced interplanetary shock and Helium enriched driver gas, *J. Geophys. Res.*, 75, 1-15, 1970.
- Hundhausen, A.J. and R.A. Gentry, Numerical simulation of flare-generated disturbances in the solar wind, *J. Geophys. Res.*, 74, 2908-2918, 1969.
- Lemaire, J., and L.F. Burlaga, Diamagnetic boundary layers: A kinetic theory, *Astrophys. Space Sci.*, 45, 303, 1976.
- Lepping, R.P. and R.D Argentiero, Single spacecraft method of estimating shock normal, *J. Geophys. Res.*, 76, 4349-4359, 1971.
- Marsch, E., K.H. Mülhåuser, H. Rosenbauer, R. Schwenn, and K.U. Denskat, Pronounced proton core temperature anisotropy, ion differential speed, and simultaneous Alfvén wave activity in slow solar wind at 0.3 AU, submitted to *J. Geophys. Res.*, 1981c.

- Musmann, G., F.M. Neubauer, A. Maier, E. Lammers, The fluxgate probe magnetic field experiment (E2), Space Travel Research, 19, Volume 5, 232-236, 1975.
- / Musmann, G., F.M. Neubauer, F.O. Gliem, and R.P. Kugel, Shock-identification-computer onboard of the spacecrafts Helios 1 and Helios 2, IEEE Trans. on Geosci. Electron., 92-95, 1979.
- / Musmann, G., F.M. Neubauer, and E. Lammers, Radial variation of the interplanetary magnetic field between 0.3 AU and 1.0 AU, J. Geophys., 42, 591-598, 1977.
- / Neubauer, F.M., the fluxgate probe and the search coil experiment of the solar probe Helios, Section 1: Demands on the experiment from the scientific research perspective, Institute for Geophysics and Meteorology at the Technical University of Braunschweig, GAMMA 8, 1969.
- / Neubauer, F.M., H.J. Beinroth, H. Barnstorf, and G. Dehmel, Initial results from the Helios 1 search coil magnetometer experiment, J. Geophys., 42, 599, 1977a.
- / Neubauer, F.M., G. Musmann, and G. Dehmel, Fast magnetic fluctuations in the solar wind: Helios 1, J. Geophys. Res., 82, 3201, 1977b.
- / Neubauer, F.M., Recent results on the sector structure of the interplanetary magnetic field, Pleins feux sur la physique solaire [Spotlight on Solar Physics], Proc. of the 2nd European Solar Physics [Conference], Toulouse, 8-10 March, 1978.
- / Neubauer, F.M., and H. Barnstorf, Recent observational and theoretical results on discontinuities in the solar wind, Proc. of the 4th solar wind conference, Burghausen, F.R.G., printed in the Lecture Notes in Physics, Springer 1981.

- / Riesebieter, Wolfgang, Three-dimensional model calculations for the Solar wind, Doctoral Dissertation, Institute for Geophysics and Meteorology at the Technical University of Braunschweig, February 1977.
- / Riesebieter, W. and F.M. Neubauer, A comparison of 3D solar wind predictions with observations, Pleins feux sur la physique solaire [Spotlight on Solar Physics], Proc. of the 2nd European Solar Physics Conference, Toulouse, 8-10 March 1978.
- / Riesebieter, W. and F.M. Neubauer, Direct solution of Laplace's equation for coronal magnetic fields using line-of-sight boundary conditions, Solar Physics, 63, 127-133, 1979.
- Rosenberg, R.L., and C.R. Winge, The latitude dependencies of the solar wind, in "Solar Wind Three", C.T. Russell, editor, 1974.
- Smith, E.J., B.T. Tsurutani, and R.L. Rosenberg, Observations of the interplanetary sector structure up to heliographic latitudes of 16°: Pioneer 11, J. Geophys. Res., 83, 717-724, 1978.
- Sonnerup, B.U.Ö, and L.J. Cahill, Jr., Magnetopause structure and attitude from Explorer 12 observations, J. Geophys. Res. 72, 171-183, 1967.
- Svalgaard, L., J.M. Wilcox and T.L. Duvall, A model combining the polar and sector structured solar magnetic fields, Solar Phys. 37, 157-172. 1974.